L1CAM AND PLANAR CELL POLARITY MAINTAIN THE SOX2+ PROGENITOR-LIKE STATE IN LUNG CANCER METASTASIS

by

Yasemin Kaygusuz

A Dissertation

Presented to the Faculty of the Louis V. Gerstner, Jr.

Graduate School of Biomedical Sciences,

Memorial Sloan Kettering Cancer Center

in Partial Fulfillment of the Requirements for the Degree of

Doctor of Philosophy

New York, NY

December, 2022

_____ _____

Joan Massagué, PhD
Dissertation Mentor

Date

ABSTRACT

The majority of cancer-related deaths are caused by metastases, which are generated by disseminated metastasis-initiating cells (MICs) exhibiting stem-like properties. However, the origins of MICs and mechanisms supporting their stem-like properties are poorly understood. We previously identified L1 cell adhesion molecule (L1CAM) as a functional marker of MICs in many cancer model systems metastasizing to multiple organs in the body. L1CAM expression emerges upon the loss of epithelial integrity and is required for growth reinitiation in cancer organoids. The goals of this study were to describe the extracellular matrix (ECM) ligands of L1CAM in MICs, to determine at which step of tumorigenesis L1CAM emerges and is necessary for tumor progression, to identify the developmental trajectory and regenerative characteristics of L1CAM+ MICs, and to investigate whether L1CAM functions via only mechanotransduction pathways in MICs.

The first chapter of this work delineates the regenerative characteristics and ECM interactions of the L1CAM+ cell state, demonstrating that L1CAM+ MICs in CRC represent malignant versions of normal regenerative progenitors.

In the second chapter, using the *Kras*$^{LSL\text{-}G12D}$; *Trp53*$^{flox/flox}$; *Rosa26*$^{LSL\text{-}Cas9\text{-}EGFP}$ (KP) LUAD mouse model, I first showed that L1CAM is dispensable for carcinoma initiation but provides a growth advantage in *in vitro* tumoroid growth and is essential for the ability of KP tumoroids to establish metastasis in multiple organs after inoculation into athymic mice. Furthermore, I found that L1CAM is necessary to support the expression of SOX2, a master developmental transcription factor expressed in the foregut endoderm and early lung epithelial progenitors, in KP tumoroids and metastases. Knockdown of L1CAM in KP tumoroids downregulated the SOX2 expression while causing the premature differentiation of LUAD cells into more mature SOX9+ progenitor stages.

We further investigated the KP and KPL1 primary tumors and tumoroids by single-cell transcriptomic profiling. L1CAM+ SOX2+ KP cells form a unique cluster showing enrichment for the expression of stem cell markers. In addition, L1CAM and SOX2 expression was closely associated with the expression of the non-canonical Wnt signaling (planar cell polarity (PCP)) and cilium assembly genes and with the transcriptional signature of the chromatin remodeler CHD1. The PCP pathway is known to activate the Jun transcription factor and regulate SOX2 expression. I demonstrated that L1CAM, is required for the FZD6 expression, a key receptor driving the PCP pathway and Jun nuclear localization in the KP tumoroids. CHD1 is previously shown to facilitate open chromatin and mediate self-renewal and pluripotency in embryonic stem cells. In KP tumoroids, CHD1 knockdown downregulates the SOX2 expression. I propose that SOX2 expression in LUAD MICs is supported by the complementary inputs of the chromatin remodeler CHD1 and Jun activation by the L1CAM-dependent assembly of PCP-JNK signaling.

Altogether, the study demonstrates that the regenerative characteristics of L1CAM+ MICs originate from epithelial regenerative and developmental progenitors as shown by the recapitulation of the SOX2+ early-stage progenitor-like state in LUAD tumoroids and metastasis. It highlights the essential role of L1CAM in promoting the progenitor-like state during tumoroid growth and metastatic colonization, and shows that L1CAM facilitates the PCP pathway and cooperates with chromatin regulation to maintain SOX2 expression. This work expands our knowledge of the role of L1CAM in the establishment of regenerative stem cell phenotypes co-opted by the tumors for relapse at distant sites.

ACKNOWLEDGEMENTS

First and foremost, I would like to thank my thesis mentor, Dr. Joan Massagué, for providing me with the training, guidance, and resources to develop as a scientist. Thank you for sharing your enthusiasm for science with me. I am grateful to my fellow lab members for their support, advice, and exciting scientific discussions - Dr. Karuna Ganesh for her mentorship and collaboration during my first few years in the lab, and Dr. Jin Suk Park and Lan He for their collaboration.

Second, I thank my thesis committee - Dr. Richard White and Philipp Niethammer for their guidance and invaluable insights, and for Drs. Tuomas Tammela and Srinivas Malladi, for accepting to be the Chair and external examiner in my examining committee, respectively.

Third, I would like to thank the Gerstner Sloan Kettering Graduate School, our Dean Dr. Mike Overholtzer, administrative staff, and fellow students. Your leadership and guidance create an environment supporting our independent growth and developing our scientific curiosity.

Finally, I thank my family for their endless love and support. My parents, Hatice and Ahmet, and my sister Deniz have always supported my interest in science and encouraged me to pursue my goals. And, lastly, I am grateful to my husband Kayahan for his love, support, and compassion.

Table of Contents

List of Tables

List of Figures

List of Abbreviations

ARL13B	ADP-ribosylation factor-like 13B
BBS	Bardet-Biedl syndrome
BSA	Bovine serum albumin
CHD1	Chromodomain helicase DNA binding protein 1
ChEA	ChIP Enrichment Analysis
CRC	Colorectal cancer
CSC	Cancer stem cell
CTC	Circulating tumor cell
Dox	Doxycycline
DSS	Dextran sodium sulfate
DTC	Disseminated tumor cell
DVL	Dishevelled
ECD	Extracellular domain
ECM	Extracellular matrix
EGFP	Enhanced green fluorescent protein
EGFR	Epidermal growth factor receptor
EMT	Epithelial-to-mesenchymal transition
ENCODE	The Encyclopedia of DNA Elements
FGFR	Fibroblast growth factor receptor
FOXA2	Forkhead box A2
FZD6	Frizzled 6
GO	Gene ontology

ICD	Intracellular domain
ILK	Integrin-linked kinase
JNK	c-Jun N-terminal kinase
KP	*Kras*$^{LSL\text{-}G12D/+}$; *Trp53*$^{flox/flox}$; *Rosa26*$^{LSL\text{-}Cas9\text{-}EGFP}$
KPL1	*Kras*$^{LSL\text{-}G12D/+}$; *Trp53*$^{flox/flox}$; *Rosa26*$^{LSL\text{-}Cas9\text{-}EGFP;}$ *L1cam*$^{flox/flox}$
KRAS	Kirsten rat sarcoma
LGR5	Leucine rich repeat containing G protein-coupled receptor 5
LUAD	Lung adenocarcinoma
L1CAM	L1 cell adhesion molecule
MIC	Metastasis-initiating cell
NET	Neutrophil extracellular traps
NKX2-1	NK2 homeobox 1
NSCLC	Non-small cell lung cancer
PAK	p21-activating kinase
PCP	Planar cell polarity
PROM1	Prominin 1
SCLC	Small cell lung cancer
SOX2	SRY-box transcription factor 2
SOX9	SRY-box transcription factor 9
YAP	Yes-associated protein

Chapter 1: Introduction

1.1 Metastasis-Initiating Cells

Metastasis is the main cause of cancer-related deaths. Despite recent developments in therapies, many patients often suffer from metastatic disease, which is the regrowth of cancer cells at distant sites. The metastatic cascade begins with the dissemination of cancer cells from the primary tumor to local sites and distant organs, followed by a dormancy period, and is completed by the colonization of host tissues. Metastasis requires certain traits to complete each step of the metastatic cascade, to survive the challenges of the new microenvironments, lack of attachment, and immune attacks, and to regenerate tumors at distant sites from scratch. Cancer cells that exhibit adaptability to acquire the necessary traits to survive the metastatic cascade and successfully colonize at distant sites are called metastasis-initiating cells (MICs).

1.1.1 The Metastatic Cascade

Cancer cell dissemination and seeding of distant organs may start at the early stages of tumor development[1-6] and continue until the primary tumor is resected[7]. Single or small clusters of disseminated tumor cells (DTCs) are capable of remodeling the extracellular matrix (ECM) and undergoing epithelial-to-mesenchymal transition (EMT), which enables migrating and invading the tissue parenchyma, migrating towards blood and lymphatic vessels, and intravasation[4,8-10].

MICs travel via blood or lymphatic circulation and are also named circulating tumor cells (CTCs). Because circulation is challenging for most CTCs, their survival and ability to leave circulation at a distant site depend on cell-intrinsic characteristics and cell-microenvironment interactions. While the majority of CTCs circulate singly, some may travel in clusters and may include stromal cells[8,11,12]. Clustering of CTCs has been shown to induce alterations in DNA methylation that resemble stem-like epigenomic states and enable metastatic seeding[13] and to allow growth-promoting nanolumenal signaling between clustering cells[14]. Moreover, platelets can form a shield surrounding CTCs, which enables immune evasion and provide protection from the physical stresses of blood circulation[15,16]. Neutrophils may also participate in CTC clustering, which prevents leukocyte-mediated killing and mediate CTC survival[17].

Surviving CTCs are caught in the capillaries and leave blood vessels by migrating through endothelial cells, a process called extravasation[1,4]. After extravasation, MICs stay in the vicinity of capillaries and invade the host tissue by migrating along the capillaries[18-20].

MICs undergo dormancy for extended periods of time to survive the physical, nutritional, and immune challenges set by the foreign microenvironment of host tissues[4,21-25]. Dormant cells may start proliferating and colonizing the distal sites months to years following the primary tumor treatment[26]. Our understanding of how dormant cells awaken is limited but recent studies have shown that the balance

between growth-promoting and dormancy signals determines when MICs exit from dormancy[21,27]. More work on neutrophil extracellular traps (NETs) also showed that NETs induced by cancer cells or during inflammation promoted the regrowth of dormant cancer cells[28-30].

After surviving the challenges of the metastatic cascade, MICs display certain traits to reinitiate growth. MICs disseminated from multiple cancer types including lung, breast, colorectal, and renal cell carcinomas express L1 cell adhesion molecule (L1CAM), which facilitates the spreading of MICs on the abluminal surface of the vasculature, a process called vascular cooption[18,31]. L1CAM, in cooperation with β1 integrins, interacts with the perivascular basement membrane and triggers the integrin-linked kinase (ILK) and p21-activating kinase (PAK), which activate the mechanotransduction effectors YAP and MRTF to promote proliferation and initiate metastatic colonization (Figure 1-1)[31]. In line with these findings, actin remodeling and forming filopodia-like protrusions by integrins, ILK, and β-parvin have been previously shown to promote stemness and metastatic colonization[32,33].

Similar to engagements with laminins in the basement membranes, MICs can coopt growth-promoting signals of stroma in the host tissues. MICs can invade stem cell niches found in the bone marrow[34,35] or establish stem-like niches by secreting tenascin C to induce a stem-like phenotype[36]. Studies on interactions with stromal cells also showed that MICs and metastatic progression may benefit

from engagements with astrocytes[37,38], neurons[39], osteoblasts[40], microglia[41], fibroblasts[36,42], and other cell types[4,30,43].

In addition to activating growth-promoting signals, MICs are able to evade the immune cell-mediated killing by altering the expression of NK cell and T cell ligands[44], effectors of signaling pathways that detect cytosolic DNAs[45], and MHC class I molecules[46,47]. Moreover, MICs are able to adapt to the changing metabolic conditions by activating oxidative phosphorylation[48,49], modifying metabolic pathways[50-52], preventing oxidative stress upon changes in the oxygen levels[48,53,54], and upregulating the fatty acid receptor CD36 to increase lipid uptake specifically in brain metastases[55,56].

1.1.2 Phenotypic Plasticity of MICs

The long and challenging journey of MICs requires the acquisition of certain traits to leave the primary tumor, survive and reinitiate growth at secondary sites, and also show therapy resistance. A subset of these MIC traits might be already present in tumor-initiating cells, also known as cancer stem cells (CSCs), and might depend on the oncogenic mutations. However, MICs have been shown to exhibit further specialized traits, such as motility, reversible dormancy, and the ability to regenerate a tumor from scratch at a secondary site, unlike both CSCs and the rest of the cells found in primary tumors. The acquisition of these traits is determined by the adaptability of MICs, which is driven by phenotypic plasticity and enables MICs to modify gene expression programs and change cell states under

the changing conditions of the microenvironment during the metastatic cascade[57-59].

Multiple studies have searched for genetic alterations specific to metastases in matched primary tumors and metastases of patients with lung cancer and other cancer types; however, only a handful of somatic mutations and chromosomal instability have been identified as metastasis-associated genetic alterations. Although these genetic alterations are not directly responsible for metastatic traits, they might contribute to tumor progression and therapy resistance in cancers, which are associated with metastatic ability[4,60-64]. Notably, the metastatic samples showed higher tumor metastatic burden[65] and increased copy number alterations associated with a higher risk of lung cancer recurrence[66]. Nonetheless, accumulating evidence in the literature suggest that the metastatic traits of MICs depend on their phenotypic plasticity established by non-genetic alterations instead of metastasis-specific mutations, which regulate the expression of metastasis-associated genes[4,67-74].

A key metastasis-promoting trait of MICs, phenotypic plasticity, enables MICs to reenact epithelial stem and progenitor cell states for tumor regeneration. Stem and progenitor cells of epithelial tissues display a fluid stem cell phenotype that enables transitions between different cell states that mediate motility, proliferation, ECM remodeling, or secretion of cytokines depending on the conditions under homeostasis and tissue injury[75,76]. For example, in the intestinal epithelium,

LGR5+ stem cells are responsible for tissue homeostasis[77] but if LGR5+ stem cells are ablated experimentally or by injury, the LGR5- regenerative progenitors in the intestine can regenerate the intestinal epithelium and give rise to new LGR5+ cells in the process[75,78,79]. Recent findings on how intestinal cells regenerate *in vitro* and form organoids demonstrated that although both LGR5+ and LGR5- cells have the capacity to initiate organoid growth, all cells acquire the LGR5- regenerative state during organoid growth initiation[78,80]. In colorectal cancer (CRC), while the LGR5+ stem cells are the CSCs, the majority of MICs in colorectal cancer (CRC) are LGR5-[81]. LGR5- MICs are capable of initiating metastasis either by re-expressing LGR5[81] or by establishing an LGR5- regenerative state[82,83].

Recent studies on phenotypic plasticity in metastasis in our lab showed that L1CAM, the cell adhesion protein that mediates cell-endothelial cell adhesion in the perivascular niche[18,31], is dynamically expressed and mediates a regenerative phenotype in MICs in CRC[68]. L1CAM is a neuronal cell adhesion molecule and its abnormal upregulation at tumor invasive fronts is associated with poor prognosis and survival across multiple cancer types, including CRC[84]. Although L1CAM is not expressed in the normal intestinal epithelium, its expression is upregulated in the injured intestinal epithelium and is necessary for restoring epithelial integrity[68]. This L1CAM-dependent regenerative phenotype displayed by intestinal progenitor cells is reenacted by L1CAM+ MICs during CRC organoid formation and metastasis initiation in CRC[68].

In sum, there is a growing body of evidence in the literature indicating that MICs are capable of acquiring certain traits to overcome the challenges of the metastatic cascade and reinitiate a tumor from scratch at a distant site by mimicking the regenerative phenotypes of adult stem and progenitor cells. However, the dynamics and mechanistic foundations of regenerative phenotypes in MICs are poorly understood. The aim of this thesis is to expand our knowledge of how regenerative phenotypes emerge and which molecular mechanisms mediate establishing the regenerative phenotypes in MICs.

1.2 Lung Adenocarcinoma Biology

1.2.1 Lung Cancer Subtype Specification and Targeted Therapies

Lung cancer is the second most frequently diagnosed cancer type and remains the leading cause of cancer-related deaths worldwide[85-88]. Lung tumors are classified based on their clinicopathological characteristics, and approximately 85% of diagnosed tumors have a histological subtype classified as non-small cell lung cancer (NSCLC) while the remaining 15% of tumors are SCLC[86]. The majority (40%) of NSCLC tumors are further classified as adenocarcinoma while the rest belong to the squamous-cell carcinoma subtype and others[86,89]. Lung cancer incidence is associated with cigarette smoking because smoking is responsible for more than 80% of the lung cancer tumors in the United States[85,90], and has been declining since 2009 as more people quit smoking[85].

Based on studies on mouse LUAD tumor models, these tumors originate from alveolar type 2 (AT2) cells[91,92]. The most frequent oncogenic mutations in LUAD are detected in the Kirsten rat sarcoma (KRAS) and epidermal growth factor receptor (EGFR) genes, which have been considered tumor-initiating mutations and studied heavily as potential targets to treat LUAD[88,93]. Notably, KRAS and EGFR mutations are mostly mutually exclusive and might be accompanied by additional mutations in p53 (TP53), BRAF, MET, ERBB2, ALK, RET, and ROS1[86,88]. KRAS mutations are detected in approximately 30% of LUAD tumors but less frequently in squamous carcinoma[86]. Compared to EGFR, KRAS is more frequently mutated in smokers than in non-smokers and shows distinct nucleotide substitutions due to C>A transversions associated with carcinogens in tobacco[94]. While G12C is the most common mutation in KRAS in smokers (41%), G12D is more frequent in non-smokers (56%)[94]. KRAS-mutant LUAD tumors have been associated with high PD-L1 expression, inflammatory stroma, and high mutation burden, which suggest that the KRAS-mutant LUAD tumors might have a high response rate to immunotherapy[95-97].

The dependence of lung cancer cells on these oncogenic mutations led to the development of therapeutic strategies targeting patient-specific mutations[86,88]. In addition to surgery and radiotherapy, targeted therapies against oncogenic mutations in certain proteins such as EGFR, ALK, MET, or BRAF have shown benefits but patients may show therapy resistance. Recently, immunotherapy has been applied in combination with chemotherapy for tumors with PD-L1 expression,

which provided additional clinical benefits[86]. Although KRAS mutations have been previously considered “undruggable”, recently the KRAS G12C inhibitor sotorasib has been shown to provide clinical benefit in NSCLC patients with KRAS G12C mutation[98].

1.2.2 Phenotypic Plasticity in Lung Adenocarcinoma

Despite the recent advances in the standard-of-care regimen for patients[99], 30-55% of NSCLC patients suffer from local and distant recurrence by five years after the initial diagnosis[100,101]. While many studies delineated the biology and order of genetic changes during tumor development[61,102], increasing evidence in the literature demonstrates that metastatic capacity and therapy resistance are driven by diverse cancer cell states equipped with high phenotypic plasticity[4].

Recent studies have been illuminating the importance of phenotypic plasticity in LUAD and unveiling the mechanisms by which tumor cells adopt phenotypic plasticity in tumor progression and metastasis. Latency-competent metastatic cancer cells have been shown to express SOX transcription factors and acquire a stem-like phenotype which facilitates their reversible quiescence and evasion from natural killer cell-mediated immunity[21]. After extravasation, MICs of LUAD have also been shown to express the neural cell adhesion protein L1CAM to achieve a pericyte-like spreading ability to co-opt capillaries and reinitiate growth by activating mechanotransduction signaling via YAP and MRTF[18,31].

The use of single-cell transcriptomics in LUAD patient primary tumor and metastasis samples and in a mouse model of metastatic lung cancer has recently shown the reenactment of lung epithelial developmental and regenerative phenotypes in disease[103]. While regenerative cell signatures and cell states from all stages of lung epithelial development are detected in primary tumor samples, cell states representing the less differentiated lung epithelial progenitors are remarkably enriched in metastatic samples, further supporting the acquisition of developmental and regenerative states during metastasis initiation[103]. The emergence and role of phenotypic plasticity have recently been demonstrated by the characterization of a highly plastic phenotypic state in mouse LUAD tumor models using single-cell transcriptomics[104]. “The high-plasticity cell state” in LUAD mouse tumors exhibits both a striking ability for proliferation, differentiation, and chemoresistance and a strong association with poor survival in multiple cancer types[104]. In line with these findings, single-cell epigenomics in mouse LUAD tumors delineated epigenomic alterations leading to loss of differentiated cell identity during tumor progression and metastasis[69].

In addition to the dedifferentiated and regenerative cell states, MICs are also capable of entering cell states that show quiescence[21], express drug efflux transporters[105], induce growth upon cytokines released by dying or senescent cancer cells[106,107], exclude immune cells from the tumors to evade from immunotherapy[108-110], and manipulate the tumor microenvironment[111-113]. Therefore, characterizing the phenotypic plasticity and its molecular underpinnings

in MICs might be key to understanding why current therapies fail and how new strategies might be developed to overcome MIC plasticity to prevent and treat metastatic LUAD.

Collectively, these data provide evidence for the acquisition and role of phenotypic plasticity in establishing a less differentiated and regenerative phenotype required for growth reinitiation *in vitro* and in metastasis. However, there is an immediate need for understanding the foundations of regenerative phenotypes observed in LUAD progression and metastasis. This thesis aims to explain how regenerative phenotypes emerge and the role of L1CAM and cooperating molecular mechanisms in establishing the regenerative phenotypes in LUAD metastasis.

1.3 L1 Cell Adhesion Molecule in Cancer

1.3.1 L1CAM Expression, Structure, and Function

L1CAM is a single-pass transmembrane glycoprotein with a 200-220 kDa molecular weight and was identified as a neuronal cell surface protein in 1984[114,115]. The extracellular domain (ECD) of L1CAM is composed of six immunoglobulin-like (Ig) domains and five fibronectin type III repeats whereas the intracellular domain (ICD) is short but highly conserved[115,116]. L1CAM is crucial for axon outgrowth, fasciculation, myelination, and neuronal cell adhesion and migration during neural development[117]. Genetic knockout of L1CAM in mice leads to neurological defects[118,119], and L1CAM mutations in humans are responsible for neurological disorders[120]. L1CAM is a member of the L1 subfamily of cell adhesion

molecules, which also includes Close Homolog of L1 (CHL1), NrCAM, and Neurofascin[117]. The other L1 subfamily members exhibit similarities in their structure and function in neural development with L1CAM; however, their expression and role in cancer are poorly understood and remain an open question[117,121,122]. The L1CAM ECD can mediate homophilic L1CAM-L1CAM interactions *in trans* at cell-cell interfaces. It can also interact with integrins, neurocan, neuropilin-1, and CD24, epidermal growth factor receptor (EGFR) and fibroblast growth factor receptor (FGFR) *in cis* and *in trans*[116,117,123-125]. The L1CAM ICD can engage with the cytoskeletal proteins ezrin-radixin-moesin (ERM), ankyrin, and spectrin[126,127]. In addition to its membrane-bound form, L1CAM ECD solubilized by ADAM proteinases can interact with integrins in an autocrine fashion[128]. In addition to the membrane proteins, the membrane-bound L1CAM ECD can also facilitate interactions between neurons and ECM proteins such as fibronectin but L1CAM-ECM interactions have been shown to depend on integrins and the interacting ECM proteins have been poorly studied[117].

L1CAM expression in adult tissues is restricted to neurons[117], certain myeloid cells[129], pericytes[31], and kidney collecting duct epithelium[130]. However, aberrant expression of L1CAM has been reported in many cancer types including colorectal, lung, breast, pancreatic ductal, renal cell, gastric, prostate, ovarian, endometrioid, and hepatocellular carcinoma, melanoma, cholangiocarcinoma, glioma, and neuroblastoma and associated with poor prognosis and short survival[84] . Multiple studies investigating how L1CAM expression is induced found that L1CAM

expression is influenced by various pathways in different cancer model systems[84]. L1CAM expression is influenced by the Wnt/β-catenin signaling at the invasive front of CRC tumors[131]. Studies on endometrial and pancreatic cancer cells showed that transforming growth factor-beta1 (TGF-β1) signaling and the transcription factor SLUG regulated L1CAM expression[132-134]. Another mechanism identified in L1CAM gene expression is the neural restrictive silencer factor/RE1 silencing transcription factor (NRSF/REST), which suppresses the neuronal gene expression in non-neuronal cells[135]. Loss of REST expression has been associated with breast cancer recurrence[136-138] and bad prognosis and induces L1CAM expression in small cell lung cancer[139]. In addition, certain microRNAs[140-142] and DNA methylation[143,144] can also influence L1CAM expression in cancer cells. However, which of these signals impinge directly on *L1CAM* transcription and the interaction partners of L1CAM in cancer cells and ECM remain unknown.

1.3.2 Role of L1CAM in Cancer

L1CAM expression has been associated with CSCs and MICs but only a number of studies have defined its direct role in supporting stem-like traits. Studies on CRC demonstrated that L1CAM is not expressed in the EpCAM+, CD133+, and CD44+ CSCs but its overexpression promoted metastasis via NF-κB signaling[145]. Later, L1CAM expression has been detected in LGR5+ CSCs and enhanced metastatic capacity of CRC cells by inducing the clusterin (CLU) expression, independent of NF-κB signaling[146]. More recent studies identified Achete scute-like (ASCL2)[147], a key transcription factor expressed in LGR5+ cells regulating stemness, and

phospho-ERK1/2[148] as the downstream effectors of L1CAM in CRC. Recent work on multiple cancer model systems, including lung, breast, colorectal, and renal cell carcinoma in the Massagué Lab showed that L1CAM is expressed in MICs and required for spreading on and migrating along blood capillaries after extravasation[18,31], and that L1CAM interactions with both β1 integrins in *cis* and the vascular basement membrane activate ILK and PAK activate the mechanotransduction transcription factors YAP and MRTF to induce proliferation and metastatic colonization (Figure 1-1)[31].

The expression and role of L1CAM in CSCs and MICs raised interest in developing antibody-based therapies to treat many types of cancer[149-151]. Neutralizing monoclonal antibodies and radioimmunoconjugates against L1CAM showed great potential in preclinical models of ovarian carcinoma and neuroblastoma[84,152]. In addition to L1CAM-targeting therapies, radioimmunoconjugates have been also used in tumor imaging in mice[152,153] and in patients[154]. Moreover, studies also demonstrated that L1CAM-specific chimeric antigen receptor-redirected T (CAR-T) cells are effective in eliminating cancer cells in vitro[155] and in mice[156] and feasible in neuroblastoma patients[157].

To sum, there is accumulating clinical and experimental literature on the expression, role, and therapeutic targeting of L1CAM in many cancer types. The role of L1CAM in mediating stem-like traits in cancer cells has been solidified over the last 20 years. Despite its clear mechanism of action in neuronal development,

studies suggest that the expression, interactions, and downstream effectors of L1CAM are dynamic and context-dependent in cancer cells and require further investigation. This thesis aims to clarify how L1CAM expression is induced, which molecular mechanisms play a role in L1CAM-dependent traits, and which developmental and regenerative states are reenacted in L1CAM+ MICs.

1.4 Planar Cell Polarity Pathway and Cilium Signaling in Cancer

1.4.1 Planar Cell Polarity Pathway

Cell polarization refers to the asymmetrical organization of molecules and cellular functions within cells. Synchronized cell polarity across cell layers is highly critical in establishing specialized tissues and functions in multicellular organisms. The most prominent example of cell polarity is observed in epithelial tissues, which exhibit two modes of polarity in space. Apical-basal cell polarity is the asymmetrical localization of molecular components and functions between the opposite surfaces along the apical-basal axis of a cell layer whereas planar cell polarity (PCP) refers to the organization along an axis orthogonal to the apical-basal axis in the plane of a cell layer[158]. The main function of PCP is to enable cell-cell communication on polarity information across the tissue plane in development and homeostasis[159]. PCP is established by the organization of key PCP proteins in a mutually exclusive pattern on opposite sides of a cell, which is repeated in the adjacent cells generating a consecutive pattern within the cell layer. As initially defined in *Drosophila melanogaster*, asymmetric distribution of protein complexes formed by Frizzled (Fz; FZD in vertebrates), Dishevelled (Dsh; DVL in vertebrates) and Diego

(Dgo; ANKRD6 in vertebrates) at one side of the cell, Van Gogh (Vang; VANGL in vertebrates) and Prickle (Pk; PRICKLE, PK1 in vertebrates) at the opposite side, and Flamingo (Fmi; CELSR in vertebrates) localization at both sides, establishes PCP patterns (Figure 1-2)[158,160-164].

PCP is triggered by asymmetric molecular signals, but it is established and propagated within the cell layer by intercellular interactions. The seven-pass atypical cadherin Fmi engages in homophilic interactions at cell-cell junctions and enables intercellular communications of PCP[165-168]. Homophilic Fmi interactions connect PCP signaling components in adjacent cells and generate complementary and repeating polarity complexes across the cell layer[158]. While Fmi is essential on both sides of the cell-cell junction and Fzd is necessary to induce polarity at the junction, Vang is not necessarily required for initiating polarization but found to be mediating the polarization of the adjacent cells[166,167,169]. Upon the engagement of Fz and Vang, Dsh and Dgo are recruited to Fz and Pk associates with Vang, which stabilizes and amplifies the PCP signal[170,171].

The downstream effectors of PCP pathway include small GTPases Rho and Rac, Rho-associated kinase (ROCK in vertebrates), and c-Jun N-terminal kinase (JNK)[159]. While ROCK regulate cytoskeletal rearrangements and actomyosin contractility, JNK stimulates the nuclear accumulation and transcriptional activity of c-Jun[159,172-175]. PCP pathway is also known as the non-canonical Wnt/PCP pathway because it signals via Fz receptors and Dvl in a β-catenin-independent

manner. The role of Wnt in PCP in *D. melanogaster* is not well understood [165,176] but multiple studies showed that Wnts are essential cues to induce PCP in vertebrate development[177-179].

Despite being first defined in cilia formation and positioning for wing hair organization and eye development *D. melanogaster*[158,180], PCP pathway components are present in vertebrates and are necessary for tissue polarity in development and homeostasis. PCP is required for the formation of multiciliated cells in the airway, central nervous system, ear hair cells, and oviduct[181], and also for convergent extension[178,182,183], neural crest migration[184,185], axon guidance[186,187], and neural migration[188-190]. Although the formation and positioning of cilia are regulated by PCP pathway[180], work on ciliated cells revealed PCP signaling can be regulated by cilia. Ciliary proteins Inversin and Bardet-Biedl syndrome (BBS) protein act as a switch between canonical and non-canonical Wnt/PCP pathways and are necessary for PCP-dependent development of epithelial tissues[191-193].

Wnt/PCP pathway proteins are abnormally expressed in multiple cancer types and have been associated with motility. FZD2/6, DVL1, VANGL1, PK1, and WNT5A/11 are necessary for cell migration in many cancers including breast, lung, and prostate cancer[194-198]. In breast cancer cells, FZD6 and DVL1 are localized at the invading leading edge in response to WNT11 signal and induce polarization and motility[196]. Similarly, PK1 suppresses RhoA GTPase activity at the rear edge of

migrating cancer cells, which allows the formation of RhoA-mediated focal adhesions at the leading edge, promoting cell motility[199]. Recent work on melanoma cells revealed that WNT11-FZD7-DAAM1 signaling activates Rho, ROCK1/2, and Myosin II, which induce a proliferative and invasive amoeboid cell state capable of migration, stem-like gene expression profile (SOX2+ and ALDH1A+), and metastatic colonization[200]. Collectively, these findings indicate that PCP may be utilized by cancer cells for tumor progression and metastasis.

1.4.2 Cilium Signaling

PCP signaling is essential for the polarized positioning of centrioles, which determines the location and orientation of cilia at the apical surface[158,180]. Cilia are complex microtubule-based organelles extending from centrioles localized at the apical membrane into the extracellular space. After cilium formation is complete, the cilium structure is still dynamic as the tubulin incorporation continues at the steady-state[201] and ciliary proteins, including membrane proteins, are transported in and out of the cilium by ciliary trafficking[202].

Primary cilium (monocilium) in mammalian cells is immotile and acts as a cellular antenna that detects microenvironmental cues such as light, proteins, or mechanical signals[203]. In addition to sensory capabilities, accumulating evidence in the literature demonstrate that primary cilia are hubs for multiple signaling pathways including Hedgehog, Notch, and Wnt signaling[204,205]. In unstimulated cells, the receptor Ptch1 is localized on the cilium membrane and excludes Smo

from the cilium membrane[204]. Upon Shh stimulation, Shh-bound Ptch1 leaves the cilium while Smo enters it, leading to activation of Gli transcription factors[204]. The co-localization of Notch receptors and Notch-processing enzymes in the ciliary membrane and positioning of Presenilin in the cilium basal body allows regulation of Notch signaling by cilia[205-207]. Primary cilia are also implicated in canonical Wnt signaling in vertebrates, but this role is controversial and context-dependent. While mutations in ciliary trafficking genes in zebrafish and mice showed normal Wnt signaling[208,209], loss of the ciliary protein Inversin resulted in Dishevelled degradation and diminished canonical Wnt signaling[193]. On the other hand, multiple studies demonstrated that ciliary defects cause canonical Wnt signaling[210-213]. In addition to their roles in development, Hedgehog, Notch, and Wnt signaling play essential roles in cancer cell stemness and therapy resistance [214-216].

Although primary cilia are involved in growth- and stemness-promoting signaling pathways in cancer cells, the role of cilia in tumor formation is still debated. While many studies show that primary cilia are lost at the early steps of tumorigenesis[217,218] and that inhibiting ciliogenesis promotes Wnt and Hedgehog signaling, and malignant traits[219,220], primary cilia contribute to tumorigenesis in certain cancer types that heavily depend on Hedgehog signaling, such as medulloblastoma and basal cell carcinoma[221,222]. Taken together, cilia formation is regulated by PCP, but primary cilia can influence PCP as well. In addition, primary

cilia play a key role in regulating tumor-promoting multiple signaling pathways in a context-dependent manner.

Chapter 2: L1CAM Expression in Regenerating Epithelia and Interactions in Colorectal Cancer

2.1 Introduction

Metastasis is responsible for the majority of cancer deaths. Despite the recent advances in treatments, many patients often experience a lethal relapse of cancer, which is initiated by MICs exhibiting stem-like properties and immune evasion abilities disseminated by tumors[1,4,10]. Understanding the molecular mechanisms that mediate the emergence and persistence of MICs is essential to developing therapeutic strategies to prevent and treat metastatic cancers.

Tumors seed invasive cancer cells into the circulation starting from the early stages of tumor development[1-3]. Although a majority of DTCs fail to survive in the circulation or after exiting from capillaries, a minority may successfully infiltrate host tissues. After the dissemination phase, DTCs enter a stage of quiescence driven by the physical, metabolic, and immune challenges present at the host parenchyma[4,223]. Studies show that DTCs can exit dormancy when the proliferative signals overcome the antimitotic barriers of the host parenchyma and therapy and colonize the host tissue[4,21,27,224]. MICs that can undergo phenotypic plasticity and acquire certain traits are capable to grow upon exit from dormancy leading to metastatic outgrowth[4]. We have identified the cell adhesion molecule L1CAM as a marker of MICs which provides growth-promoting signals leading to metastatic colonization in multiple cancer types[18,31].

Although L1CAM is only expressed in neurons, myeloid cells, pericytes, and the specialized epithelial cells in kidneys and ovaries in homeostasis, its aberrant expression has been reported in many human cancer types and found to be associated with poor prognosis[84,225]. However, the mechanism of how L1CAM contributes to tumor development and progression was poorly studied. As reviewed in Chapter 1, two consecutive studies from our lab showed that L1CAM enables metastatic cells to spread on blood capillaries at distant sites by interacting with the vascular basement membrane and this interaction activates the mechanotransduction transcription factors YAP and MRTF, leading to proliferation and metastatic growth[18,31]. These studies highlighted the essential role of L1CAM in metastatic colonization in many cancer types metastasizing to multiple organs in the body and pointed out that L1CAM is an actionable target for the treatment of metastatic cancers.

Understanding the conditions that drive L1CAM expression and the interaction partners of L1CAM in metastasis is needed to develop therapeutic strategies to target L1CAM+ MICs. However, our knowledge of how MICs gain L1CAM expression limited because the regulation of L1CAM expression in cancer has been poorly studied[84]. Studies led by Dr. Karuna Ganesh in the Massagué Lab showed that L1CAM expression in CRC emerges in the invasive front of primary tumors and is further enriched in metastasis samples. Next, Dr. Ganesh found that L1CAM-high cancer cells isolated from CRC primary tumors and metastases have higher organoid generation capacity than L1CAM-low cells, which is a trait of stem-

like cells and regeneration[226,227], and are not necessarily LGR5+, suggesting that L1CAM+ MICs and LGR5+ CSC are different subsets of tumor cells[68]. These findings implicated an association between L1CAM expression and tissue disruption and regrowth. Indeed, more work from Dr. Ganesh showed that L1CAM expression is upregulated when CRC organoids are dissociated into single cells by the release of the transcriptional repressor REST from the L1CAM promoter upon disassembly of E-cadherin adherens junctions[68]. Based on these findings, we hypothesized that induction of L1CAM expression upon loss of tissue integrity would originate from epithelial regeneration.

At the start of my work to understand whether L1CAM expression was induced upon disruption of epithelial integrity and whether L1CAM upregulation in cancer cells is associated with epithelial regeneration, I joined efforts in the Massagué Lab using a mouse intestinal injury model to study L1CAM expression. Using this model, we showed that although it is not detected in the homeostatic intestinal epithelium, L1CAM is expressed in regenerating mouse intestinal epithelium and is required for intestinal regeneration.

In addition to its transcriptional regulation, L1CAM ligands in cancer have not been clearly defined[84]. I hypothesized that the relevant ECM ligands in metastatic cells would be a component of vascular basement membrane. To test this hypothesis, I applied protein-protein interaction and cell adhesion assays using CRC organoids and recombinant ECM proteins and demonstrated that L1CAM can form direct

interactions with epithelial and vascular laminin isoforms and facilitates CRC cell interactions with laminins. Therefore, we propose that MICs can express L1CAM to engage with the laminins of the perivascular basement membrane and acquire an L1CAM-dependent regenerative state to survive and proliferate upon the loss of epithelial integrity.

2.2 Results

2.2.1 L1CAM Is Upregulated and Necessary for Regeneration upon Loss of Epithelial Integrity

Studies led by Dr. Ganesh showed that in addition to the CRC organoids, L1CAM was upregulated when normal mouse and human colon epithelial cells are isolated from colon tissue and grown as organoids in culture although L1CAM is not expressed in the normal intestinal epithelium[68]. Therefore, we hypothesized that normal intestinal tissue would induce L1CAM expression upon tissue damage and would require L1CAM to regenerate the epithelium.

To determine if L1CAM expression is induced in epithelial regeneration in vivo, we used the dextran sulfate sodium (DSS)-induced colitis model. In this model, DSS added to drinking water causes epithelial cell injury and loss of epithelial monolayer barrier[228]. DSS treatment for 9 days induced colitis in C57BL/J mice, indicated by severe weight loss, diarrhea, and fecal bleeding (Figure 2-1). After reaching maximal colitis by day 9, the mice were treated with water to allow tissue repair. Although not detected in the mice treated with water, L1CAM was expressed in

colon epithelial cells found at wound beds, intermediate epithelial structures that are called “wound channels”[229], and regenerating crypts (Figure 2-2). Notably, cells in the wound-channel invaginations showed stronger L1CAM expression, suggesting a role for L1CAM in the specialization or differentiation of the intermediate epithelial cells into regenerating crypts.

To test whether L1CAM plays a role in colon epithelial regeneration, Dr. Ganesh generated conditional L1CAM-knockout mice by crossing *L1cam*$^{fl/y}$ mice[118] with *Vil1-cre* mice[230], which allows Cre recombinase expression specifically in intestinal epithelial cells. While the loss of L1CAM in intestinal epithelial cells did not result in any aberrations in body weight and intestinal morphology during homeostasis, L1CAM-knockout mice suffered from body weight loss, diarrhea, and fecal bleeding and failed to recover from colitis after DSS treatment[68]. These data show that L1CAM expression is upregulated upon disruption of epithelial integrity in intestinal epithelium and required for regeneration in normal colon epithelia and CRC primary and metastasis tumors and organoids. Therefore, we propose that during organoid growth and metastatic colonization CRC MICs adopt the L1CAM+ regenerative cell state of the damaged intestinal epithelium.

2.2.2 L1CAM Facilitates CRC Cell Adhesion to Laminins

Cancer cells at the tumor invasive front and disseminated metastatic cells in host tissues interact with extracellular matrix proteins in the microenvironment. The Massagué Lab previously demonstrated that L1CAM enables the pericyte-like

spreading of metastatic cells on endothelial cells, which depends on the interactions of L1CAM and β1 integrin with vascular basal lamina[18,31]. The basal lamina is composed of collagen IV and laminin isoforms 111, 411,421, 511, and 521 in the vasculature[231] and epithelial tissues[232]. Of note, organoid formation cultures require Matrigel, which contains 60% laminin-111 and 30% collagen IV[233].

Although previous studies have reported that L1CAM forms homophilic interactions between neurons[234] and heterophilic interactions in neurons with extracellular matrix proteins, such as fibronectin and laminin[117,235], ECM ligands of L1CAM in cancer cells were not clearly defined. To address this question, I first confirmed that L1CAM established homophilic interactions and heterophilic interactions with laminins in cancer cells by using recombinant L1CAM extracellular domain and extracellular matrix proteins (Figure 2-3a & b). To identify the ligand of L1CAM, I applied a solid-phase binding assay using recombinant and purified extracellular matrix proteins. Using the recombinant L1CAM extracellular domain, I confirmed that L1CAM established homophilic interactions as previously shown in neurons and heterophilic interactions with collagen IV and laminin isoforms 111, 411, 421, 511, and 521 (Figure 2-3a & b).

Next, I hypothesized that metastatic CRC cells would utilize L1CAM to adhere to laminin-rich perivascular basement membrane during metastatic colonization. To test this hypothesis, I applied a cell adhesion assay using CRC organoid cells and recombinant ECM proteins. CRC organoid cells lost the capacity to adhere to

laminin-coated surfaces upon L1CAM knockdown using doxycycline-inducible shRNAs (Figure 2-4). Collectively, these data show that basement membrane laminins are the preferential ligands of L1CAM and L1CAM-laminin interactions are essential for the binding of MICs to basement membranes in the perivascular niche and in vitro culture, which is necessary for metastatic colonization and organoid growth.

2.3 Conclusions and Discussion

My findings about L1CAM+ regenerative state and laminins as the preferred ligands for L1CAM in MICs contribute a key piece of knowledge to our understanding of the role of L1CAM+ MICs. Cancer cells disseminating from primary tumors experience loss of epithelial integrity at all steps of the metastatic cascade, from invading the parenchyma and circulation to surviving at distant sites after extravasation. Metastases are initiated by the DTCs that can exhibit phenotypic plasticity and acquire certain traits under the selective pressure of the metastatic cascade. Our work defined a clear relation between the L1CAM+ regenerative state in MICs and epithelial tissue regeneration by demonstrating that L1CAM expression is upregulated in response to the loss of epithelial integrity and required to reinitiate growth in normal intestinal epithelial regeneration after colitis and in metastasis.

Although L1CAM expression and role in tumor development and metastasis have been studied by others, the ECM ligands of L1CAM have not been well identified[84].

My findings showed that L1CAM forms direct interactions with epithelial and vascular basement membrane laminins. L1CAM mediates both cell adhesion to the laminins of the perivascular basement membrane and cell-cell adhesions via homophilic interactions, which overcome the loss of epithelial integrity and lack of attachment and promotes growth reinitiation in regenerating epithelium and metastasis.

This work also showed that MICs are not necessarily CSCs. The cell of origin of CRC tumors is LGR5+ stem cells found in the intestinal crypts[236]. Oncogenic mutations in homeostatic LGR5+ stem cells result in uncontrolled cell division and adenoma initiation[236]. Studies on intestinal epithelium found that LGR5- cells of the crypt might also initiate tumorigenesis after acquiring an LGR5+ phenotype[79,237-239]. Similar to LGR5+ CRC cells, we found a remarkable ability of some L1CAM- CRC cells to maintain the phenotypic plasticity required for upregulating L1CAM and exhibiting a regenerative state following the loss of epithelial integrity, suggesting a fluid but not a fixed stem-like state[68]. Moreover, according to Dr. Ganesh's findings, L1CAM+ cells are not always LGR5+ and not necessary for adenoma initiation but are required for the regrowth of tumor cells as organoids, transplanted tumors, and metastases[68], which concludes that metastasis initiation depends on L1CAM+ MICs but not on LGR5+ CSCs. The dynamic emergence of the L1CAM+ regenerative state is also reminiscent of injury-driven regenerative stem cells employed in tissue repair. There is abundant evidence that differentiated epithelial cells act as regenerative stem cells during injury repair in numerous

tissues, including the intestinal epithelium[59,78,240-242], and that the LGR5+ homeostatic stem cell gene signature is downregulated during repair after colitis[243]. Based on these findings, we suggest that MICs are different from CSCs and are able to reenact a regenerative progenitor-like state which resembles stem cells emerging after tissue damage, promoting reinitiation of tumor growth at distant sites.

L1CAM has multiple interaction partners well-defined by studies on neuronal development. While interactions with the laminins of the basement membrane in cooperation with integrins trigger mechanotransduction signaling via YAP and MRTF which promote cell proliferation[31], our findings also showed significant L1CAM expression at cell-cell junctions in metastases, CRC organoids, and regenerating intestinal epithelium. L1CAM has been previously shown to engage in homophilic interactions in neurons and cancer cells[84,244]; however, L1CAM homophilic interactions have been considered static adhesions rather than motility-promoting[244]. Little is known about the implications of different L1CAM interactions on phenotypic states acquired by cancer cells. Clarifying the role of L1CAM homophilic interactions and the molecular underpinnings of different cell states mediated by L1CAM became the next objective of my research. Moreover, this work has been largely confined to investigating the role of L1CAM+ regenerative state in CRC. L1CAM expression has been associated with poor prognosis in multiple cancer types[84] and with metastasis to many organs in the body[31]. The role

and molecular details of L1CAM+ regenerative state in metastasis of other cancer types require further investigation.

Chapter 3: L1CAM and Planar Cell Polarity Maintain the SOX2+ Progenitor-Like State in Lung Adenocarcinoma Metastasis

3.1 Introduction

To address the questions mentioned above, I focused on the role of L1CAM in metastasis initiation in the context of LUAD. Lung cancer is the leading cause of cancer deaths worldwide[85-88]. Despite recent advances in targeted therapies, lung cancer patients suffer from therapy resistance and metastasis[86]. At the time of diagnosis, lung tumors may have already shed large numbers of cancer cells into the circulation[4,245]. Even though a majority of these cancer cells fail to survive in circulation or after extravasation, a subset infiltrates the host tissues leading to metastatic colonization. Therefore, understanding the mechanisms and vulnerabilities of metastasis initiation is crucial to prevent and to treat LUAD metastasis.

Previous studies have defined the nature and emergence of genetic changes in tumor development and metastasis[61,102], but accumulating evidence suggests that phenotypic plasticity and diverse cell states determine the metastatic capacity of cancer cells. One such example, L1CAM+ regenerative state in MICs of many cancer model systems, including lung adenocarcinoma, to multiple organs has been identified by the Massagué Lab[18,31]. Our work demonstrated a key role of phenotypic plasticity in metastasis by showing that the L1CAM+ regenerative state in MICs emerges upon loss of epithelial integrity and promotes growth reinitiation

of organoids and metastasis in CRC by mimicking the regenerative progenitor cells of intestinal epithelial tissue[68].

A number of traits of tissue regenerative and developmental progenitor cells are recapitulated in MICs. Recent work on LUAD patient tumors and a mouse model of metastasis demonstrated that primary tumor cells exhibit regenerative cell phenotypes and multiple cell phenotypes that include nearly all stages of lung epithelium development[103]. On the other hand, metastasis samples displayed enrichment for the key lung epithelial progenitor transcription factors (e.g., SOX2) and resemble a more primitive and stem-like phenotype[103]. SOX2 is expressed by endoderm and early lung epithelial progenitors in lung development and is essential for lung tissue formation and epithelial regeneration upon tissue injury[246-248]. Moreover, SOX2 expression in LUAD is associated with CSC traits[249]. Given the role of L1CAM+ regenerative cell phenotypes during metastasis initiation and epithelial tissue regeneration in CRC, we hypothesized that L1CAM+ regenerative state would promote LUAD tumor development and metastasis and recapitulate lung epithelial progenitor phenotypes in LUAD metastasis.

Our understanding of the L1CAM+ regenerative phenotype has been limited by the use of patient-derived xenograft models (i.e., cancer cell lines and patient-derived organoids), which show cell line- and patient-specific differences and lack the intact mouse immune system. In this chapter, to investigate how L1CAM expression emerges upon loss of epithelial integrity at the invasion front of primary

tumors and during tumoroid growth in vitro and metastatic colonization, we used a mouse LUAD tumor model and tumoroids. We generated a genetic knockout of L1CAM in the mouse LUAD tumor model and demonstrated that L1CAM is dispensable for carcinoma initiation in mouse LUAD. However, L1CAM provides a growth advantage in tumoroid growth in vitro and is required for metastatic colonization and for acquiring a progenitor-like regenerative state. By applying single-cell transcriptomic analyses and in vitro perturbation experiments, we define how L1CAM mediates the activation of the Wnt/PCP pathway and leads to the reenactment of a progenitor-like regenerative state defined by the expression of early lung epithelial progenitor transcription factor SOX2.

3.2 Results

3.2.1 L1CAM Is Expressed in Metastases and Organoids in Lung Adenocarcinoma

To investigate the expression pattern of L1CAM in LUAD, I, together with Dr. Jin Suk Park in our lab, analyzed a panel of primary and metastasis tumor samples from LUAD patients and LUAD patient-derived xenografts (PDX) tumors. Although L1CAM was expressed in LUAD primary tumors at low levels, it was enriched both in the metastatic cells locally disseminated into the pleural fluid and lung (pleural metastasis) and in the metastases in distant organs such as bone, brain, and liver (Figure 3-1a & b). Moreover, strong L1CAM expression was also detected in PDX tumors derived from LUAD primary tumors and metastases (Figure 3-1a & b) and in LUAD PDX organoids (Figure 3-2). Increased L1CAM expression in LUAD cells

during their regrowth as metastases, PDX tumors, and patient-derived organoids further supports our previous finding in both intestinal tissue and CRC tumors that L1CAM is expressed in regenerating cells upon loss of epithelial integrity[68] (Figure 3-1c).

3.2.2 L1CAM Is Expressed at the Invasive Front of Mouse LUAD Tumors

PDX models are promising tools to study cancer biology but they have critical limitations, such as patient-specific differences due to mutations and chemotherapy exposure, and the lack of an intact mouse immune system when used in xenograft studies. Moreover, because we aimed to determine whether L1CAM is required for carcinoma initiation and progression using a well-defined and genetically traceable tumor model system, we decided to continue our study using the *Kras*$^{LSL\text{-}G12D/+}$; *Trp53*$^{flox/flox}$; *Rosa26*$^{LSL\text{-}Cas9\text{-}EGFP}$ (KP) genetically engineered mouse model (GEMM) of LUAD[250,251]. In the KP model, the Cre recombinase is introduced to the lungs via intratracheal injection of the Lenti-SPC-Cre lentivirus and drives the oncogenic KRAS-G12D expression and the homozygous deletion of the p53 tumor suppressor in AT2 cells of the lung (Figure 3-3)[250,251], which are the well-known origin of LUAD[91,92]. This model precisely recapitulates the molecular and histopathological characteristics of human lung adenocarcinoma[250-252].

I delivered the lentivirus encoding Cre recombinase to KP mice via intratracheal instillation and allowed LUAD formation for at least 14 weeks. We monitored tumor formation and progression by bioluminescence imaging (BLI) and micro-

computerized tomography (micro-CT) (Figure 3-4). Then, I collected tumor-bearing lungs from KP mice at the adenoma/adenocarcinoma transition (10-19 weeks post-initiation) and adenocarcinoma (20+ weeks post-initiation) stages to investigate L1CAM expression by immunohistochemistry. Although L1CAM was not detected in normal mouse lungs, it was expressed at the invasive front of KP tumors (Figure 3-5) and significantly increased in the late-stage KP tumors (Figure 3-6), similar to the L1CAM expression pattern in LUAD patient primary tumors[84,253]. Furthermore, L1CAM expression was detected mostly at the cell-cell junctions in addition to the cell-matrix interface (Figure 3-5).

3.2.3 L1CAM Is Enriched During LUAD Cell Regrowth as Tumor Organoids

I isolated EGFP+ KP tumor cells from the tumor-bearing mouse lungs at the adenocarcinoma stage by FACS to grow tumor organoids ("tumoroids") *in vitro*. Isolated KP tumor cells were grown in Matrigel supplemented with 2% FBS-containing LUAD tumoroid media[104]. While only ~5% of KP primary tumor cells were L1CAM+ (Figure 3-6), L1CAM+ cells were enriched in the KP tumoroid culture and reached to ~20% in 7 days (Figure 3-7). When KP tumoroids were dissociated into single cells and re-seeded in Matrigel, L1CAM expression was sustained in the next passage at similar levels (Figure 3-7). Similar to the KP LUAD tumors, L1CAM expression in KP LUAD tumoroids was strongly localized at the cell-cell junctions in addition to the cell-matrix interface (Figure 3-8).

3.2.4 L1CAM Is Dispensable for KP Primary Tumor Growth

To investigate whether L1CAM was required for carcinoma initiation and progression, I generated a L1CAM-null KP LUAD tumor model, named KPL1, by crossing the KP mice with the conditional L1CAM knockout mice (*L1cam*$^{flox/flox}$) (Figure 3-9)[118]. I monitored LUAD tumor growth in KP and KPL1 mice by BLI and micro-CT after the Lenti-SPC-Cre intratracheal instillation and showed that L1CAM was not required for the carcinoma initiation and development in mouse LUAD (Figure 3-10).

I sacrificed the KP and KPL1 mice at the 22-week time point and collected tumor-bearing lungs to perform histological analyses. KP and KPL1 tumors were both high-grade and invasive to the adjacent lung parenchyma and exhibited a combination of tubular and solid growth patterns (Figure 3-11). Both KP and KPL1 carcinoma cells showed round to polygonal morphology (Figure 3-11).

3.2.5 L1CAM+ KP LUAD Cells Have a Growth Advantage as Tumor Organoids

I isolated EGFP+ KP and KPL1 tumor cells from mouse lungs at the 22-week time point by FACS and generated KP and KPL1 tumoroids cultures (Figure 3-12a). After 7 days of culture, KP and KPL1 cells showed similar tumoroid growth capacities as determined by the number of tumoroids generated by KP and KPL1 single cells seeded *in vitro* (Figure 3-12b). However, when we sorted L1CAM-high and L1CAM-low cells from KP tumoroids by FACS and seeded them into Matrigel, we found that L1CAM-high cells had a 4.6-fold higher tumoroid formation capacity

than L1CAM-low cells (Figure 3-13). These data show that L1CAM-high cells exhibit superior tumoroid reinitiation capacity.

3.2.6 L1CAM Is Required for KP LUAD Metastasis

To investigate the role of L1CAM in metastatic colonization by LUAD tumoroids, I used a series of *in vivo* metastasis assays in athymic nude mice. I delivered FACS-sorted L1CAM-high and L1CAM-low KP tumoroid cells, and KPL1 tumoroid cells into athymic mice via tail vein to model lung colonization (Figure 3-14), intracardially model multi-organ metastasis (Figure 3-15), or intratracheally (Figure 3-16) to model spread through air spaces in LUAD (STAS)[254]. In all three metastasis assays, L1CAM-high KP tumoroid cells exhibited the highest colonization capacity while KPL1 tumoroid cells failed to colonize the lung and other organs in mice. L1CAM-low KP tumoroid cells were also able to colonize the lung after tail vein injection; however, they trend towards lower metastatic capacity compared to L1CAM-high KP tumoroid cells after intracardiac and intratracheal injections. Metastatic lesions formed by the inoculation of L1CAM-low KP tumoroid cells into the circulation showed abundant L1CAM+ cells. We previously showed that FACS-sorted L1CAM-low CRC organoid cells were able to re-express L1CAM *in vitro*[68]. The finding that L1CAM-low tumoroid cells re-expressed L1CAM *in vivo* and established L1CAM+ lung colonies after tail vein injection into mice suggests phenotypic plasticity in L1CAM-low cells (Figure 3-17), which further supports our previous findings that L1CAM expression is dynamically induced upon loss of epithelial integrity and during growth reinitiation.

To test the growth reinitiation capacity of KPL1 tumoroid cells *in vivo*, we repeated the tail vein injection of FACS-sorted KP L1CAM-high, KP L1CAM-low, and KPL1 tumoroid cells into athymic mice with 5-times higher number of cells per mouse (Figure 3-18) than the previous tail vein injection experiment (Figure 3-14). Similar to the lung colonization experiment in Figure 3-14, the growth reinitiation capacity of FACS-sorted L1CAM-high and L1CAM-low KP tumoroid cells were comparable (Figure 3-18). When injected at a high concentration, KPL1 tumoroid cells were also able to form small colonies in the mouse lungs (Figure 3-18). In addition to the smaller size, the KPL1 tumoroid-derived colonies were also histologically different from KP tumoroid-derived colonies. The KP tumoroid-derived colonies exhibited highly invasive, ECM-rich, and solid growth patterns accompanied by (under these rapidly growing conditions) hemorrhage in the mouse lungs. In contrast, the KPL1 tumoroid-derived lung colonies showed more tubular and differentiated morphology (Figure 3-18c), which is similar to the morphology of KP and KPL1 primary tumors (Figure 3-11). Taken together, these data showed that L1CAM is required both for growth reinitiation at distant sites and for the manifestation of heterogeneity and invasiveness in metastases of KP LUAD.

3.2.7 KP LUAD Metastases Exhibit a SOX2+ Early-Stage Progenitor-Like State

The striking growth reinitiation capacity of the L1CAM-high KP LUAD cells *in vitro* and *in vivo* led us to investigate the regenerative progenitor phenotype in LUAD

metastasis. Previously, our lab showed that LUAD patient metastatic samples are composed of more primitive and less-differentiated cell phenotypes defined by expression of the early-stage lung epithelial progenitor cell transcription factor SOX2 whereas primary tumors displayed cell phenotypes from many stages of lung epithelial development, including more differentiated states defined by the expression of later stage progenitor factors NKX2-1, FOXA2 and SOX9[103]. The transcription factor SOX2 is crucial both for branching and cell differentiation in lung epithelial development and for lung epithelial regeneration after injury, and was shown to be associated with the metastatic phenotype in LUAD by Laughney et al.[103]. To find whether the less differentiated morphology and high metastatic capacity of KP tumoroid cells are associated with a more primitive cell phenotype, I investigated the SOX2 expression in KP and KPL1 tumoroid-derived metastatic colonies. The lung colonies derived from KP and KPL1 tumoroids that exhibited significant differences in morphology and mesenchymal characteristics also demonstrated a dramatic difference in SOX2 expression (Figure 3-19a). The KP tumoroid-derived lung colonies were highly SOX2+ whereas the small colonies formed by KPL1 tumoroids lacked SOX2 expression (Figure 3-19b) and were enriched for the later-stage progenitor factor SOX9 (Figure 3-19c). These findings suggest that KP LUAD cells are capable of recapitulating early-stage progenitor factor SOX2+ cell states whereas KPL1 LUAD cells exhibited more differentiated cell states in metastasis. Therefore, I hypothesized that the emergence of early-stage progenitor factor SOX2+ cell states is associated with L1CAM expression in LUAD.

3.2.8 L1CAM Maintains the SOX2+ Progenitor-Like State in KP LUAD

Next, to determine the molecular mechanisms that establish and characterize the progenitor-like and metastatic phenotype in L1CAM+ LUAD cells, I, together with Dr. Park, performed single-cell RNA sequencing (scRNA-seq) of KP and KPL1 cells freshly isolated from lung tumors, and from tumoroids that were grown for 2 days or 7 days in culture (Day 0: 15044, Day 2: 2406, and Day 7: 15983 cells) (Figure 3-20a). All scRNA-seq data were merged, processed, and normalized to generate UMAP clusters corresponding to each time point. Clustering revealed that KP and KPL1 cells exhibited a transition of cell states during the 7-day culture (Figure 3-20b).

Next, we focused on finding differentially expressed transcriptional signatures between KP and KPL1 primary tumors and tumoroids. Intrigued by the differential expression of SOX2 in lung colonies derived from KP and KPL1 tumoroids (Figure 3-19), we investigated the expression of SOX2 and later-stage progenitor cell transcription factors NKX2-1, FOXA2, and SOX9 in the single-cell RNA-seq dataset to identify the association between more primitive cell states[103] and L1CAM expression.

Unsupervised clustering and heatmap analysis of mean gene expression revealed that multiple clusters expressed L1CAM at all time points (Figure 3-21). While L1CAM-high and L1CAM-low cells were assembled in multiple clusters and

exhibited mixed expression of epithelial progenitor markers, we noticed that the clusters with the highest L1CAM expression were always SOX2-high (Figures 3-21 and 3-22), In addition to SOX2, L1CAM-high cells also showed expression of the transcription factors NKX2-1, FOXA2, and SOX9 that specify the later stage progenitors of the lung epithelial development, and the expression of NKX2-1 and FOXA2 becomes more enriched in L1CAM+ clusters on days 2 and 7 (Figure 3-21). Moreover, we observed that the L1CAM+ SOX2+ cells were also enriched for the expression of the lung and LUAD stem cell marker PROM1 (CD133)[91] and the LUAD stem cell marker ALDH1A1[255] (Figure 3-22), which indicates that L1CAM+ SOX2+ LUAD cells exhibit a progenitor and stem-like phenotype.

I confirmed the association between L1CAM and SOX2 expression by showing that SOX2 expression cells are maintained and amplified in KP tumoroids but lost in KPL1 tumoroids by immunostaining for L1CAM and SOX2 (Figure 3-23). Moreover, when KP tumoroids were sorted into L1CAM-high and L1CAM-low populations by FACS, L1CAM-high KP tumoroid cells showed higher SOX2 expression than L1CAM-low KP tumoroid cells (Figure 3-24), which further confirms the strong association of L1CAM and SOX2 expression in KP LUAD.

In addition to the KP LUAD model, we also noted the association between L1CAM and SOX2 in the primary and metastatic tumor samples from LUAD patients. SOX2 expression was enriched in the fluid and solid metastatic samples (Figure 3-25a) and correlated with high L1CAM expression (Figure 3-25b & c). Collectively, these

data demonstrated that L1CAM+ cells exhibit a SOX2+ early-stage epithelial progenitor state in mouse and human LUAD primary tumors and metastases.

Next, to determine whether SOX2 expression is dependent on L1CAM in KP LUAD, I transduced KP tumoroids with lentiviruses that direct doxycycline-inducible expression of short-hairpin RNAs (shRNAs) targeting L1CAM. Upon doxycycline treatment, L1CAM knockdown in KP tumoroids decreased the SOX2 expression and promoted SOX9 expression (Figure 3-26). Additionally, when we overexpressed L1CAM in KP tumoroids, SOX2 expression was upregulated while SOX9 expression was downregulated (Figure 3-27).

These data showed that L1CAM is required for the maintenance and expansion of SOX2 expressing LUAD cells and suggested that the SOX2+ progenitor-like state maintained by L1CAM might be promoting the regenerative phenotype in LUAD metastasis. Upon loss of L1CAM, LUAD cells lose SOX2 expression and transition into a more differentiated SOX9+ phenotype.

3.2.9 The Chromatin Remodeler CHD1 Maintains the SOX2+ Progenitor-Like State in KP LUAD

How might L1CAM mediate SOX2 expression in LUAD cells? L1CAM has a short cytoplasmic tail that enables interaction with the cytoskeleton, but it is not a signal transduction molecule[84,117]. L1CAM interactions in *cis* and in *trans* with signaling molecules, such as integrins and FGFR, have often been found to trigger signal

transduction[31,116,244]; however, the role of L1CAM in signal transduction pathways is not well understood[225]. To find the mechanism of how L1CAM could regulate SOX2 expression, we investigated the transcriptional regulators that are specifically active in L1CAM+;SOX2+ LUAD cells based in our scRNA-seq dataset.

First, we identified the L1CAM+ SOX2+ clusters in all time points (Figure 3-21) and investigated the differentially expressed genes in these clusters. All three clusters showed high expression of lung developmental and regenerative stem cell markers p63[256,257], KRT5[256], KRT14[256], SLC16A3[256], PLSCR[256], RASSF9[256], LY6D[256], LY6A[258], ITGB4[258], and SOX21[259], in addition to the LUAD stem cell markers PROM1 (Cd133)[91] and ALDH1A1[255] (Figure 3-22), which further supports that L1CAM+ SOX2+ cells show a progenitor-like transcriptional profile in LUAD primary tumors and during tumoroid growth.

Next, to find the transcriptional regulatory programs associated with, and potentially responsible for SOX2 expression in these cells, we analyzed the differentially upregulated genes of the L1CAM+ SOX2+ clusters using ChEA (ChIP Enrichment Analysis)[260] and ENCODE (The Encyclopedia of DNA Elements)[261]. By integrating the results of both analyses, we were able to identify a strong enrichment for CHD1 and MYC transcriptional signatures in the L1CAM+ SOX2+ clusters (Figure 3-28).

MYC is a pleiotropic transcriptional regulator and a proto-oncogene[262] and shares many target genes with SOX2[263,264]. Therefore, the enrichment of MYC transcriptional signature observed in SOX2+ cells may reflect the functional overlap of these two transcription factors in early-stage progenitors, rather than a role of MYC in driving SOX2 expression. However, no such link is known in the case of CHD1. CHD1 (Chromodomain Helicase DNA Binding Protein 1), is a chromatin remodeler and a nucleosome assembly factor associated with active transcription[265-267]. CHD1 binding was detected in the *Sox2* loci and shown to promote self-renewal and pluripotency in embryonic stem cells[267]. A recent study in mesenchymal stromal cells also noted that CHD1 knockdown reduced both colony-formation capacity and expression of stem cell transcription factors, including SOX2, OCT4, and NANOG[268].

Using publicly available ChIP-seq datasets[269] for CHD1 and ReMap[270], I identified three putative CHD1 binding sites in the mouse *Sox2* locus[271] and in the distal enhancer that regulates *Sox2* expression in mouse embryonic stem cells[272] (Figure 3-29). Indeed, knocking down CHD1 using independent shRNAs sharply reduced SOX2 expression in KP tumoroids (Figure 3-30). Taken together, these data suggest that CHD1 is necessary for SOX2 expression in KP LUAD.

Although CHD1 is required for SOX2 expression in KP tumoroids, its expression is not restricted to the L1CAM+ SOX2+ clusters as shown by scRNA-seq (Figure 3-31). However, as the ChEA and ENCODE analyses showed that the

transcriptional activity of CHD1 is uniquely associated with SOX2 expression, I hypothesized that CHD1 additionally requires a second input that is specific to L1CAM+ SOX2+ cells and that the second input either activates or cooperates with CHD1 in regulating the SOX2 expression in KP LUAD cells.

3.2.10 L1CAM Maintains SOX2 Expression by Establishing Planar Cell Polarity Pathway in KP LUAD

Although we identified CHD1 transcriptional activity specifically in association with the L1CAM+;SOX2+ cells, the expression of CHD1 was not limited to this cluster (Figure 3-31). Chromatin remodeling in the Sox2 locus might be mediated by CHD1, but the L1CAM-SOX2 association raises the possibility that SOX2 expression additionally requires a second input that is specific to L1CAM+ cells. To test this possibility, I decided to investigate the biological processes and signaling pathways enriched in the L1CAM+ SOX2+ clusters identified in the scRNA-seq (Figure 3-21). I analyzed the differentially expressed genes of the clusters of interest using the Gene Ontology (GO) tool[273] and detected distinct biological processes at all three time points (Figure 3-32).

In KP primary tumors (Day 0), L1CAM+ SOX2+ KP LUAD cells showed significant enrichment in the GO terms of cilium assembly and movement, mitochondrial ATP synthesis, and G2/M transition in the cell cycle (Figure 3-32a). Interestingly, this cluster shows strong enrichment in cilium assembly signature due to the differential expression of FOXJ1, ARL13B, CEP19, TEKT1, TEKT2, NEK1, TUBA1A,

DYNC2H1 and other cilium-associated components. The L1CAM+ SOX2+ cluster of the Day 0 time point is also enriched for the expression of CDKN1A, RB1, and CHEK2, suggesting that the cell cycle is negatively regulated. In addition, the expression of aerobic electron transport chain genes points out that the mitochondrial electron transport chain might be active in these cells.

After 2 and 7 days of in vitro culture, L1CAM+ SOX2+ cells continued to present enrichment in the GO terms of cilium assembly and movement and G2/M transition in the cell cycle but also showed significant enrichment in additional GO terms including non-canonical Wnt/PCP pathway, regulation of establishment of planar polarity, homophilic cell adhesion via plasma membrane adhesion molecules, and hemidesmosome assembly, which suggested that L1CAM+ SOX2+ cells in growing tumoroids might have established and utilized cell-cell junctions to activate the Wnt/PCP pathway (Figure 3-32b & c). The cells express the hemidesmosome components ITGB4 and COL17A1, and homophilic cell adhesion genes CELSR2, BSG, NPTN, CDH13, NECTIN1, and EMB in addition to L1CAM. The ligands WNT4, WNT7, and WNT11, the receptors FZD3 and FZD6, and the Wnt/PCP signaling component DAAM1 were upregulated in the Day 2 and 7 clusters. When the Wnt/PCP pathway signaling is activated, the downstream effector JNK phosphorylates and promotes the nuclear translocation of the transcription factor Jun[274]. Interestingly, the Wnt/PCP pathway, JNK, and Jun have been previously shown to regulate SOX2 expression[200,275-280] and cell migration and metastasis[281,282] in many cancer model systems. Moreover, activation of the

Wnt/PCP pathway requires cell-cell adhesion molecules[168,283]. Therefore, we hypothesized that the Wnt/PCP pathway might regulate the SOX2 expression and SOX2+ cell state in KP LUAD cells in an L1CAM-dependent manner.

Firstly, we showed that the Wnt/PCP components and ciliary gene expression were enriched in the L1CAM+ SOX2+ clusters in the scRNA-seq dataset (Figure 3-33) suggesting that the FZD6-dependent Wnt/PCP pathway and primary cilia might be established in the L1CAM+ SOX2+ KP cells. Because we failed to detect FZD3 expression in the Day 2 dataset, we decided to focus only on FZD6. We confirmed the presence of primary cilia in L1CAM+ and SOX2+ cells by immunostaining for the ciliary small GTPase ADP-ribosylation factor-like 13B (ARL13B) (Figures 34 & 35), which would suggest that L1CAM facilitates cilium assembly and that these cells are equipped with primary cilia and able to activate cilia-dependent signaling pathways, such as Hedgehog or Notch pathways, upon stimulation. While SOX2 expression and cilia are tightly associated on day 2, ciliated SOX2+ cells become a minority as tumoroids develop (Figure 3-35). The decrease in ciliated SOX2+ cells in tumoroids could be attributed to the asymmetrical inheritance of primary cilia[284]. Primary cilia are disassembled during cell division but the mother centriole is endocytosed together with the ciliary membrane, which persists through the cell division and is inherited by one of the daughter cells, resulting in asymmetric inheritance of primary cilium in embryonic stem cells[284]. The daughter cell receiving the mother centriole reassembles the primary cilium and also retains stem cell phenotype[284,285]. Based on this, the early

progenitor character of ciliated and non-ciliated SOX2+ KP tumoroid cells requires further investigation.

To determine the association between L1CAM, SOX, and PCP, we first confirmed the nuclear localization of the effector transcription factor of PCP and FZD6, Jun, by immunostaining and showed that Jun colocalizes with the L1CAM+;SOX2 KP tumoroid cells (Figure 3-36). Next, I surveyed the Jun binding sites in the mouse Sox2 locus[271] and the distal enhancer that regulates Sox2 expression in mouse embryonic stem cells[272] the PROMO tool[286,287]. I found five Jun binding sites in the Sox Regulatory Regions (SRR1 and SRR2) and six in the Sox2 distal enhancer (Figure 3-37), which supports our hypothesis that Jun might regulate Sox2 transcription.

Then to find whether the Wnt/PCP pathway depends on L1CAM, we analyzed the FZD6 expression in KP tumoroids that stably express doxycycline-inducible shRNAs that target L1CAM. While L1CAM knockdown in KP LUAD tumoroids have not affected the FZD6 mRNA levels (Figure 3-38), it dramatically reduced the membrane expression of FZD6 protein (Figure 3-39), which shows that the establishment of the Wnt/PCP pathway is dependent on L1CAM expression in KP LUAD tumoroids. Furthermore, L1CAM knockdown using doxycycline-inducible shRNAs in KP tumoroids reduced the nuclear localization of the transcription factor Jun (Figure 3-40). These results demonstrated the role of L1CAM in establishing and promoting the activation of the Wnt/PCP pathway and Jun nuclear localization

in KP LUAD tumoroids. Taken together, the evidence suggests that the FZD6-directed Wnt/PCP pathway and Jun nuclear localization in KP LUAD cells depend on L1CAM-mediated cell-cell adhesion and might regulate SOX2 expression.

To determine the role of FZD6 signaling in SOX2 regulation, we transduced KP tumoroids using lentivirus directing the expression of doxycycline-inducible shRNAs targeting FZD6 and showed that knocking down FZD6 reduced SOX2 expression in KP tumoroids (Figure 3-41). Next, we treated the KP tumoroids with the JNK inhibitor (SP600125)[276] to inhibit the phosphorylation and nuclear translocation of Jun. Chemical inhibition of Jun activation reduced SOX2 transcription in KP tumoroids, which demonstrates that SOX2 expression is regulated by the transcription factor Jun (Figure 3-42). Taken together, these data demonstrate the key role of L1CAM in promoting the SOX2+ progenitor-like state by mediating the establishment of the Wnt/PCP pathway and Jun transcriptional activity.

3.3 Conclusions and Discussion

Our results show that L1CAM expression is essential for metastatic colonization and for the establishment of a progenitor-like state in LUAD metastasis. L1CAM expression emerges at the invasive front of primary tumors and is enriched during regrowth as LUAD tumoroids and metastases. L1CAM+ cells exhibit superior growth reinitiation capacity in tumoroid culture and metastatic colonization and represent an L1CAM-dependent SOX2+ progenitor-like state. In addition to its

expression at the cell-ECM interface, L1CAM is expressed at cell-cell junctions and facilitates the activation of the Wnt/PCP pathway and the nuclear localization of the transcription factor Jun. Jun drives transcription at the Sox2 locus, which is primed for transcription by the chromatin remodeler CHD1. As a result, L1CAM+ cells maintain the SOX2+ progenitor-like state and growth reinitiation capabilities in LUAD tumoroids and metastasis (Figure 3-43).

This work emphasizes both the important roles of phenotypic plasticity and progenitor-like state in metastasis initiation and the distinction between CSCs and MICs. The ability to exhibit phenotypic plasticity and to acquire stem and progenitor-like traits is essential for MICs to reinitiate growth at distant sites and distinguishes them from CSCs[68,81,239,288-290]. While CSCs originate from adult homeostatic stem cells carrying oncogenic mutations and drive tumorigenesis, both emerging evidence in the literature and our previous work on L1CAM in CRC show that metastases are not seeded by CSCs but by MICs, which are phenotypically distinct cancer cell populations and reminiscent of tissue regenerative stem cells[4,68,81,239]. Our findings in LUAD confirm that L1CAM+ MICs are not CSCs as they are dispensable for carcinoma initiation. On the other hand, our study provides further evidence to demonstrate that L1CAM+ progenitor-like state emerges upon loss of epithelial integrity and promotes growth reinitiation in LUAD tumoroid culture and metastasis by using a genetically tractable tumor model. The observation that L1CAM is necessary for the Wnt/PCP signaling, which regulates SOX2 expression in cooperation with the chromatin modifier CHD1,

indicates that LUAD MICs acquire metastatic characteristics through non-genetic modifications. On the contrary, these results suggest the ability of MICs to evolve under challenging conditions of the metastatic cascade and to acquire regenerative progenitor-like traits, which molecularly and phenotypically resemble the regenerative stem cells that emerge upon tissue injury and are employed in tissue repair in lung[256,257] and other tissues[4,59,78,240-242].

Our results reveal a surprising mechanism for L1CAM in metastatic colonization. Previously L1CAM has been shown to activate the mechanotransduction transcription factors YAP and MRTF by interacting with both integrins and vascular basement membrane during metastasis initiation[31] but whether L1CAM functions only via mechanotransduction signaling and whether L1CAM might be involved in distinct signaling events when expressed at cell-cell junctions were not clearly understood. The observation that L1CAM is necessary for the establishment of Wnt/PCP pathway to maintain the SOX2+ progenitor-like state defined the molecular foundations of the regenerative capacity of L1CAM+ MICs and also proposed a new role for L1CAM at cell-cell junctions. Cell adhesion molecules in homodimers such as Fmi in *D. melanogaster* and CELSR in mammals expressed at cell-cell junctions are essential for the formation of the Wnt/PCP complexes between adjacent cells[158]. Whether L1CAM engages in homophilic interactions to enable the Wnt/PCP pathway similar to Fmi and CELSR homodimers remains an important and open question and requires further investigation. Previous studies have reported that cell adhesion molecules that support Wnt/PCP function

physically interact with other Wnt/PCP components at the membrane[165,167,169,291-293]. Because we have not found any evidence of L1CAM interaction with the Wnt/PCP pathway proteins, we attribute the requirement for L1CAM in the Wnt/PCP pathway to the formation of L1CAM-dependent cell-cell junctions that crucially favor the assembly of PCP core protein complexes. A more detailed study of the membrane recruitment of the Wnt/PCP pathway proteins is needed to find the role of L1CAM in supporting this process.

In addition to L1CAM and the Wnt/PCP pathway, SOX2 expression is also dependent on the chromatin remodeler CHD1, which indicates that the SOX2+ progenitor-like state is maintained by multiple factors including signal transduction and chromatin regulation. CHD1 has been previously shown to influence SOX2 expression and self-renewal in stem cells[267,268], but the mechanism of how CHD1 is regulated is poorly understood. The observation that CHD1 expression was not unique to the L1CAM+ SOX2+ cells but its transcriptional activity was specifically detected in the L1CAM+ SOX2+ cells suggested the presence of an additional input that activated or cooperated with CHD1 in regulating SOX2 expression, which was identified as Jun. One possible mechanism for their cooperation may be the priming of the *Sox2* locus by CHD1 and the transcriptional activation by Jun. Whether the recruitment of Jun to the *Sox2* locus depends on CHD1 needs to be determined.

Intriguingly, L1CAM+ SOX2+ cells uniquely express the cilium assembly genes and exhibit primary cilia in tumoroids. The observations on primary cilia in KP LUAD tumoroids have highlighted interesting and unique characteristics of the SOX2+ progenitor-like state and raised further questions on the formation and role of primary cilia. Although many studies show that primary cilia positioning and assembly depend on the Wnt/PCP pathway[180], it is interesting to note that primary cilia can also act as a switch between the canonical Wnt and the Wnt/PCP pathways[193]. In addition, whether the primary cilia-associated signaling pathways, such as Hedgehog signaling, are active and contribute to SOX2 expression in KP LUAD is unknown. Therefore, the relation between cilia, L1CAM, Wnt/PCP pathway, and SOX2 expression in LUAD cells remains to be determined in future studies.

The main focus of this study has been on the L1CAM+ SOX2+ progenitor-like state; however, our results show that multiple clusters of KP LUAD cells express L1CAM and the later-stage progenitor cell markers (e.g., NKX2-1 and FOXA2) at varying levels. Whether L1CAM+ SOX2- LUAD cells also exhibit phenotypic plasticity and whether L1CAM has a different role in such cells are open and important questions.

In sum, this study investigated how the L1CAM-dependent regenerative phenotype emerges in LUAD metastasis and identified a novel mechanism for how L1CAM promotes the progenitor-like state during tumoroid growth and metastatic

colonization by facilitating the Wnt/PCP pathway and maintaining the expression of the early-stage progenitor transcription factor SOX2. The interesting finding that L1CAM mediates the establishment of the Wnt/PCP pathway emphasizes the need for more detailed studies on the role of L1CAM both in cell-cell interactions and in PCP component organization on the cell membrane. Additionally, further investigation on the formation and function of the primary cilia may give rise to important insights about its association with L1CAM+ SOX2+ cells and its potential role in LUAD progression. Altogether, our findings highlight the significance of phenotypic plasticity in metastatic cells necessary to reenact the developmental and regenerative progenitor cell states in metastasis. In this regard, further investigation into the emergence and mediators of such states would unveil the underlying mechanisms driving metastasis.

Chapter 4: Materials and Methods

4.1 Molecular and Cell Biology

4.1.1 Isolating Cells from Lung Adenocarcinoma

Cancer cells were isolated from 20-32-week-old lung adenocarcinoma tumors harvested from 28-42-week-old mice. Mice were euthanized and perfused with PBS. Tumor-bearing lungs were harvested in ice-cold PBS. Entire lungs were dissociated into single cells in 1 mg/ml Collagenase III (Worthington Biochemical), 1 mg/ml Dispase II (Sigma-Aldrich), and 100 µg/ml DNase I (EMD Millipore) in Dulbecco's Modified Eagle's Medium (DMEM) at 37^{o}C for 30 min after mechanical dissociation by using GentleMACS^{TM} C Tubes (Miltenyi Biotec) and GentleMACS Dissociator (Miltenyi Biotec). The cell suspension was filtered through 70 µm EASYstrainer (Greiner Bio-one) and spun at 300 *g* for 5 min at 4^{o}C. The supernatant was aspirated, and red blood cells were lysed using RBC Lysis Buffer (eBioscience). The cells were washed with PBS and spun at 300 *g for* 5 min at 4^{o}C. The supernatant was aspirated, and the cells were resuspended in Fluorescence-Activated Cell Sorting (FACS) buffer (0.001% FBS (vol/vol) in PBS) before straining through a 35 µm filter and prepared for FACS.

4.1.2. Fluorescence Activated Cell Sorting (FACS)

Single cells resuspended in FACS buffer were stained for 20 min with before washing twice with FACS buffer. Cells were spun at 300 *g* for 5 min at 4^{o}C after washing and resuspended in FACS buffer containing DAPI (final concentration 3 µM, Fisher Scientific) to distinguish dead cells. FACS was performed at the Flow

Cytometry Core Facility at Sloan Kettering Institute/MSKCC using a BD FACS Aria Sorter with the “single cell purity” mode. Cancer cells from mouse lungs were sorted as $DAPI^-/CD45^-/EGFP^+$ live cells using anti-CD45-PE (Invitrogen). L1CAM-high KP LUAD cells from single-cell dissociated tumoroids were sorted as $DAPI^-/CD45^-/EGFP^+/L1CAM^+$ live cells. L1CAM-low KP LUAD cells from single-cell dissociated tumoroids were sorted as $DAPI^-/CD45^-/EGFP^+/L1CAM^-$ live cells.

4.1.3 Mouse 3-Dimensional Tumoroid Culture

Primary tumoroid cultures were generated from 20-32-week-old lung adenocarcinoma tumors harvested from 28-42-week-old mice. Cancer cells sorted from tumor-bearing mouse lungs by FACS were mixed in 50% Matrigel (Corning) and 50% KP LUAD media and seeded in Matrigel-coated non-tissue culture-treated plates or glass-bottom plates. Tumoroids were cultured in KP LUAD media (Advanced DMEM/F-12 (Thermo Fisher Scientific) containing 2% FBS (vol/vol, Takara Bio), 2 mM GlutaMAX (Thermo Fisher Scientific), 10 mM HEPES, 100 U/ml Penicillin/Streptomycin (Thermo Fisher Scientific), 2 μg/ml Gentamicin (Gibco)) at 37°C. Fresh media were added every 1-2 days.

4.1.4 Human CRC Organoid Culture

Primary human CRC organoids established in previously described protocol were seeded in Matrigel in uncoated non-tissue culture-treated 6-well plates and cultured in HISC medium Advanced DMEM/F12 containing Wnt-3a (conditioned medium from L-Wnt3A cells (ATCC)), R-Spondin1 (conditioned medium from m-

RSpo-Fc cells (a kind gift of C. Kuo, Stanford University), 50 ng ml^{-1} EGF, 50 ng ml^{-1} Noggin (Peprotech), 10 nM gastrin (Sigma), 10 mM nicotinamide (Sigma), 500 nM A8301 (Sigma), 10 µM SB202190, 10 mM HEPES, 2 mM glutamine, 2 mM *N*-acetylcysteine, 1 µM PGE2 (Sigma), 1:100 N2 (Invitrogen), 1:50 B27 (without vitamin A) and 100 µg ml^{-1} Primocin (InvivoGen)) was added. Y27632 (10 µM; Sigma) was added for initial organoid generation and for 48 h after every passage.

4.1.5 Generating Lenti-SPC-Cre Virus

The Lenti-SPC-Cre plasmid was constructed by cloning the *SPC* promoter sequence received from Tuomas Tammela (Sloan Kettering Institute/MSKCC) into the pLL3.7 plasmid (Addgene #11795). Lenti-SPC-Cre virus particles were generated by using HEK293T cells transfected with 9 µg Lenti-SPC-Cre plasmid, 8 µg pSPAX2, 3 µg pMD2.G using Lipofectamine 3000 diluted in Opti-MEM media (Thermo Fisher Scientific) overnight. Then, HEK293T cells were cultured in DMEM containing 10% FBS (vol/vol), 2 mM L-Glutamine (Thermo Fisher Scientific), 100 U/ml Penicillin/Streptomycin (Thermo Fisher Scientific) for 48 hours. Lentivirus-containing media were collected by spinning at 300 *g* for 5 min at 4^{o}C and straining through 0.45 µm Millex-HV filter (EMD Millipore). Lentivirus particles were concentrated using Amicon Ultra-15 centrifugal filter unit (Sigma Aldrich) according to the manufacturer's instructions.

4.1.6 Immunostaining

Mouse tissues were fixed in 4% paraformaldehyde for 24 hours before paraffin embedding. Immunohistochemistry staining was performed on 5-µm sections with standardized automated protocols on a Ventana Discovery XT machine using anti-L1CAM (clone 14.10, Biolegend), anti-SOX2 (clone Btjce, Invitrogen), and anti-SOX9 (EMD Millipore). Ultra-High-Def Mouse on Mouse (MOM) blocking reagent (StatLab) was used for L1CAM staining on mouse tissues. Hematoxylin and eosin staining was performed by Histowiz, Inc (Brooklyn, NY, US).

Mouse tissue sections were deparaffinized using Histoclear (National Diagnostics) and serial ethanol washes. Antigen retrieval was performed in the Tris-based antigen unmasking solution (Vector Laboratories) for 20 min in a steamer basket. After washing with PBS, sections were blocked by 10% normal donkey serum diluted in PBS-T (0.1% Triton X-100 in PBS) for 1 hour. Sections were incubated with primary antibodies diluted in the blocking solution overnight at 4^{o}C. Following three washes with PBS-T, sections were incubated with secondary antibodies in dark at room temperature for 1 hour. After washing sections with PBS-T three times, nuclei were stained using 1:10,000 DAPI for 5 min, followed by two washes in PBS. Sections were air-dried and mounted using ProLong Diamond antifade mountant (Invitrogen). Images were taken using an Imager.Z1 with Apotome.2 optical sectioning module (Zeiss) or a TCS SP5 confocal microscope (Leica Microsystems). Captured images were processed and quantified using FIJI.

Mouse LUAD tumoroids were cultured in Matrigel-coated 8-well chambered slides. Medium was aspirated and tumoroids were fixed in 4% paraformaldehyde for 20 min at room temperature. After washing with PBS once, tumoroids were permeabilized in 0.01% Triton X-100 in PBS for 10 min at room temperature. After washing with PBS once, tumoroids were blocked using 10% normal donkey serum in PBS for 1 hour at room temperature. Tumoroids were incubated with primary antibodies diluted in the blocking solution for 2 hours at room temperature and washed with PBS three times for 10 min each on a shaker. Tumoroids were incubated with secondary antibodies diluted in the blocking solution for 1 hour in dark at room temperature and then washed with PBS three times for 10 min each on a shaker. Nuclei were stained using 1:10,000 DAPI for 5 min, followed by two washes in PBS. Sections were air-dried and mounted using ProLong Diamond antifade mountant (Invitrogen). Images were taken using an Imager.Z1 with Apotome.2 optical sectioning module (Zeiss) or a TCS SP5 confocal microscope (Leica Microsystems). Captured images were processed and quantified using FIJI.

4.1.7 Knockdown and Overexpression in Mouse Tumoroid Culture

Doxycycline-inducible L1CAM and FZD6 knockdown was generated by lentiviral shRNAs (Horizon Discovery). Single-cell suspensions of LUAD tumoroids were mixed with lentivirus, TransDux MAX lentivirus transduction reagent, and Enhancer according to the manufacturer's instructions. Transduction mix was spun in 48-well non-tissue culture-treated plates at 1,500 *g* at 32°C for 2 hours. After spinning, cells were collected in centrifuge tubes and spun at 1,500 *g* for 5 min.

The supernatant was removed, and the cell pellet was resuspended in 50% Matrigel and 50% KP LUAD media to be seeded for puromycin selection (4 μg/ml) after 2 days for 1 week.

4.1.8 RNA Isolation and Quantitative Real-Time PCR

Mouse tumoroid cultures were incubated in Cell Recovery Solution (Corning) for 30 min at 4°C. After centrifugation at 300 *g* at 4°C for 5 min, tumoroid pellets were processed for total RNA isolation using RNeasy Mini kit (Qiagen). Total RNA (200 ng) was used to generate cDNA using the Transcriptor First-Strand cDNA synthesis kit (Roche). qRT-PCR was performed with TaqMan gene expression assay probes, and expression levels were normalized to the expression of Gapdh using an ABI Viia7 Real-Time PCR System (Applied Biosystems).

4.1.9 Solid-Phase Binding Assay

Solid-phase L1CAM ligand binding assays used recombinant human L1CAM (human Fc tag, R&D Systems; His tag, Thermo Fisher Scientific), UltraPure BSA (Thermo Fisher Scientific), purified mouse laminin-111 (Sigma-Aldrich), purified mouse collagen IV (Cultrex, R&D Systems), purified human collagen V (Sigma-Aldrich), recombinant human tenascin C (R&D Systems) and recombinant human laminin-411, laminin-421, laminin-511 and laminin-521 (Biolamina). 96-well Maxisorp plates (Nunc) were coated overnight at 4 °C with 30 nM recombinant protein, washed with PBS and blocked with protein-free blocking buffer (TBS, Thermo Fisher Scientific) for 2 h at room temperature. Human L1CAM (Fc tag) in

PBS was added to the wells, and plates were incubated for 1 h at room temperature and washed three times with 0.1% Tween-20 in PBS (PBS-T). HRP-conjugated anti-human IgG (Thermo Fisher Scientific; 0.5 μg ml^{-1} in PBS) was added to wells for 1 h at room temperature, plates were washed three times in PBS-T and enzyme activity was measured with 1-Step Ultra TMB ELISA substrate (Thermo Fisher Scientific) on a Synergy H1 Plate Reader at 450 nm.

4.1.10 Cell Adhesion Assay

To assay the L1CAM dependency of organoid cell adhesion to the basement membrane, MSK121Li organoids were treated with doxycycline (200 ng ml^{-1}) or left untreated for 48 h, dissociated and incubated for 24 h at 37 °C as single cells. 96-well Maxisorp plates (Nunc) were coated overnight at 4 °C with 30 nM laminins (purified mouse laminin-111 and recombinant human laminin-411, laminin-421, laminin-511 and laminin-521) or mouse collagen IV. After washing with sterile PBS and blocking with 5% (wt/vol) BSA (Fisher Scientific; 1 h at room temperature), 100 μl of cell suspension (3×10^4 cells per ml) in ADF was added to the wells and cells were allowed to adhere for 1 h at 37 °C. Then, wells were washed three times with prewarmed ADF and adherent cells were quantified by CellTiter-Glo assay (Promega), with data normalized to the luminescence detected immediately after cell seeding to calculate the percentage of adherent cells.

4.1.11 Single-cell RNA Sequencing and Analysis

Tumor cells from KP and KPL1 mice were isolated and collected as described in the method. For the tumoroid samples, cells were seeded in Matrigel and cultured for 2 and 7 days. To collect cells from tumoroids, Matrigel was dissolved by suspending tumoroids in Cell Recovery Solution (Corning) for at least 30 min at 4°C. Tumoroids were subsequently dissociated with TrypLE for 10 min at 37°C, and single cells were sorted in 0.04% BSA in PBS by flow cytometry with DAPI as a viability marker. Single-cell RNA-seq was performed as previously described by Ganesh et al. (2020). Briefly, single-cell samples were loaded onto the 10x Genomics Chromium platform as performed by the Single Cell Analytics Innovation Lab (SAIL). scRNA-seq libraries were prepared based on the manufacturer's protocol for 3' end reading. Single cells in gel beads in emulsion were captured and single-stranded cDNA was amplified and quantified using a SimpliAmp Thermal Cycler (Thermo Fisher Scientific). The sequencing data were demultiplexed and generated a molecule count array from raw data.

The sequencing data from day 0, 2 and 7 were concatenated and analyzed using Scanpy packages. Cells with low-complexity libraries and high mitochondrial contents were filtered out according to the respective gene readouts per cell content. A resulting number of cells was 32,266 cells with a library size of 15,217 genes. Data were normalized by median library size followed by a log transformation before downstream analysis. The phenotype clustering was calculated by the Leiden algorithm, and the differential gene expression was

ranked by the Wilcoxon test. The first 30 principal components were used to construct a Markov transition matrix and the normalized count matrix was further imputed with the MAGIC algorithm. UMAPs and force-directed layouts were used to visualize the clustering structures of cells based on the samples. Ranked counts of genes per cluster were compared to highlight genes closely associated with L1CAM. Heatmaps showing the scaled expression of L1CAM and developmental transcription factors were generated based on the imputed count matrix.

4.2 Animal Experiments

4.2.1 Mouse Models

All animal experiments were conducted in accordance with protocols approved by the MSKCC Institutional Animal Care and Use Committee (IACUC) and the Research Animal Resource Center (RARC). The mouse strains *Kras*$^{LSL\text{-}G12D}$ (B6.129S4-Kras^{tm4Tyj}/J; stock 008179), *Trp53*$^{fl/fl}$ (B6.129P2-Trp53^{tm1Brn}/J; stock 008462), *Rosa26*$^{LSL\text{-}Cas9\text{-}EGFP}$ (B6J.129(B6N)-Gt(ROSA)26Sortm1(CAG-cas9*,-EGFP)Fezh/J; stock 026175)[294] were obtained from the Jackson Laboratory. *L1cam*$^{fl/fl}$ mice were a gift from Melitta Schachner (Rutgers University)[118]. Mice were inbred on a C57BL/6J background to generate the KP-Cas9 and KPL1-Cas9 mice. To induce tumor formation, 8- to 10-week-old mice were given 2.5 x 10^4 TU of Lenti-SPC-Cre diluted in MEM medium (Gibco) via intratracheal instillation. Tumor formation and development were monitored by monthly bioluminescence imaging (BLI) by retro-orbital injection of D-luciferin (150 mg kg^{-1}) and the IVIS Spectrum Xenogen instrument (Caliper Life Sciences). Data were analyzed using

Living Image software v.4.5. Tumor volume was determined by scanning mouse chest by micro-CT equipment Inveon^{TM} PET/CT (Siemens Medical Solutions, Knoxville, TN, US) under anesthesia maintained by approximately 1.5% isoflurane/O_2 for mouse hotel scans applied via nose cone. The micro-CT acquisition consisted of 360 projections and the X-ray tube setting was 70 kV.

4.2.2 Experimental Metastasis Assays

Female athymic nude mice (Envigo, 069) at 4 to 8 weeks of age are used for *in vivo* xenograft experiments. For tail vein injections, 2 x 10^4 or 1 x 10^5 cells were delivered in 200 µl of PBS. For intracardiac injections, 5 x 10^4 cells were delivered in 200 µl of PBS. For intratracheal injections, 3 x 10^4 cells were delivered in 100 µl of S-MEM medium (Gibco Cat: 11380037). Metastatic growth was monitored weekly by BLI by retro-orbital injection of D-luciferin (150 mg kg^{-1}) and the IVIS Spectrum Xenogen instrument (Caliper Life Sciences). Data were analyzed using Living Image software v.4.5. For metastasis experiments, animals were anesthetized with 3% isoflurane/O_2 and retro-orbitally injected with D-luciferin. Isolated lungs, brains, kidneys, and livers were analyzed using IVIS Spectrum Xenogen instrument and Living Image software v.4.5.

4.2.3 Mouse Colitis Injury Model

8- to 10-week-old C57BL/6J mice were given 3-3.5% (wt/vol) dextran sodium sulfate (DSS, Affymetrix) in the drinking water ad libitum for 9 days, followed by

water up to 19 days until euthanasia. Colon paraffin sections were prepared from mice euthanized at IACUC-approved humane endpoints or on day 28.

Table 4-1 Antibodies

Antibodies		
Reagent	**Source**	**Identifier**
Mouse Anti-Mouse L1CAM Monoclonal Antibody	Biolegend	Clone 14.10 ,Cat# 826701
Chicken Anti-GFP Polyclonal Antibody	Aves Labs	Cat# GFP-1020
Rat Anti-Mouse CD45 Monoclonal Antibody, FITC	Invitrogen	Clone 30-F11, Cat#11-0451-81
Rat Anti-Mouse L1CAM Monoclonal Antibody, APC	Miltenyi Biotec	Clone 555, Cat# 130-102-864
Rat Anti-Human/Mouse SOX2 Monoclonal Antibody	Invitrogen	Clone Btjce, Cat# 14-9811-82
Rabbit Anti-Mouse SOX9 Polyclonal Antibody	EMD Millipore	Cat# AB5535
Goat Anti-Mouse FZD6 Polyclonal Antibody	R&D Systems	Cat# AF1526
Rabbit Anti-Mouse Jun Monoclonal Antibody	Cell Signaling Technology	Clone 60A8, Cat# 9165S
Rabbit Anti-Mouse Phospho-Jun (Ser73) Monoclonal Antibody	Cell Signaling Technology	Clone D47G9, Cat# 3270S

Table 4-2 Resources and Reagents

Resources and Reagents		
Reagent	**Source**	**Identifier**
Collagenase III	Worthington Biochemical	CLS-3
Dispase II	Sigma-Aldrich	D4693-1G
DNase I	EMD Millipore	260913
Matrigel	Corning	356231
Advanced DMEM/F12	Gibco	12634-010
Penicillin/Streptomycin	Gibco	15140163
Gentamicin	Gibco	15710064
L-Glutamine	Gibco	25030081
FBS	Takara	631106
Glutamax	Fisher Scientific	35-050-061
TrypLE	Gibco	12563011
Cell Recovery Solution	Corning	354253
eBioscience RBC Lysis Buffer	Invitrogen	00-4300-54
DAPI	Fisher Scientific	D3571
Ultra-High-Def Mouse on Mouse Blocking Reagent	StatLabs	P1-MOM-10HRP
ProLong Diamond Antifade Mountant	Invitrogen	P36961
Histo-Clear	National Diagnostics	HS-200
16% Paraformaldehyde	Fisher Scientific	50-980-488
Tris-Based Antigen Unmasking Solution	Vector Laboratories	H-3301-250
TransDux MAX Lentivirus Transduction Reagent	System Biosciences	LV860A-1
RNeasy Mini kit	Qiagen	74106
Transcriptor First-Strand cDNA synthesis kit	Roche	04897030001
Recombinant Human L1CAM	R&D Systems	777-NC-100
UltraPure BSA	Thermo Fisher Scientific	AM2616
Purified Mouse Laminin-111	Sigma-Aldrich	L2020-1MG
Purified Mouse Collagen IV	R&D Systems	3410-010-01

Table 4-3 TaqMan Probes

Mouse TaqMan Probes		
Reagent	**Source**	**Identifier**
L1cam	Thermo Fisher Scientific	Cat# 4331182, Probe ID# Mm00493049_m1
Gapdh	Thermo Fisher Scientific	Cat# 4331182, Probe ID# Mm99999915_g2
Sox2	Thermo Fisher Scientific	Cat# 4331182, Probe ID# Mm03053810_s1
Sox9	Thermo Fisher Scientific	Cat# 4331182, Probe ID# Mm00448840_m1
Nkx2-1	Thermo Fisher Scientific	Cat# 4331182, Probe ID# Mm00447558_m1
Foxa2	Thermo Fisher Scientific	Cat# 4331182, Probe ID# Mm01976556_s1
Fzd3	Thermo Fisher Scientific	Cat# 4331182, Probe ID# Mm00445423_m1
Jun	Thermo Fisher Scientific	Cat# 4331182, Probe ID# Mm00495062_s1
Aldh1a1	Thermo Fisher Scientific	Cat# 4331182, Probe ID# Mm00657317_m1
Prom1	Thermo Fisher Scientific	Cat# 4331182, Probe ID# Mm01211402_m1
Chd1	Thermo Fisher Scientific	Cat# 4331182, Probe ID# Mm00514308_m1

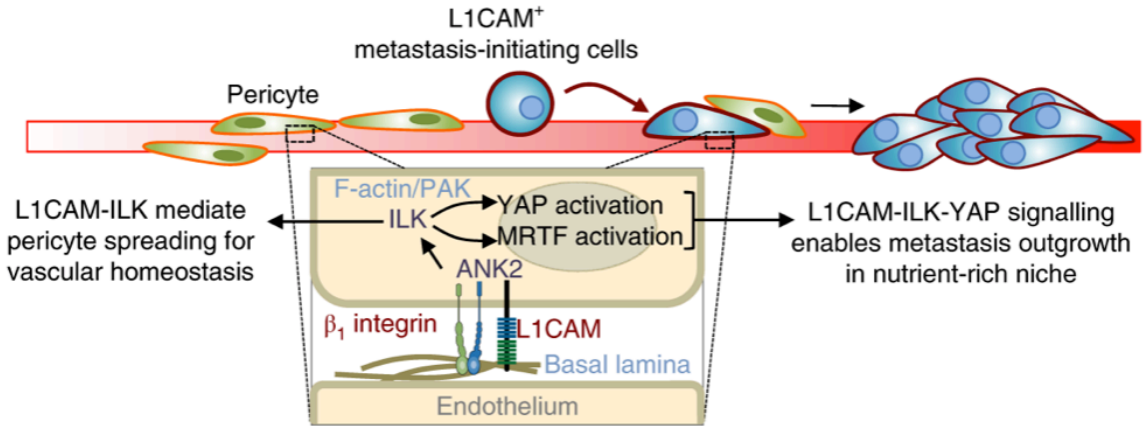

Figure 1-1. A model summarizing the molecular mechanism of L1CAM-dependent spreading of metastatic cancer cells and pericytes on blood vessels. As metastasis-initiating cells infiltrate secondary sites, they interact with the vascular basal lamina by L1CAM and β1 integrin. This engagement stimulates integrin-linked kinase (ILK) and p21-activating kinase (PAK) leading to the activation of YAP and MRTF mechanotransduction effectors. While L1CAM-ILK-dependent pericyte spreading is necessary for vascular homeostasis, metastatic cancer cells use L1CAM-ILK-YAP signaling to coopt blood vessels and initiate metastatic colonization. Adapted from Er et al. (2018). Pericyte-like spreading by disseminated cancer cells activates YAP and MRTF for metastatic colonization. Er, E.E. et al. (2018). Pericyte-like spreading by disseminated cancer cells activates YAP and MRTF for metastatic colonization. *Nature Cell Biology* 20, 966-978.

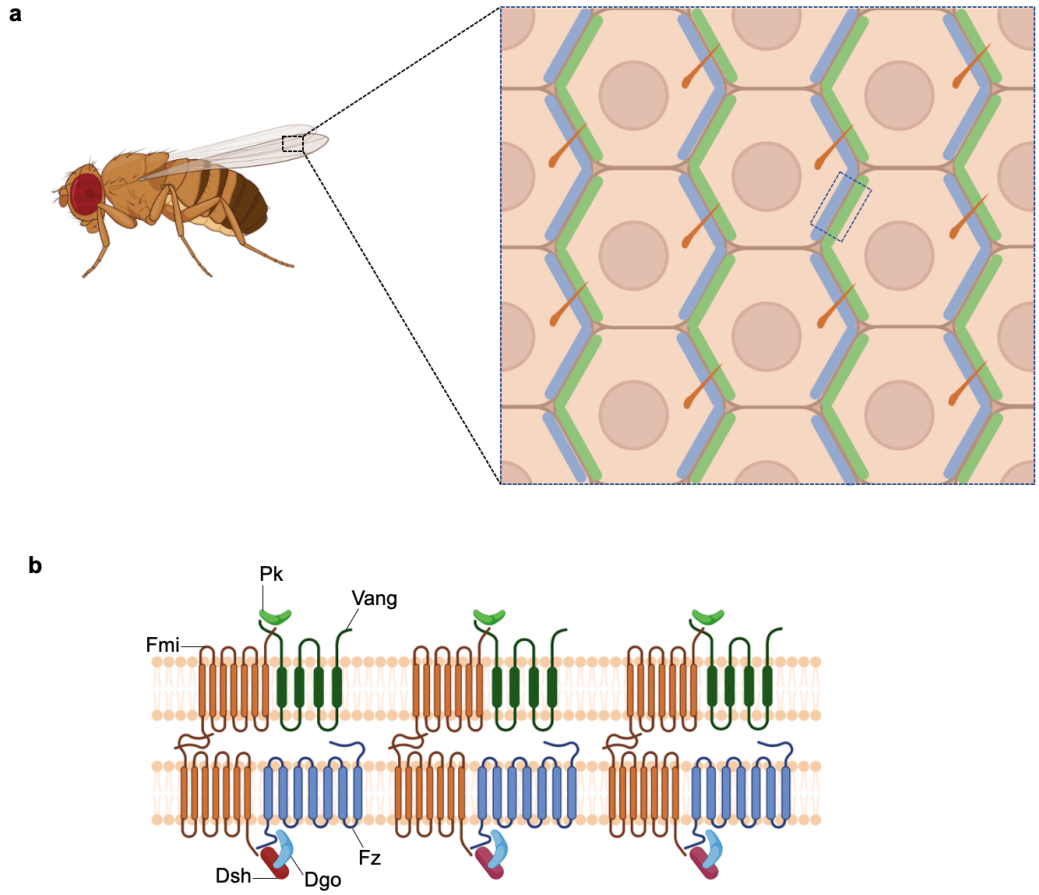

Figure 1-2. Planar cell polarity organization in the wings of *Drosophila melanogaster*. (a) Illustration of the boxed region in the *D. melanogaster* wing shows asymmetrical patterning in the wing epithelium, which determines the positioning and direction of single actin-based hairs. (b) Illustration of the organization of the PCP components at intercellular junctions. Asymmetrical accumulation of Fzd and Vang, and their physical interaction with Fmi homodimers establish junctional signaling and cell-cell communication on planar polarity. While the activity of Dsh and Dgo enables the asymmetrical distribution of Fzd and Vang within the cells, the activity of Pk enhances the formation of Fz-Vang signaling complexes between adjacent cells. Adapted from Butler, M.T. and Wallingford, J.B. (2017). Planar cell polarity in development and disease. *Nature Reviews Molecular Cell Biology 18*, 375-388.

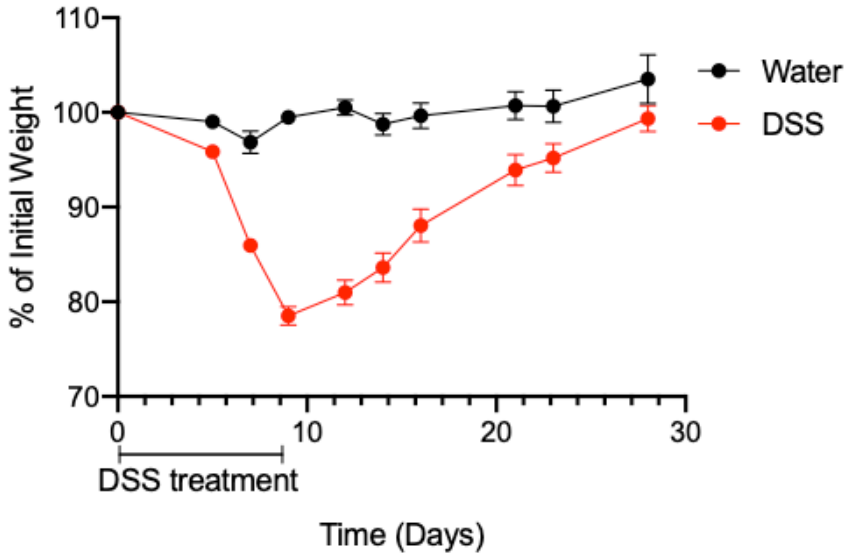

Figure 2-1. Change in the body weight of mice treated with dextran sodium sulfate (DSS) or water. C57BL/J mice were treated with 3-3.5% DSS in drinking water for 9 days, and then were provided with water without DSS for 19 days. N=24 for DSS and N=3 for water. Data by Yasemin Kaygusuz.

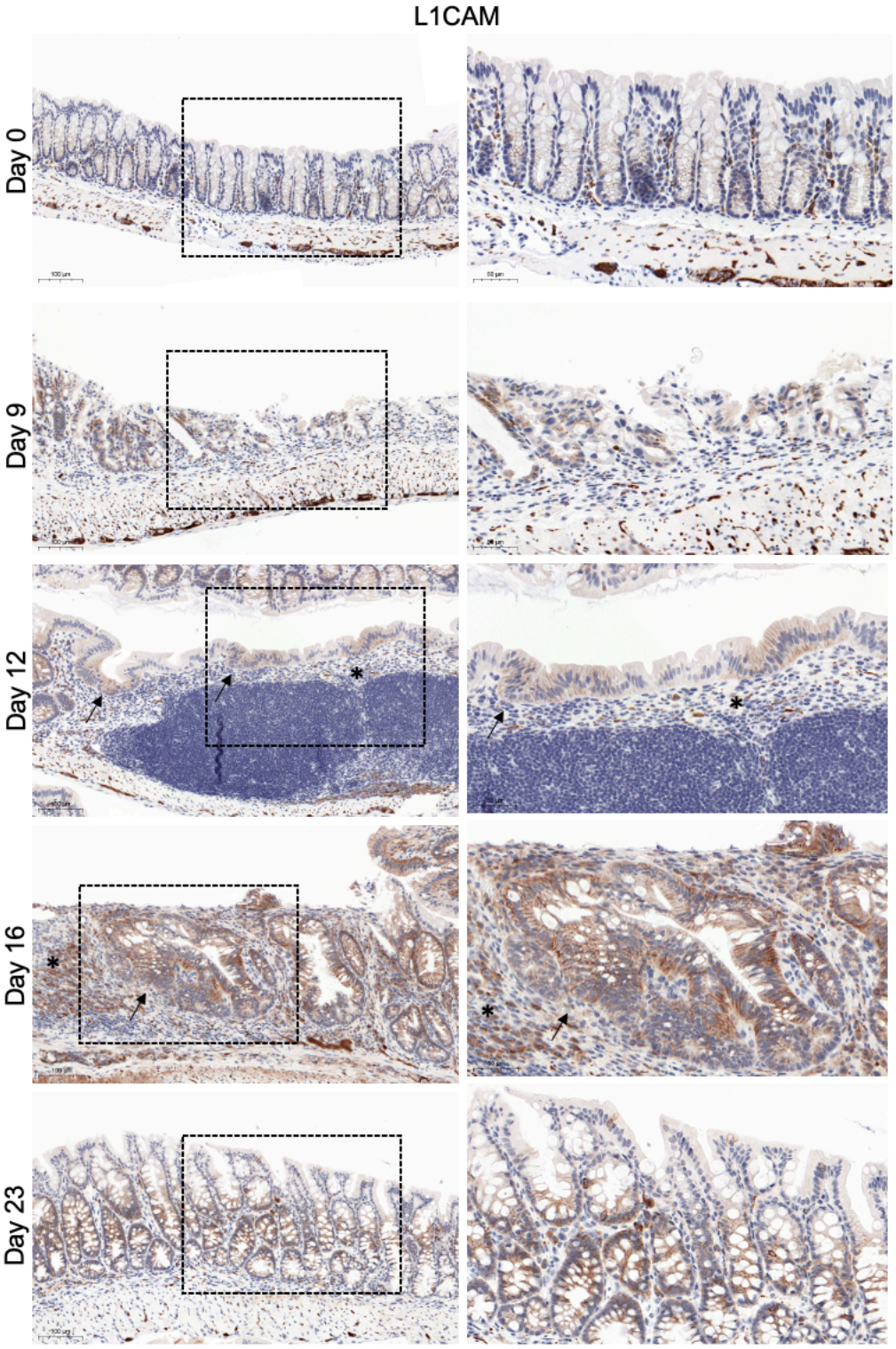

Figure 2-2. Representative images of L1CAM expression by IHC in the colon tissues of healthy mice (Day 0) and mice treated with DSS starting at Day 0 for 9 days and sacrificed at indicated time points. Asterisks show wound beds and arrows show wound-channel invaginations.

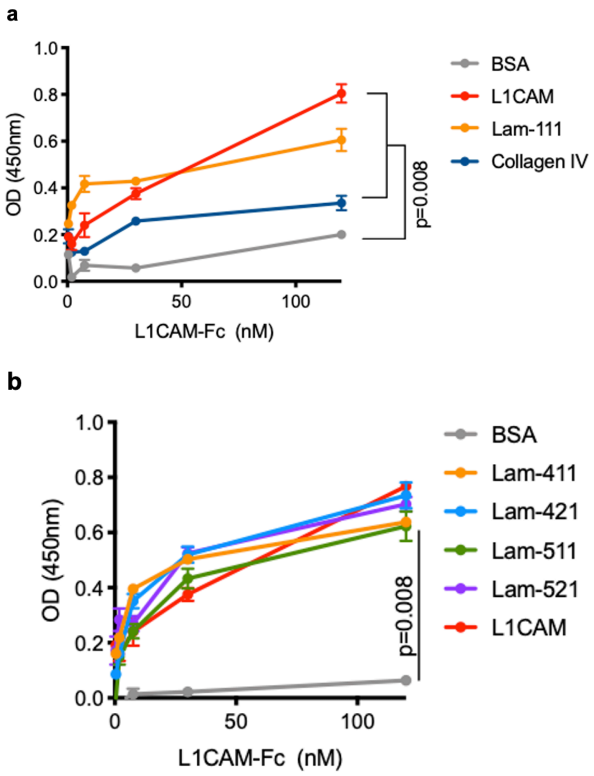

Figure 2-3. Solid-phase binding assay quantifying the dose-dependent binding of recombinant human L1CAM-Fc to plates pre-coated with **(a)** the components of Matrigel and L1CAM extracellular domain (L1CAM-ECD) and **(b)** the components of epithelial and vascular basement membrane and L1CAM-ECD at equimolar concentrations. After washing, horseradish-peroxidase (HRP)-conjugated anti-human IgG and HRP substrate were added to detect bound L1CAM-Fc by measuring optical density (OD) at 450 nm using a plate reader (mean ± s.e.m.). N=5 wells per each L1CAM-Fc concentration. Two-tailed Mann-Whitney *U* test. Data by Yasemin Kaygusuz.

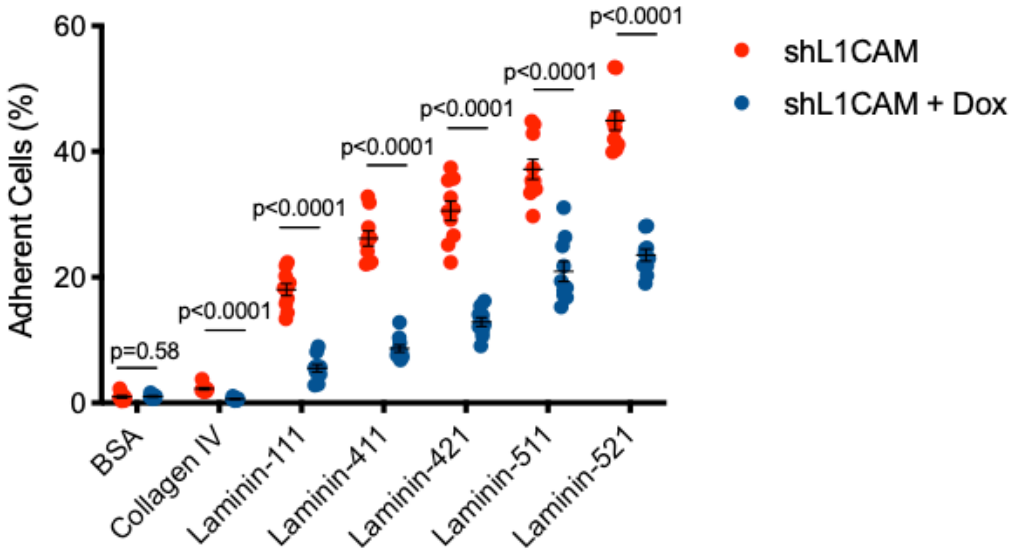

Figure 2-4. Change in the adhesion of CRC organoid-derived cells on laminin isoform-coated plates upon L1CAM knockdown by shRNAs was quantified by CellTiter-Glo. shL1CAM + Dox CRC organoids were treated with doxycycline 48 hours prior to assay to induce L1CAM knockdown. The percentage of adherent cells was calculated using the relative luminescence of each well after cell seeding and without washing. N=10 wells for each condition. Two-tailed Mann-Whitney *U* test. Data by Yasemin Kaygusuz.

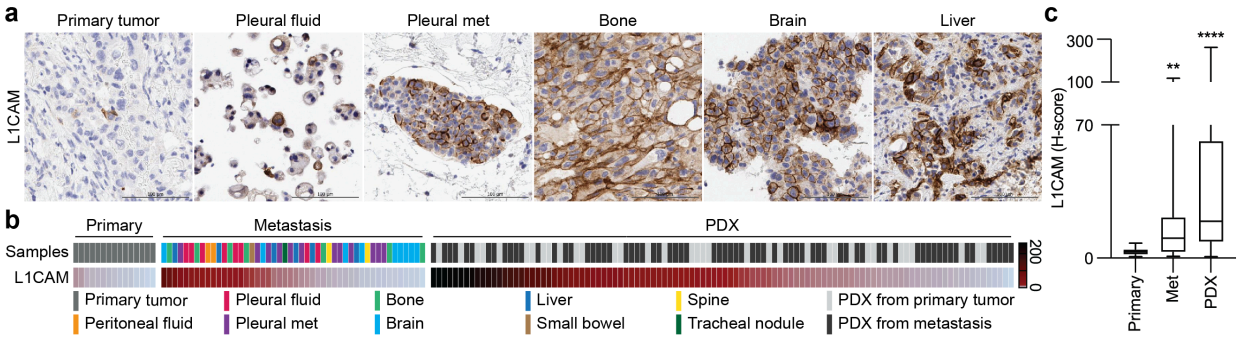

Figure 3-1: (a) Representative immunohistochemistry images of L1CAM from the primary tumor and metastasis samples of lung adenocarcinoma LUAD patients. Scale bar, 100 μm. (b) H-score of L1CAM expression in the samples from LUAD patients (primary tumor and metastasis) and patient-derived xenograft (PDX) tumors. Each column represents an independent patient. (c) Quantification of L1CAM expression in LUAD primary tumor, metastasis, and PDX tumor samples as determined. Statistical significance was assessed using two-tailed Mann-Whitney test. Data by Jin Suk Park.

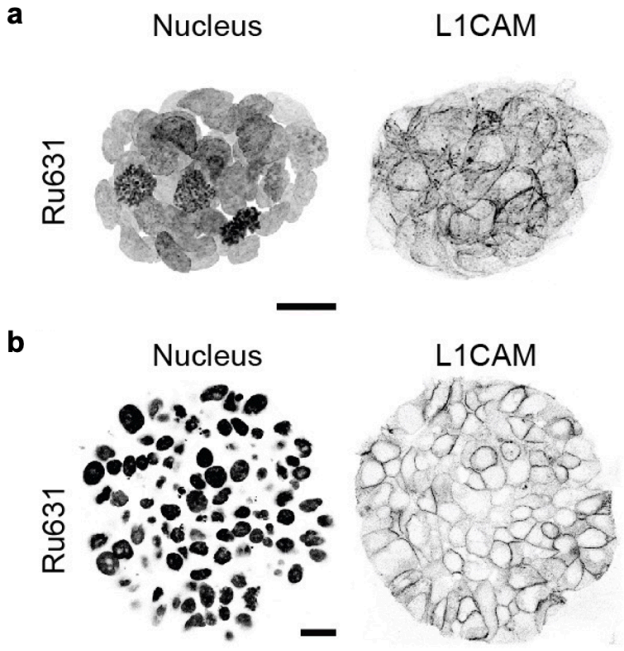

Figure 3-2: (a) A representative 3D projection and (b) a cross-section of Ru631 PDX organoid after 7 days followed by immunofluorescence staining of L1CAM and DAPI staining of nuclei. Data by Jin Suk Park.

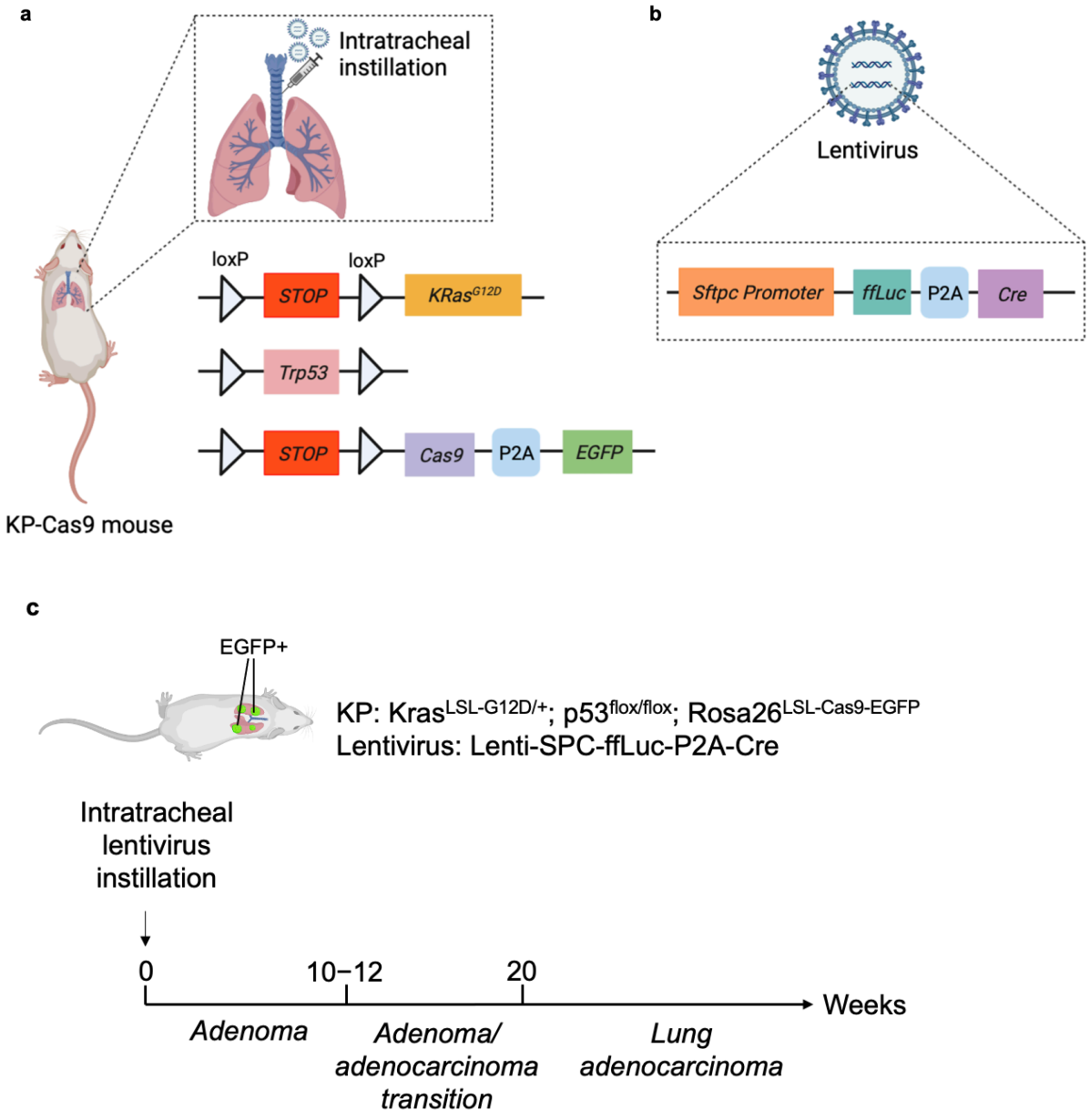

Figure 3-3. Experimental overview of the KP LUAD tumor model. (a) KP LUAD tumor formation is induced in the *Kras*$^{LSL\text{-}G12D/+}$; *Trp53*$^{flox/flox}$; *Rosa26*$^{LSL\text{-}Cas9\text{-}EGFP}$ (KP-Cas9) mice by the intratracheal instillation of the Lenti-SPC-Cre lentivirus. (b) The Lenti-SPC-Cre lentivirus directs the expression of firefly luciferase (ffLuc) and

Cre recombinase under the control of the Sftpc (SPC) promoter. (c) Timeline of KP LUAD development after the lentivirus delivery into mice. P2A encodes for the 2A self-cleaving peptide sequence. LSL: LoxP-STOP-LoxP.

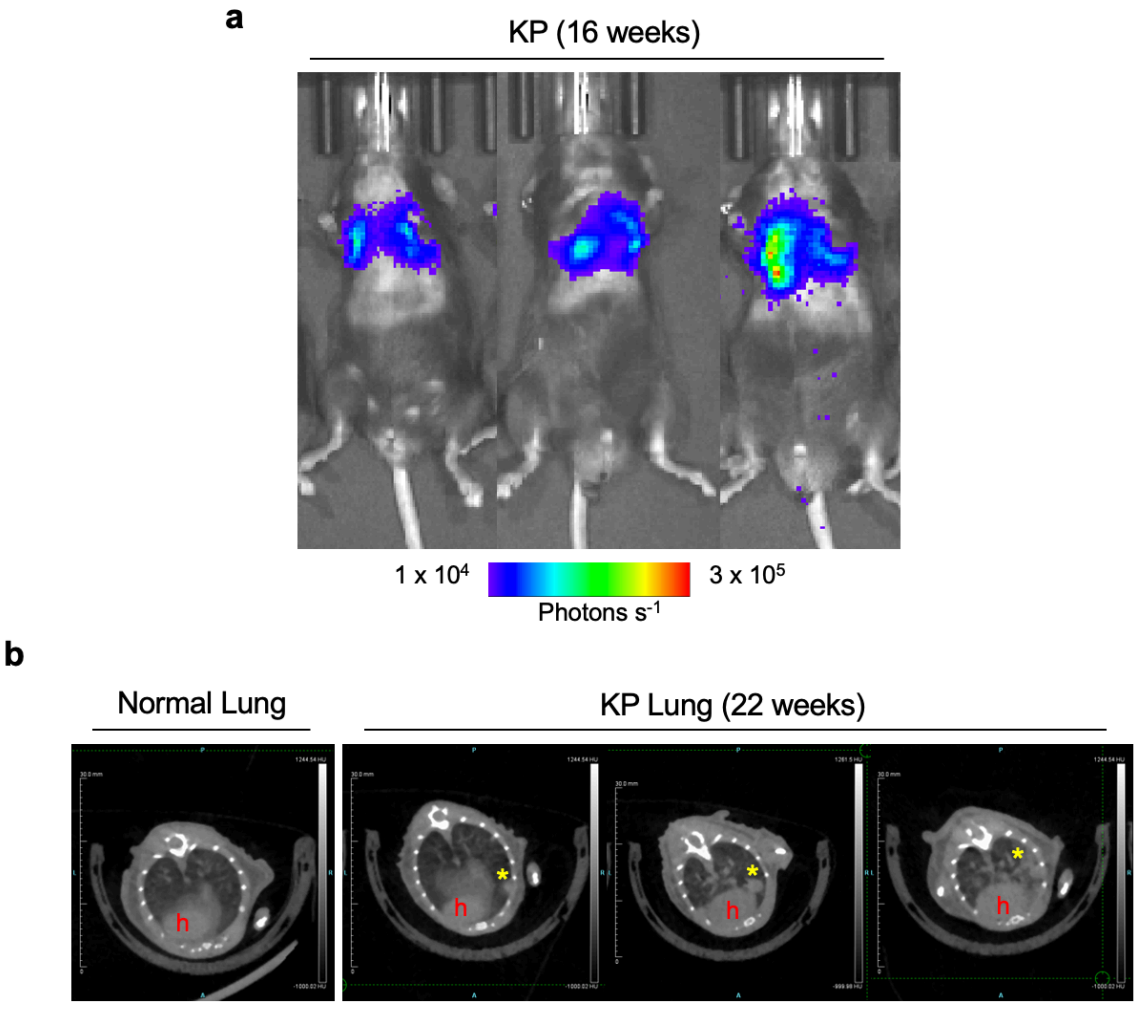

Figure 3-4. Representative (a) BLI and (b) microCT images of the KP mice injected with the Lenti-SPC-Cre virus 16 and 22 weeks after the injections, respectively (h: heart, *: lung tumors).

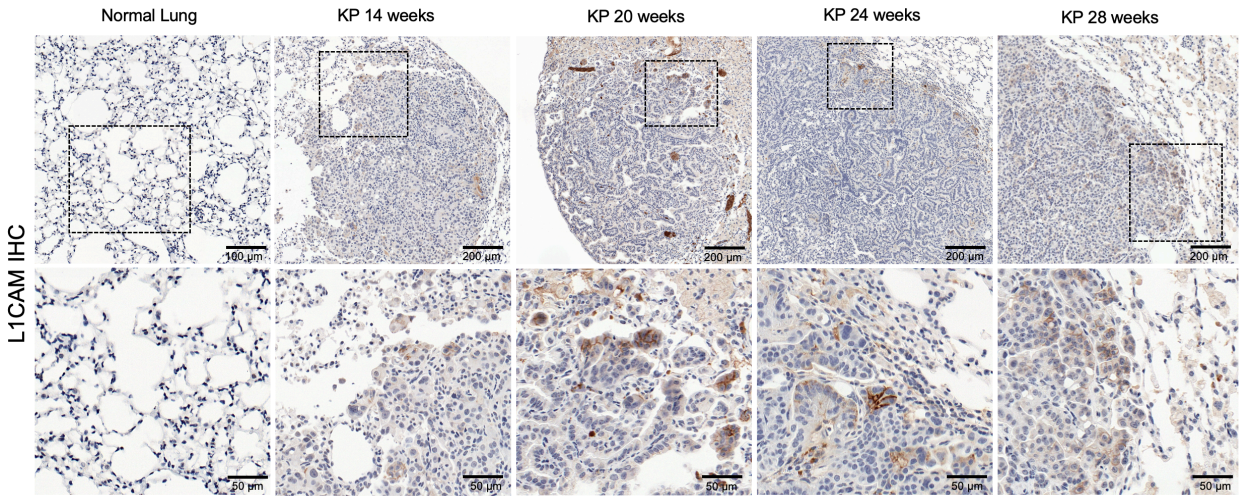

Figure 3-5. L1CAM expression in normal mouse lung and KP LUAD tumors from representative mice at indicated time points post-tumor induction by IHC.

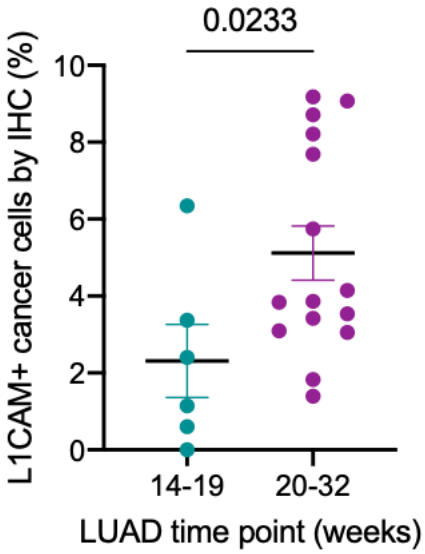

Figure 3-6. Quantification of L1CAM+ cancer cells in KP tumors harvested at indicated LUAD time points and stained for L1CAM by IHC (mean ± s.e.m.). Two-tailed Mann-Whitney *U* test. N=6 and 15, from left to right.

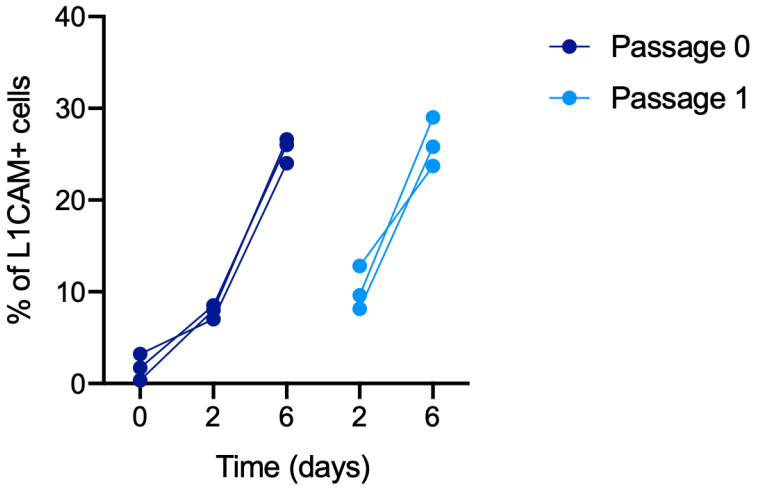

Figure 3-7. Percentage of L1CAM+ cells in KP LUAD tumoroids cultured for 2 and 7 days from two consecutive passages by flow cytometry (N=4 for each time point).

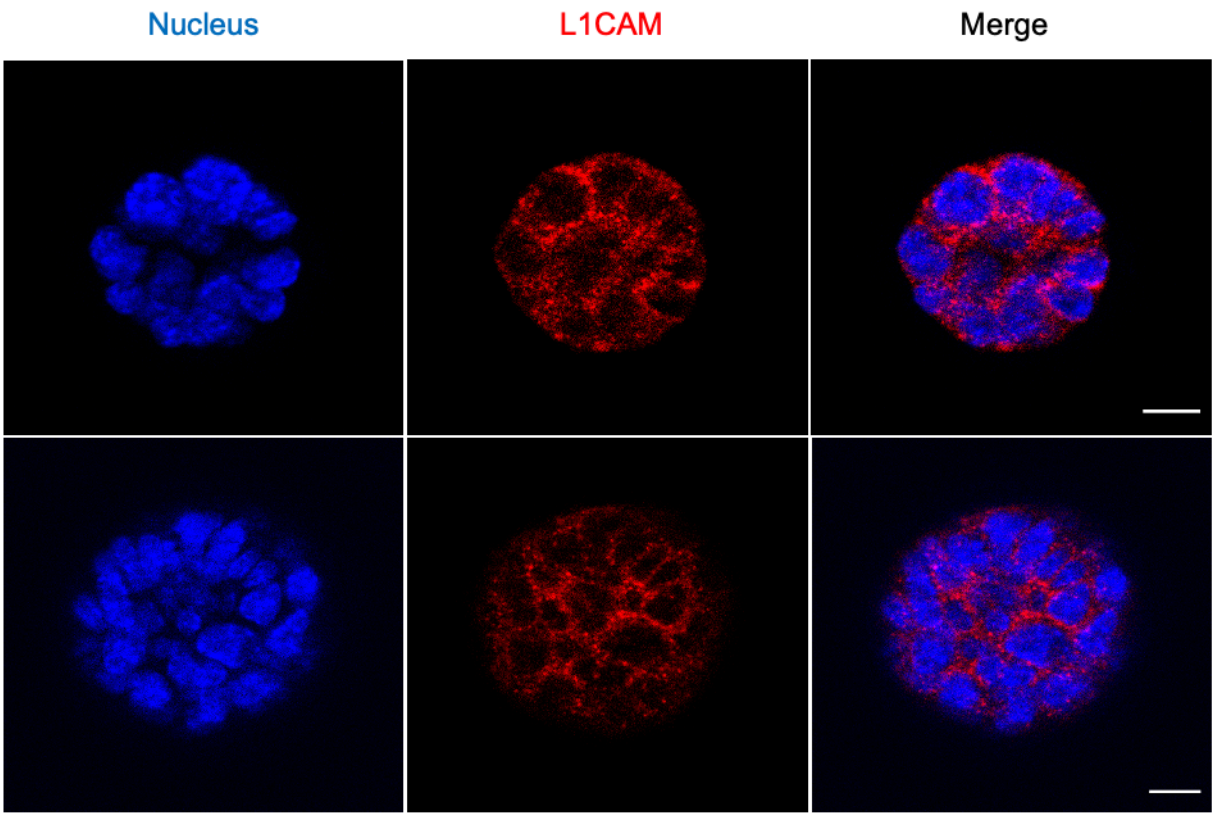

Figure 3-8. Representative KP LUAD tumoroid images of L1CAM immunofluorescence staining (scale bar: 10 μm).

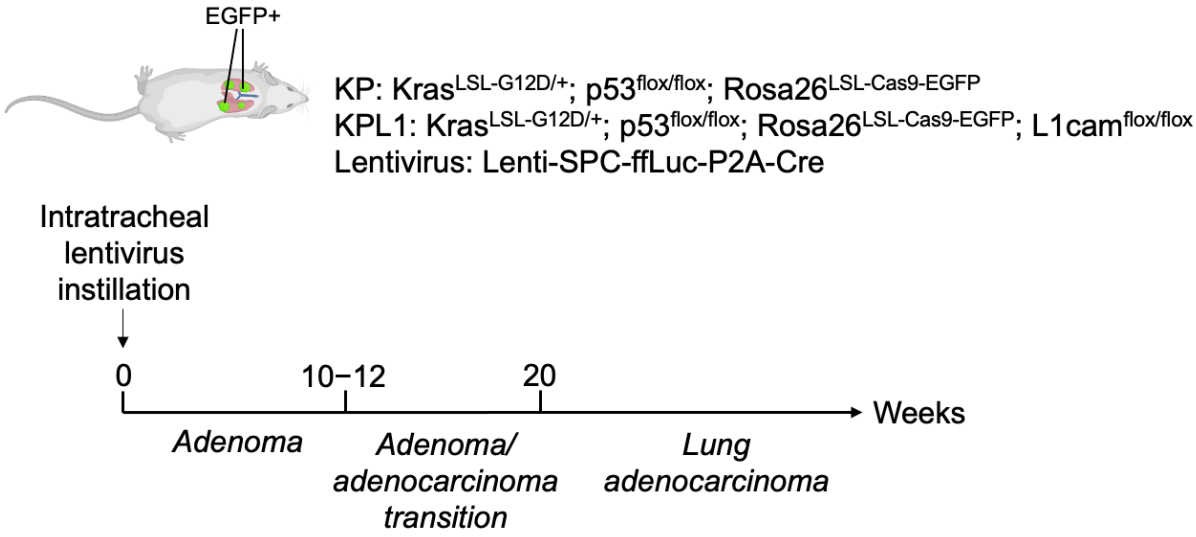

Figure 3-9: Experimental overview of the LUAD tumor induction and development in KP and KPL1 mice.

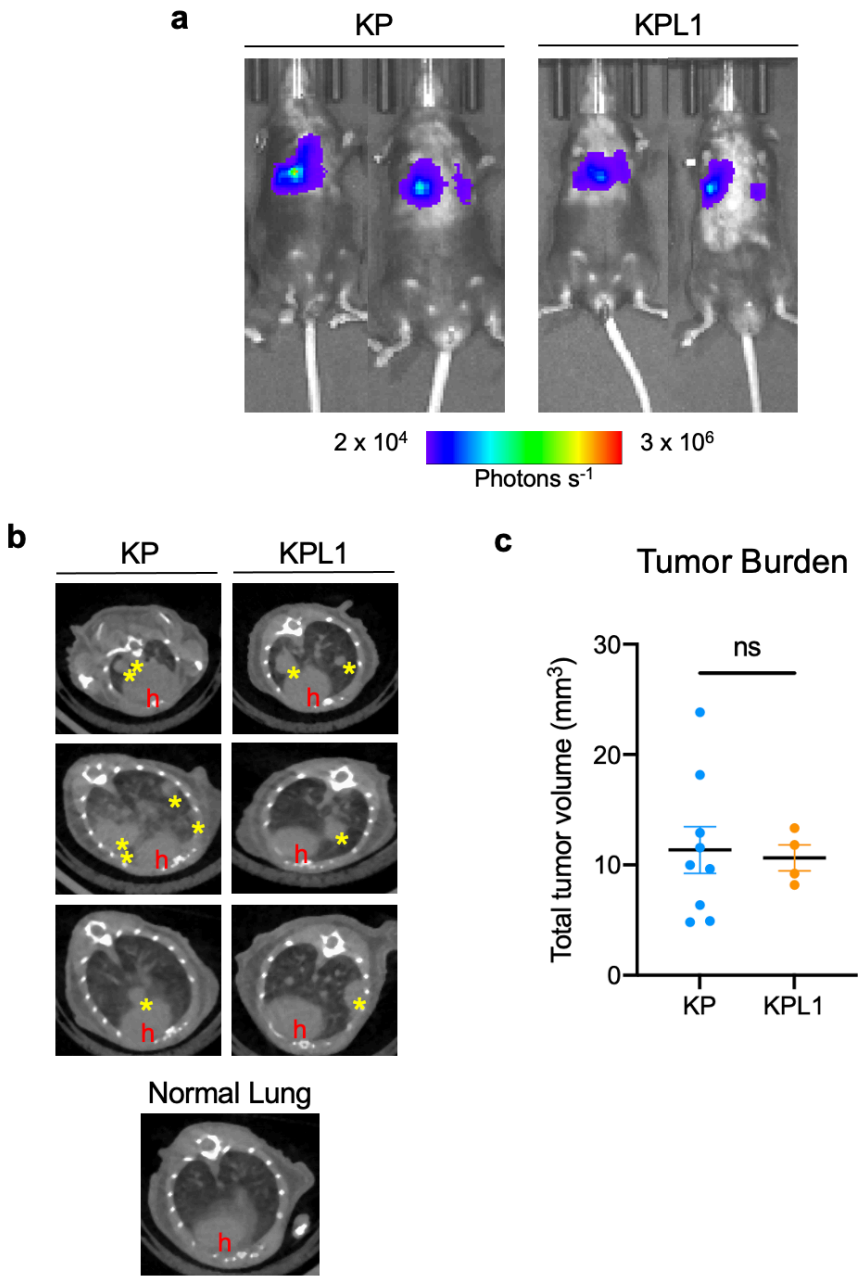

Figure 3-10: Representative (a) BLI and (b) microCT images of the KP and KPL1 mice injected with the Lenti-SPC-Cre virus 16 and 22 weeks after the injections, respectively (h: heart, *: lung tumors). (c) Quantification of total tumor volume in KP and KPL1 mice at the 22-week time point (mean ± s.e.m.). Two-tailed Mann-Whitney *U* test (N=9 and 4 mice, respectively).

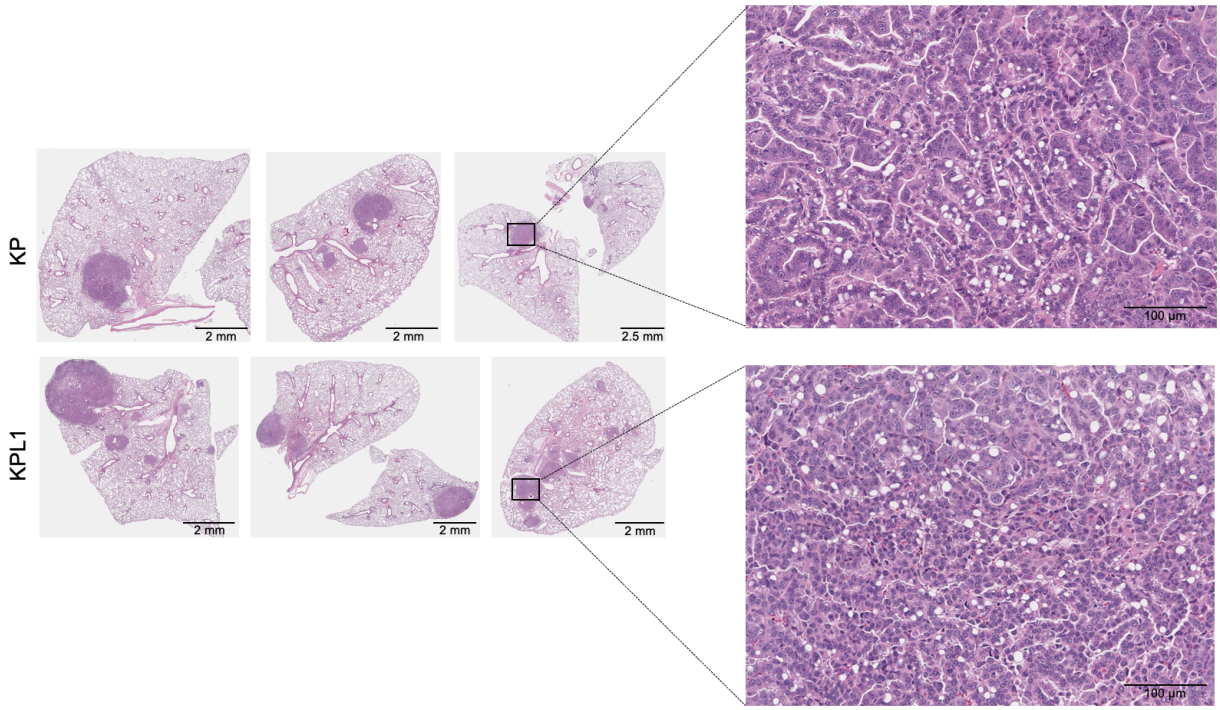

Figure 3-11: Representative H&E images of KP and KPL1 LUAD tumors at the 22-week time point.

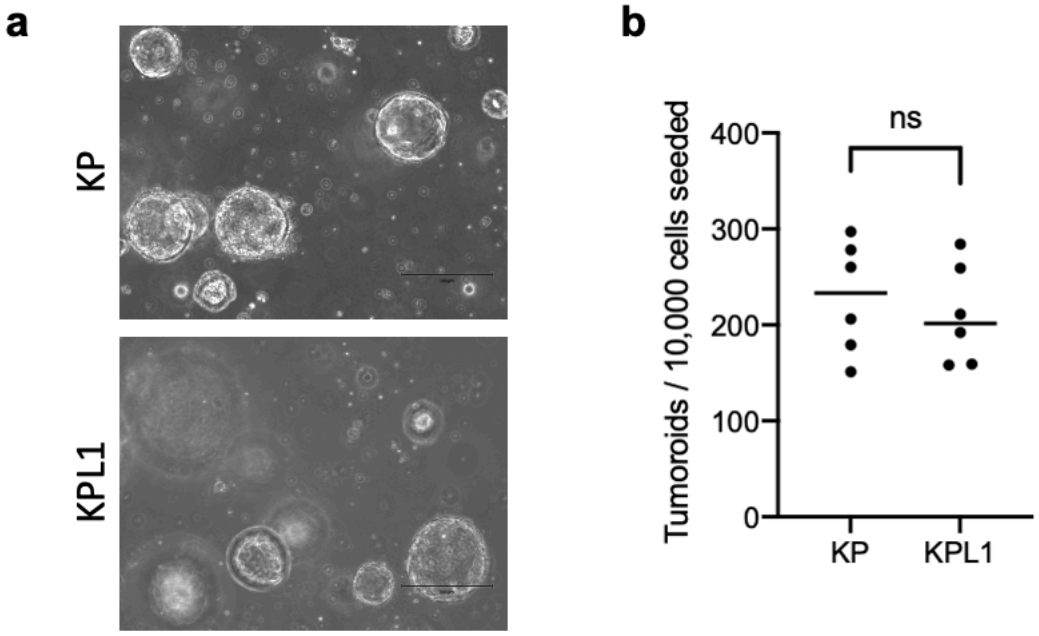

Figure 3-12: (a) Representative brightfield images of tumoroids grown from KP and KPL1 tumor cells isolated from mouse LUAD tumors. (b) The number of tumoroids established from KP and KPL1 cells per 10,000 cells plated 7 days after plating. Two-tailed Mann-Whitney *U* test. N=6 for each group.

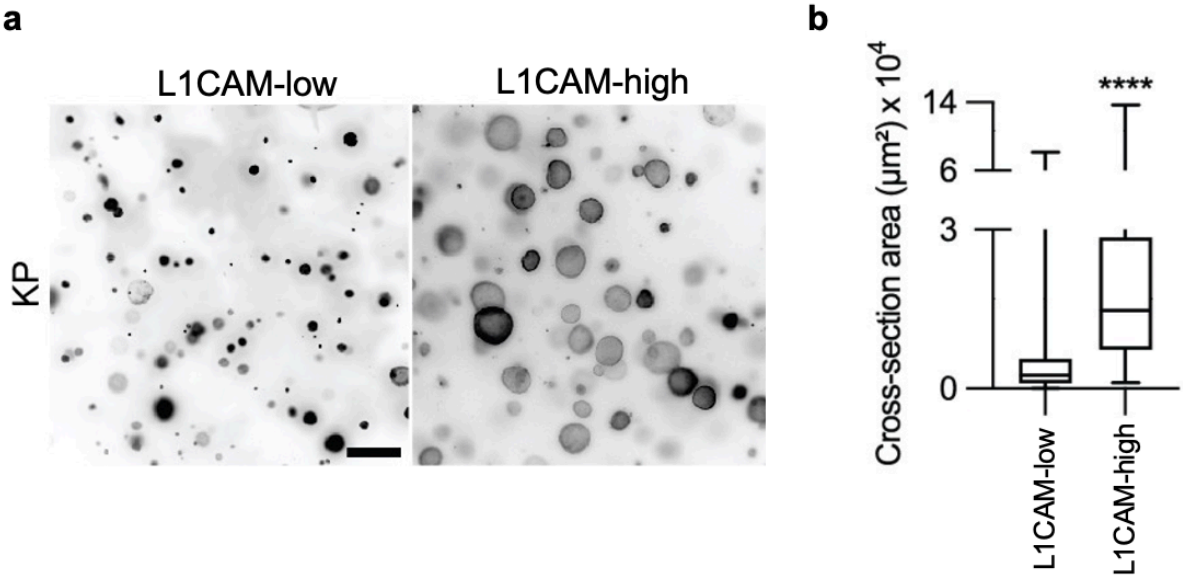

Figure 3-13: (a) Differentiated spheroid growth between L1CAM-low and L1CAM-high KP cells. Cells were sorted based on their L1CAM expression and cultured in Matrigel for 7 days. Fluorescent images of viable tumoroids were taken after staining them with calcein-AM. (b) The cross-section area of tumoroids derived form L1CAM-low and L1CAM-high cells was quantified. Statistical significance was assessed using two-tailed Mann-Whitney test. N = 807 tumoroids for L1CAM-low, 477 tumoroids for L1CAM-high. Data by JSP.

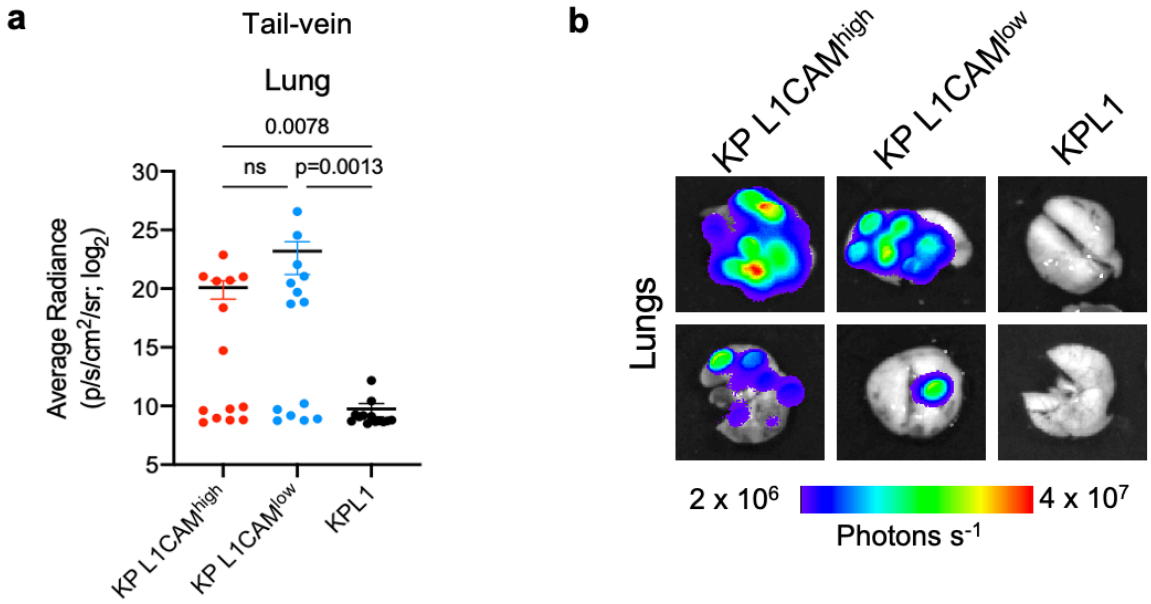

Figure 3-14: (a) Quantification and (b) representative images of lung ex vivo luminescence signal of athymic mice 5 weeks after tail-vein injection of KP L1CAM^{high}, KP L1CAM^{low}, and KPL1 tumoroid cells (20,000 cells per mouse). Two-tailed Mann-Whitney *U* test. N=14 for each group (mean ± s.e.m.).

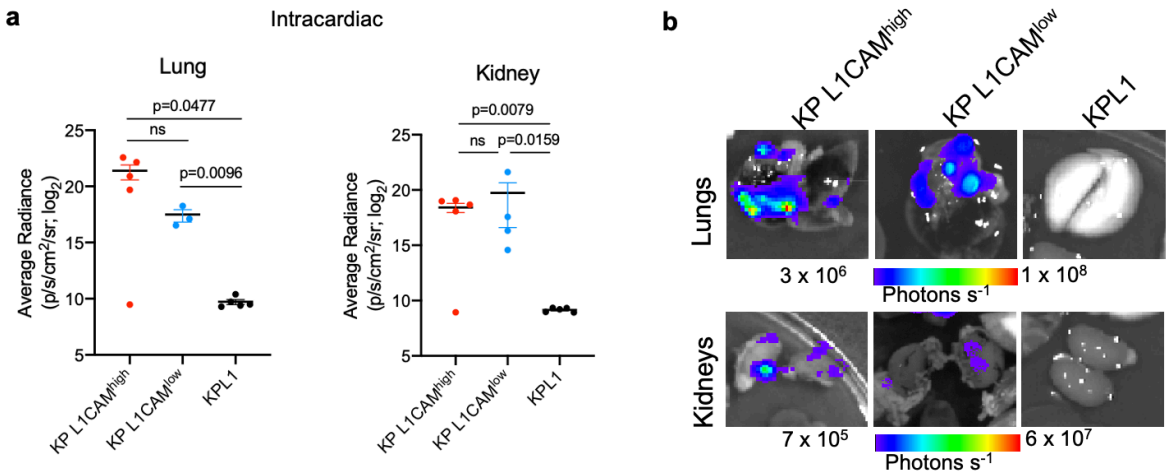

Figure 3-15: (a) Quantification and (b) representative images of lung and kidney ex vivo luminescence signal of athymic mice 3 weeks after intracardiac injection of KP L1CAM^{high}, KP L1CAM^{low}, and KPL1 tumoroid cells (50,000 cells per mouse). Two-tailed Mann-Whitney *U* test. N=5, 4, and 5 from left to right (mean ± s.e.m.).

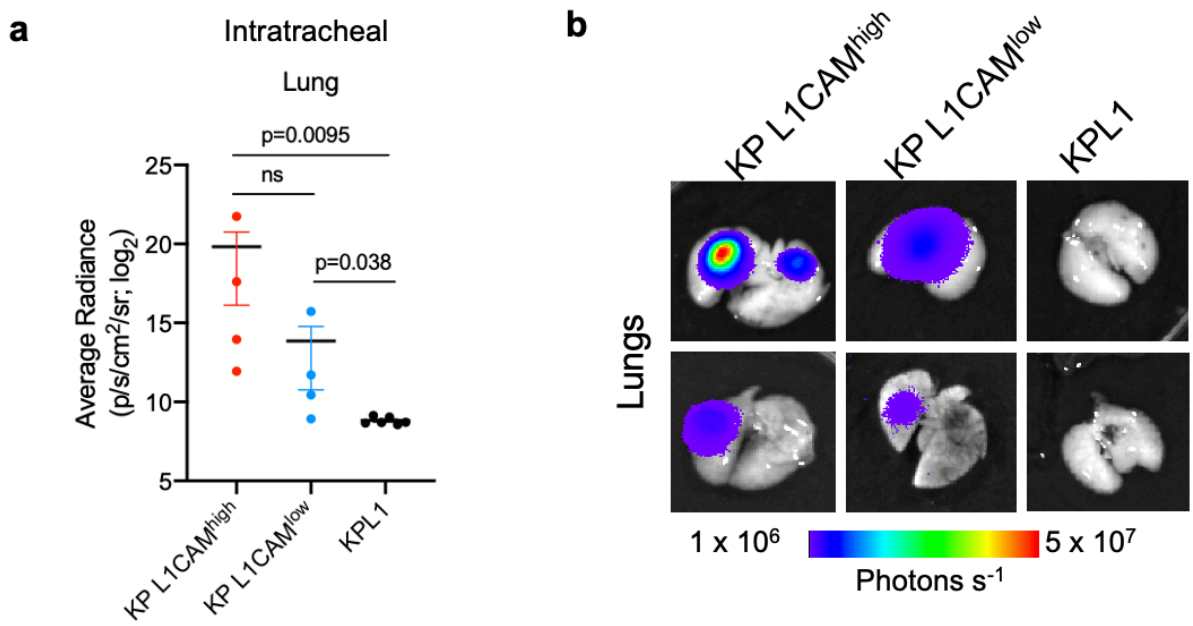

Figure 3-16: (a) Quantification and (b) representative images of lung and kidney ex vivo luminescence signal of athymic mice 5 weeks after intratracheal injection of KP L1CAM^{high}, KP L1CAM^{low}, and KPL1 tumoroid cells (20,000 cells per mouse). Two-tailed Mann-Whitney *U* test. N=4, 4, and 6 from left to right (mean ± s.e.m.).

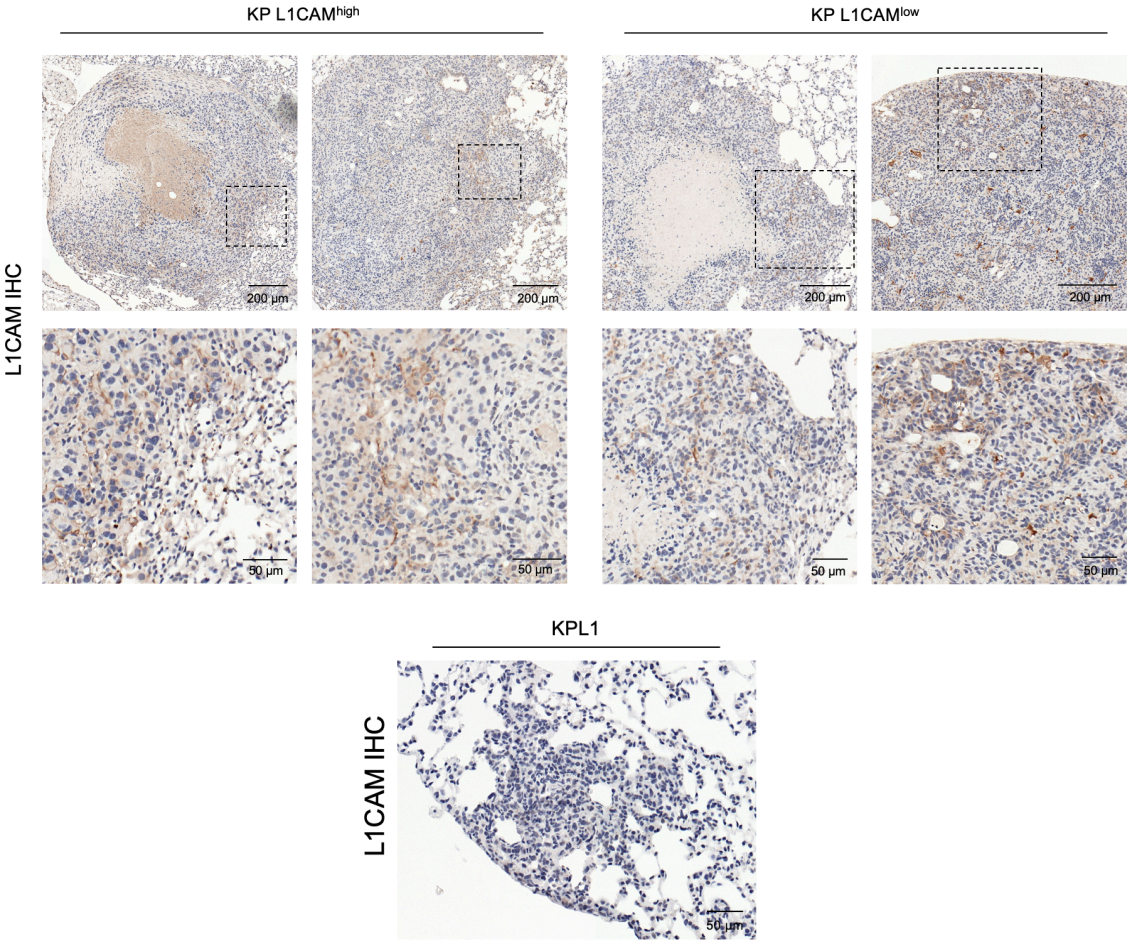

Figure 3-17: Representative images of L1CAM expression by IHC in lung colonies derived from KP L1CAM^{high}, KP L1CAM^{low}, and KPL1 tumoroids by tail-vein injection into athymic mice.

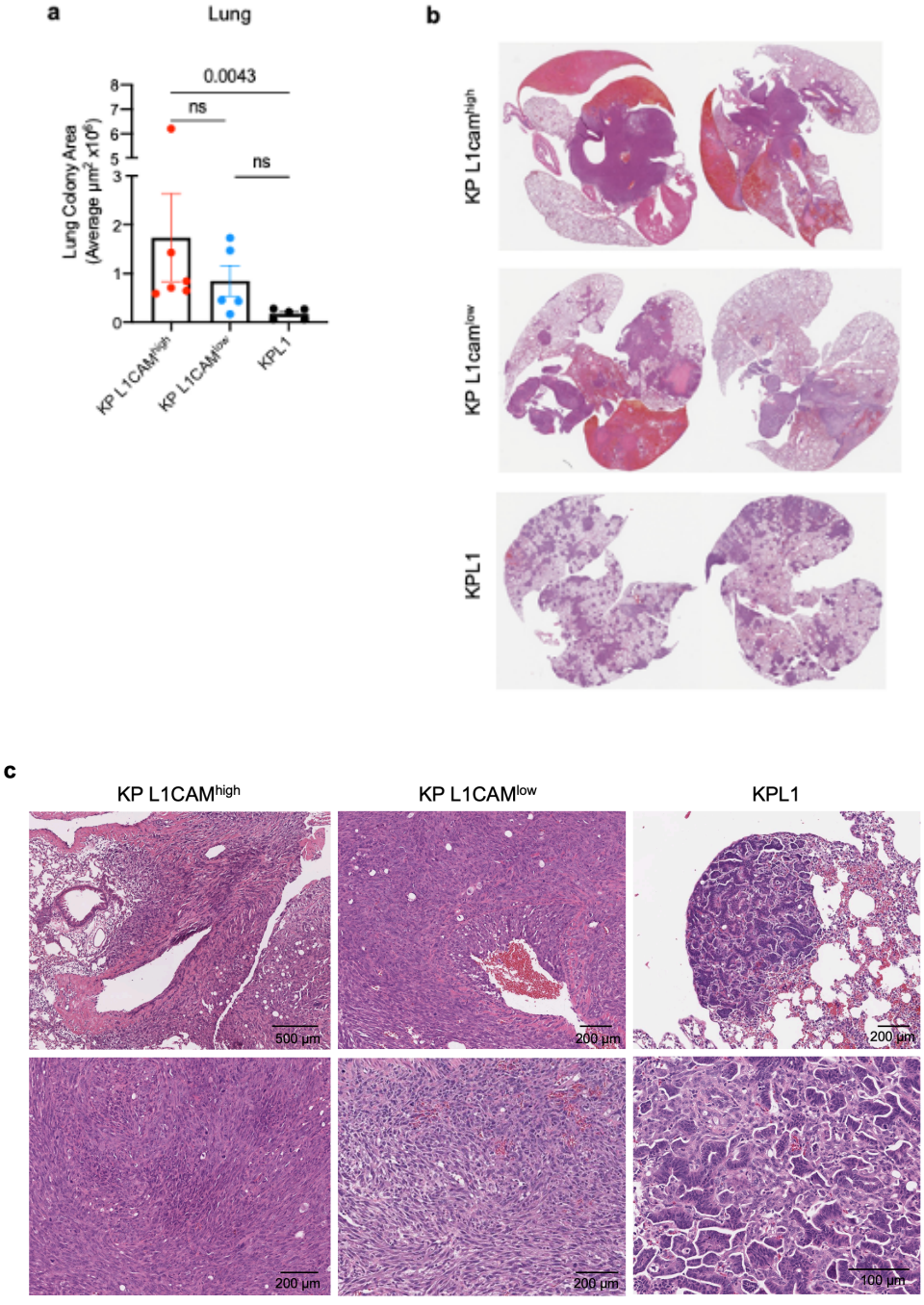

Figure 3-18: (a) Quantification of areas and (b & c) representative H&E images of lung colonies derived from KP L1CAM^{high}, KP L1CAM^{low}, and KPL1 tumoroids by tail-vein injection into athymic mice (100,000 cells per mouse). Two-tailed Mann-Whitney *U* test. N=6, 5, and 5 from left to right (mean ± s.e.m.).

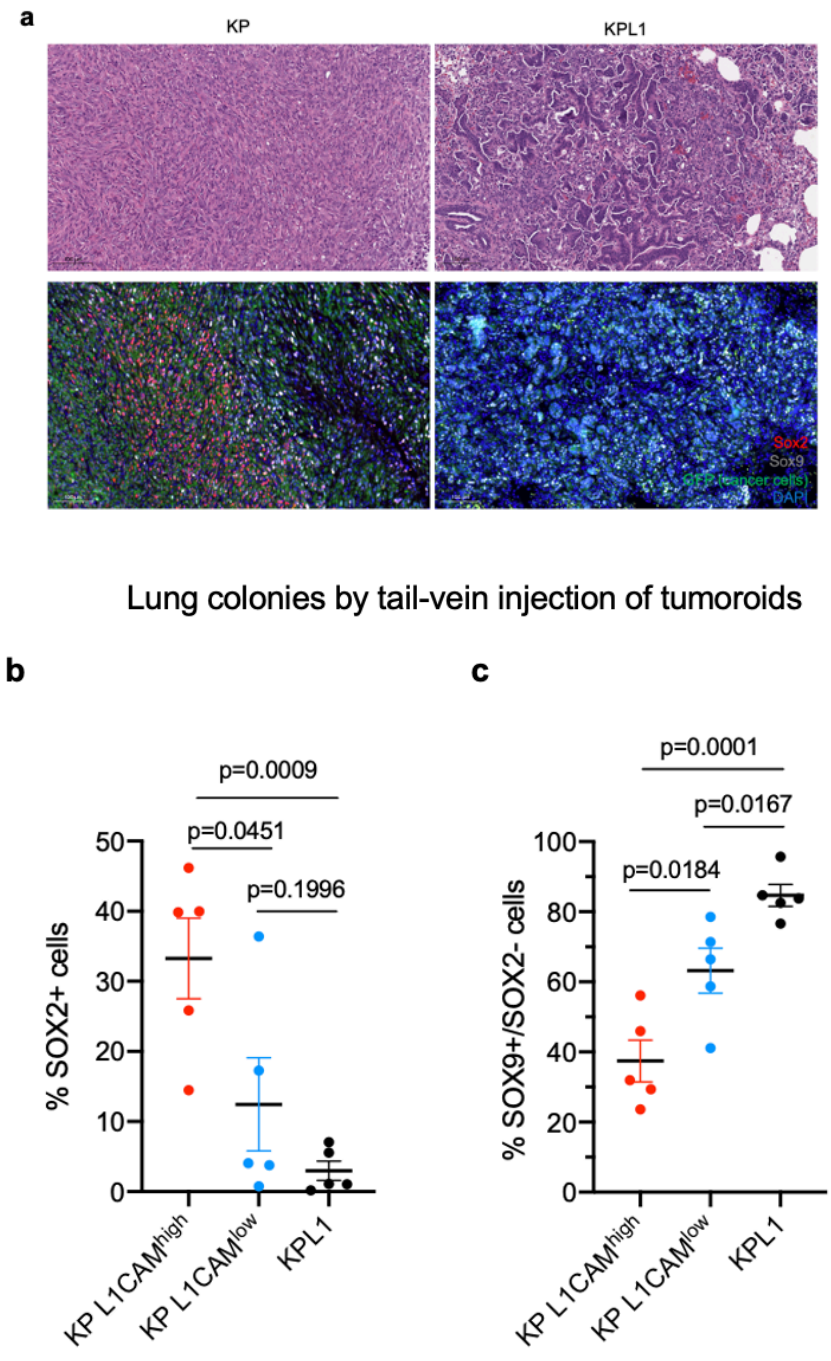

Figure 3-19: (a) Representative images of H&E and co-IF staining and quantification of (b) SOX2+ cancer cells and (c) SOX9+/SOX2- cancer cells in lung colonies derived from FACS-sorted KP and KPL1 tumoroid cells by tail-vein injection into athymic mice. Two-tailed unpaired *t* test. N=5 for each group (mean ± s.e.m.).

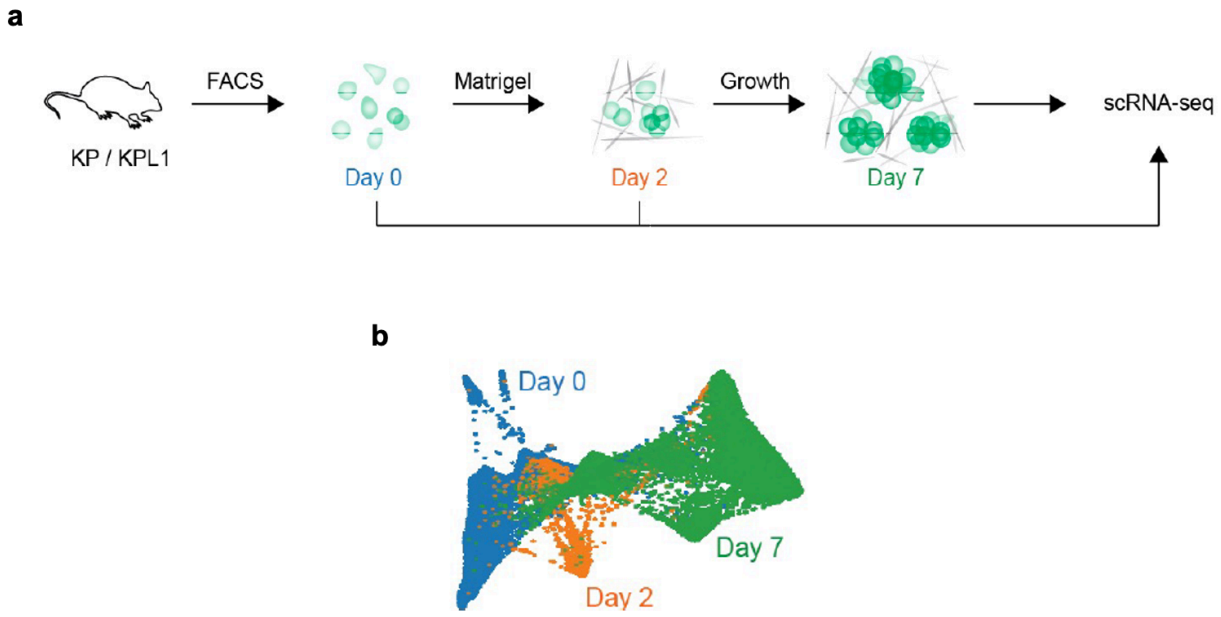

Figure 3-20: Experimental pipeline of single-cell RNA sequencing (scRNA-seq) of KP and KPL1 tumor cells freshly isolated or cultured as tumoroids in Matrigel. (a) KP and KPL1 tumor cells were isolated from respective mice after 24–26-week post-lentiviral infection. Freshly isolated cells were submitted for scRNA-seq (Day 0) or grown in Matrigel as tumoroids (Days 2 and 7) before performing scRNA-seq. (b) The force-directed layout of analyzed tumor cells (Day 0, blue; Day 2, orange; Day 7, green). Data by Yasemin Kaygusuz and Jin Suk Park.

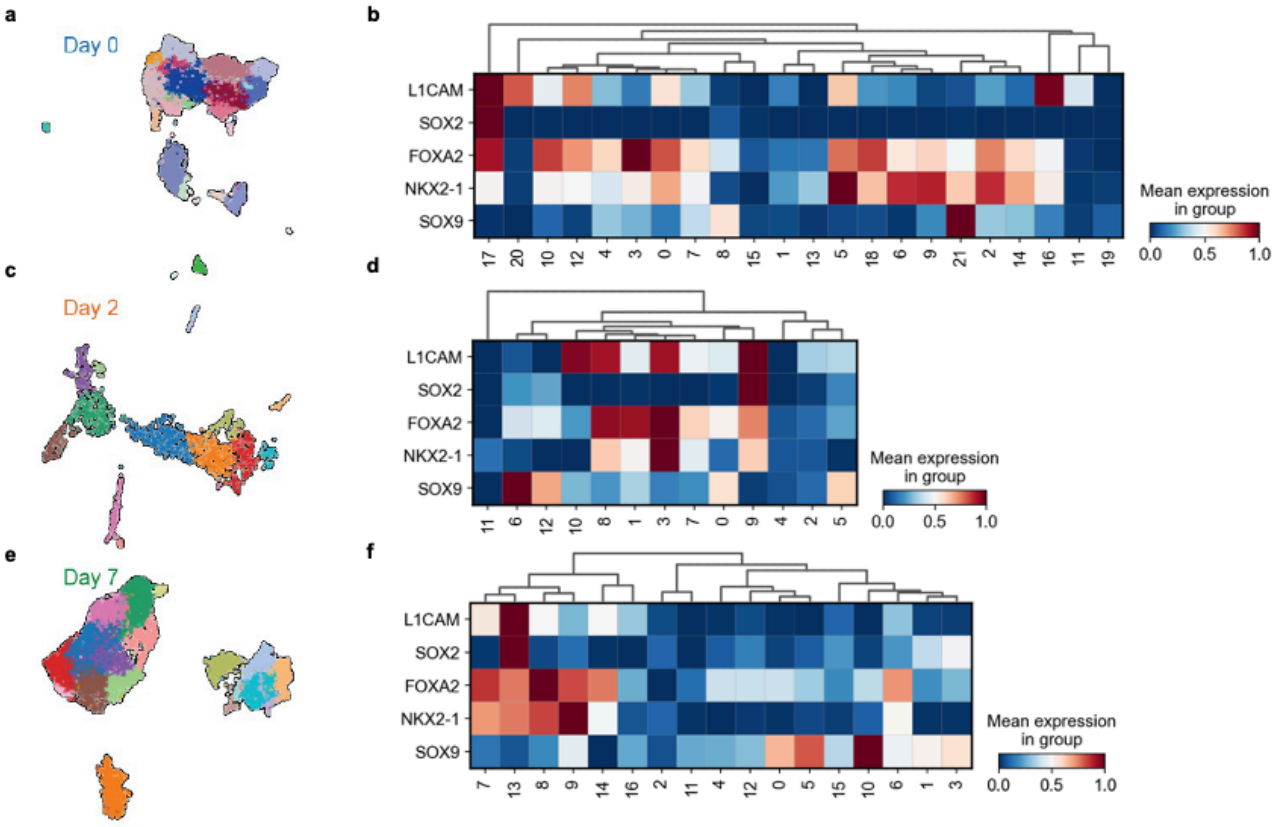

Figure 3-21: The UMAPs and heatmaps of (a) Day 0, (c) Day 2, and (e) Day 7 show the phenotype clusters calculated by the Leiden algorithm. The heatmaps of Day 0, Day 2, and Day 7 show the normalized expression of L1CAM and key transcription factors of lung epithelial development (e.g., SOX2, FOXA2, NKX2-1, and SOX9) for all individual KP and KPL1 tumor and tumoroid cells, ranked by the Wilcoxon test. Hierarchical clustering is shown as a dendrogram per heatmap. Data were normalized by median library size followed by log-transformation. The expression of each transcription factor is transformed as a standard scale (dimension between 0 and 1). Data by Yasemin Kaygusuz and Jin Suk Park.

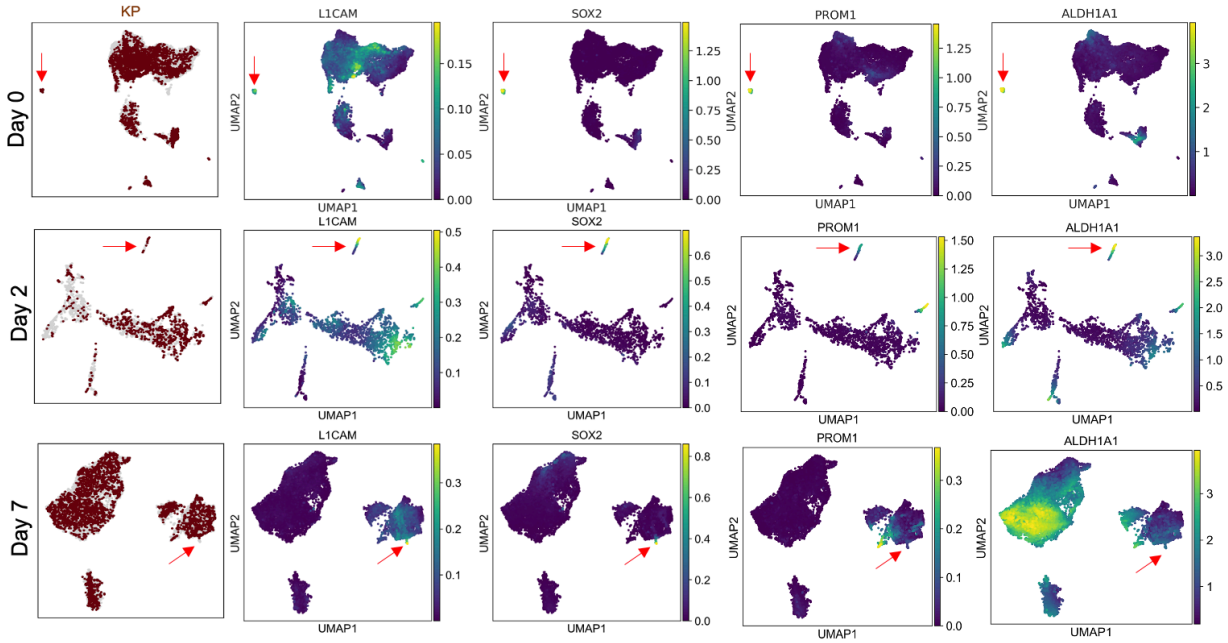

Figure 3-22: The UMAP layout of all KP and KPL1 cells from three time points colored by sample type (KP) or mean expression of L1CAM, SOX2, PROM1 (Cd133), and ALDH1A1. The red arrows show the L1CAM+ SOX2+ clusters at each time point. Data by Yasemin Kaygusuz and Jin Suk Park.

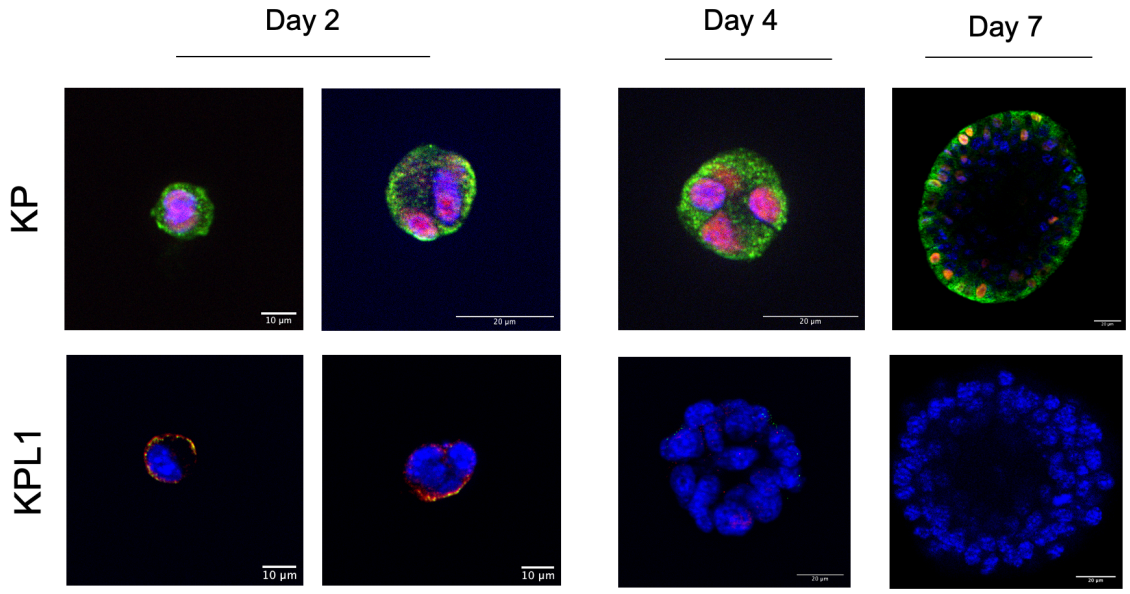

Figure 3-23: Representative images of L1CAM and SOX2 immunofluorescence staining of KP and KPL1 tumoroids at indicated time points (Blue: nuclei, Green: L1CAM, Magenta: SOX2).

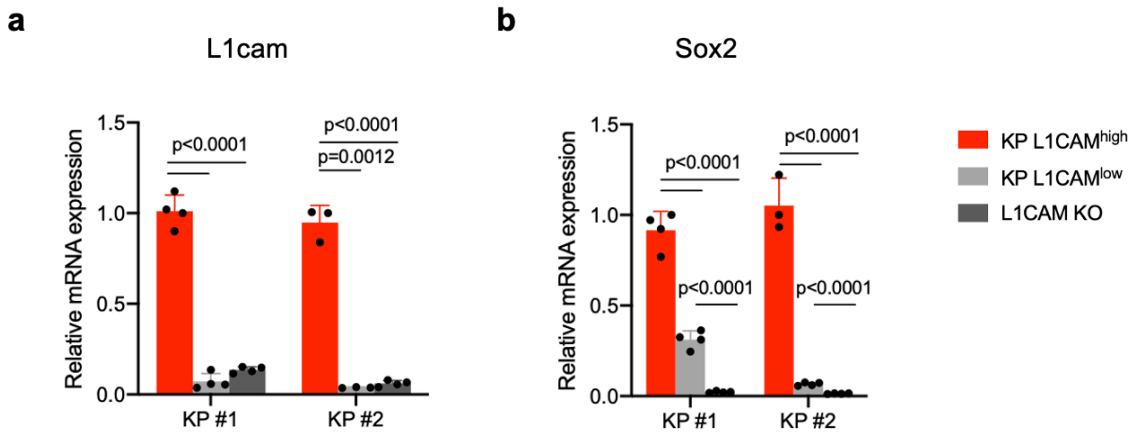

Figure 3-24: (a) L1cam and (b) Sox2 mRNA expression quantified by qRT-PCR in two KP tumoroids (KP #1 and #2) sorted by FACS into L1CAM^{high} and L1CAM^{low} populations and in two L1CAM knockout (KO) tumoroid lines (KPL1 #1 and #2). Data were normalized to Gapdh mRNA levels and to KP L1CAM^{high}. Two-tailed unpaired *t* test. N=4 for each group (mean ± s.e.m.).

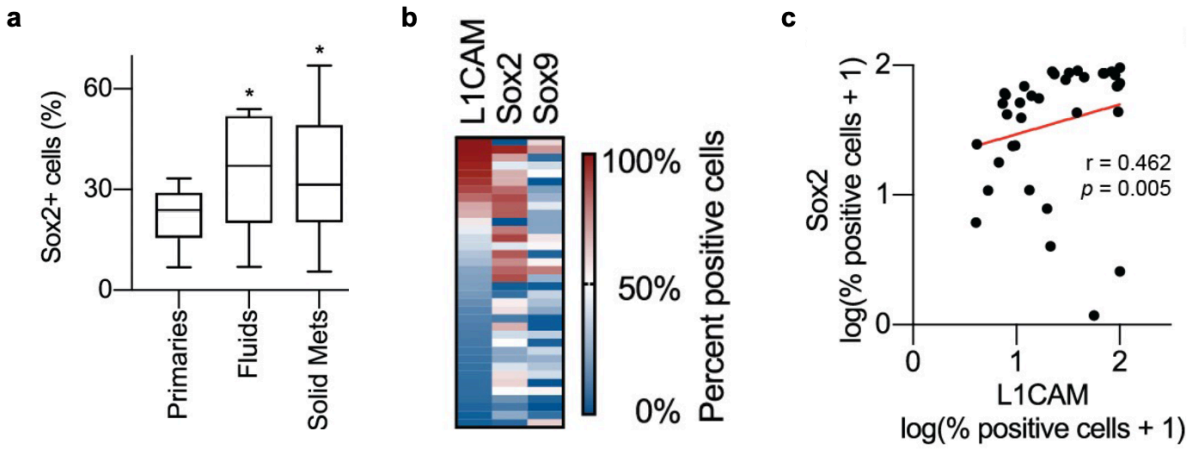

Figure 3-25: (a) Percentage of SOX2+ cells in LUAD primary tumors (N = 14 patient samples), and fluidic metastasis (N = 7 patient samples) and solid metastasis (N = 38 patient samples) by IHC staining. (b) Heatmap of PDX panels showing the percentage of positive cells for L1CAM, Sox2 and Sox9 expression. (c) Spearman correlation of Sox2+ PDX panels and L1CAM+ PDX panels. Data by Jin Suk Park.

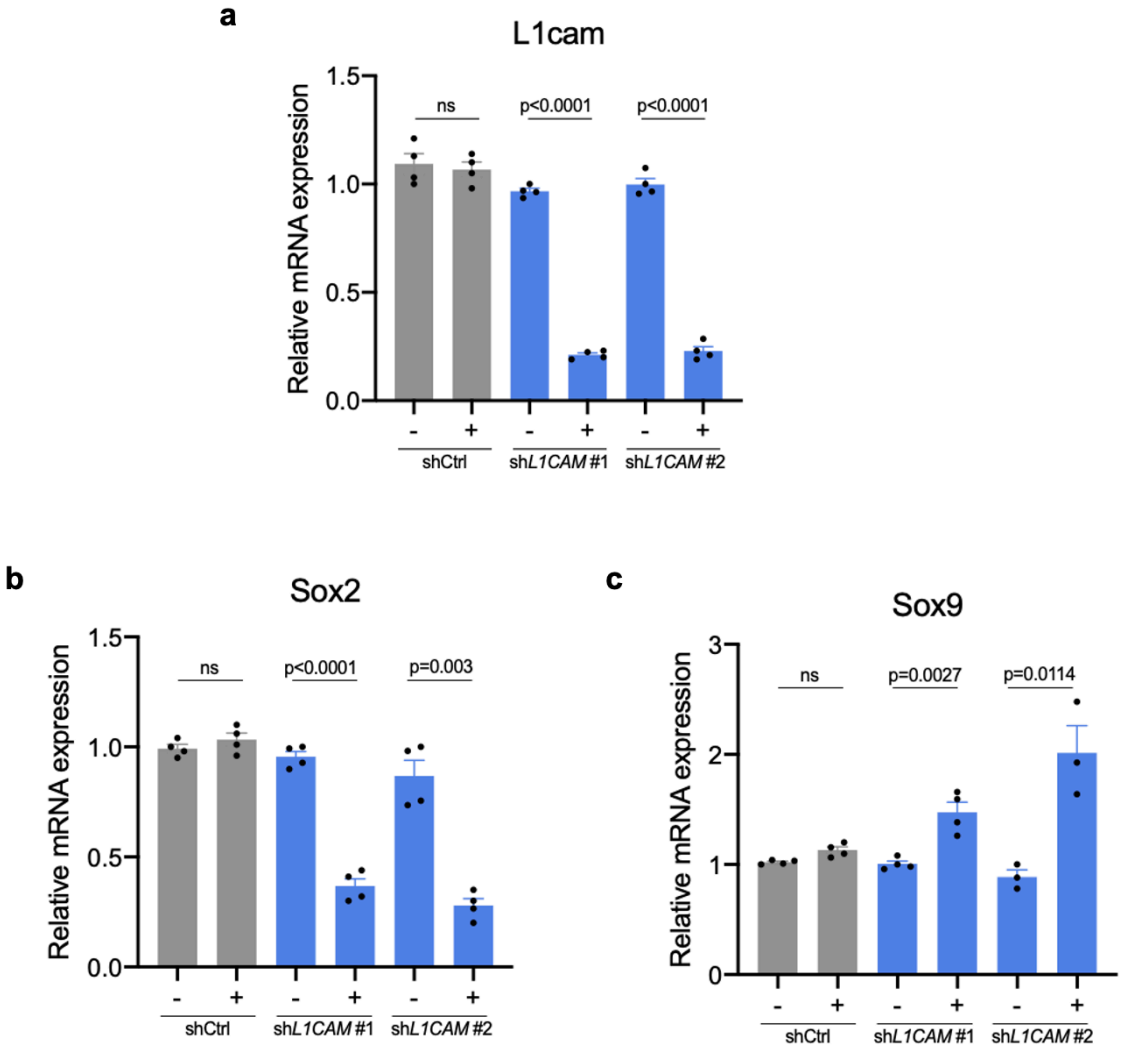

Figure 3-26: (a) L1cam, (b) Sox2, and (c) Sox9 mRNA expression quantified by qRT-PCR in two KP tumoroids stably expressing the shRNAs in the presence or absence of doxycycline (Dox) for 2 days before RNA isolation. Data were normalized to Gapdh mRNA levels and to the corresponding shControl samples. Two-tailed unpaired *t* test. N=4 for each group (mean ± s.e.m.).

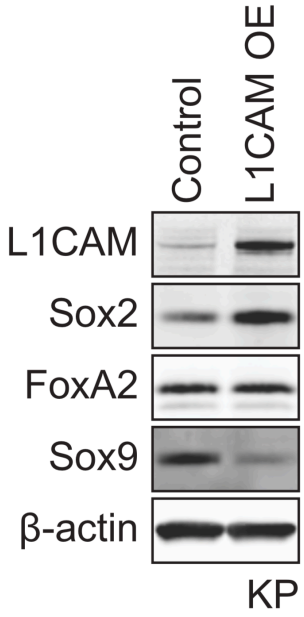

Figure 3-27: L1CAM, Sox2, FoxA2, and Sox9 immunoblots in KP tumoroids overexpressing L1CAM (L1CAM OE). β-actin, loading control. Data by and Jin Suk Park.

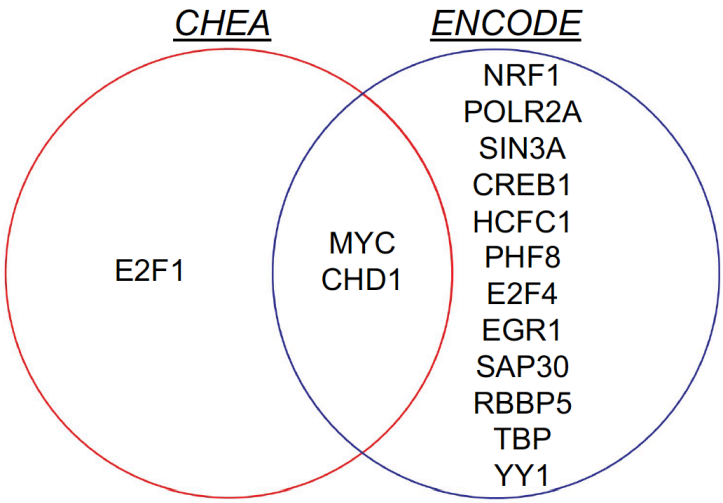

Figure 3-28: Venn diagram showing the transcriptional regulators enriched in the L1CAM+ SOX2+ clusters of the scRNA-seq dataset analyzed by CHEA (ChIP Enrichment Analysis) and ENCODE (The Encyclopedia of DNA Elements). Data by Yasemin Kaygusuz and Jin Suk Park.

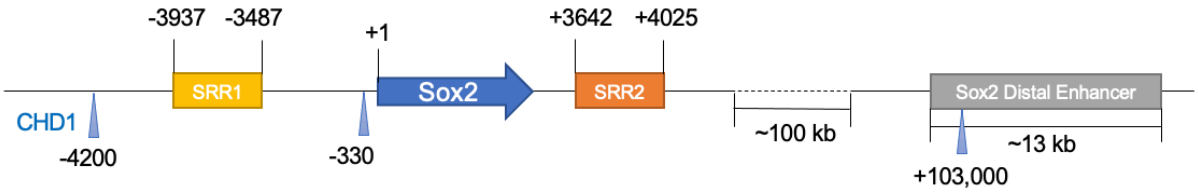

Figure 3-29: Mouse Sox2 locus and the Sox2 distal enhancer shown with the putative CHD1 binding sites (shown with blue arrowheads) identified by publicly available ChIP-seq datasets for CHD1 and ReMap (SRR: Sox Regulatory Regions).

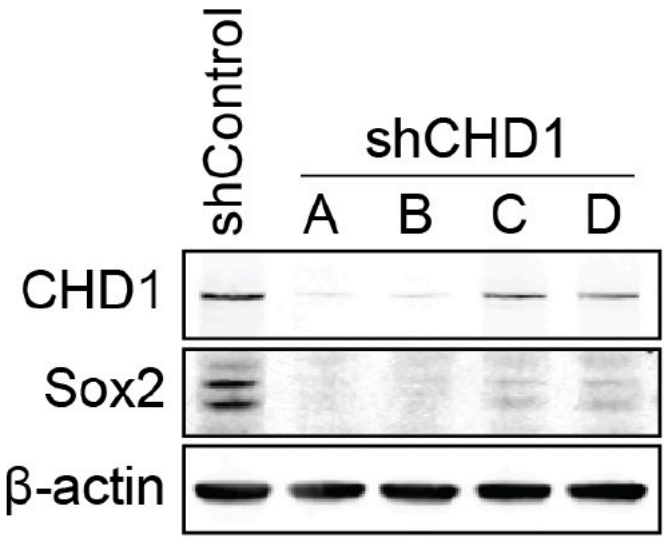

Figure 3-30: Immunoblot showing CHD1 and SOX2 protein expression in KP tumoroids stably expressing the indicated shRNAs. β-actin: loading control. Data by Jin Suk Park.

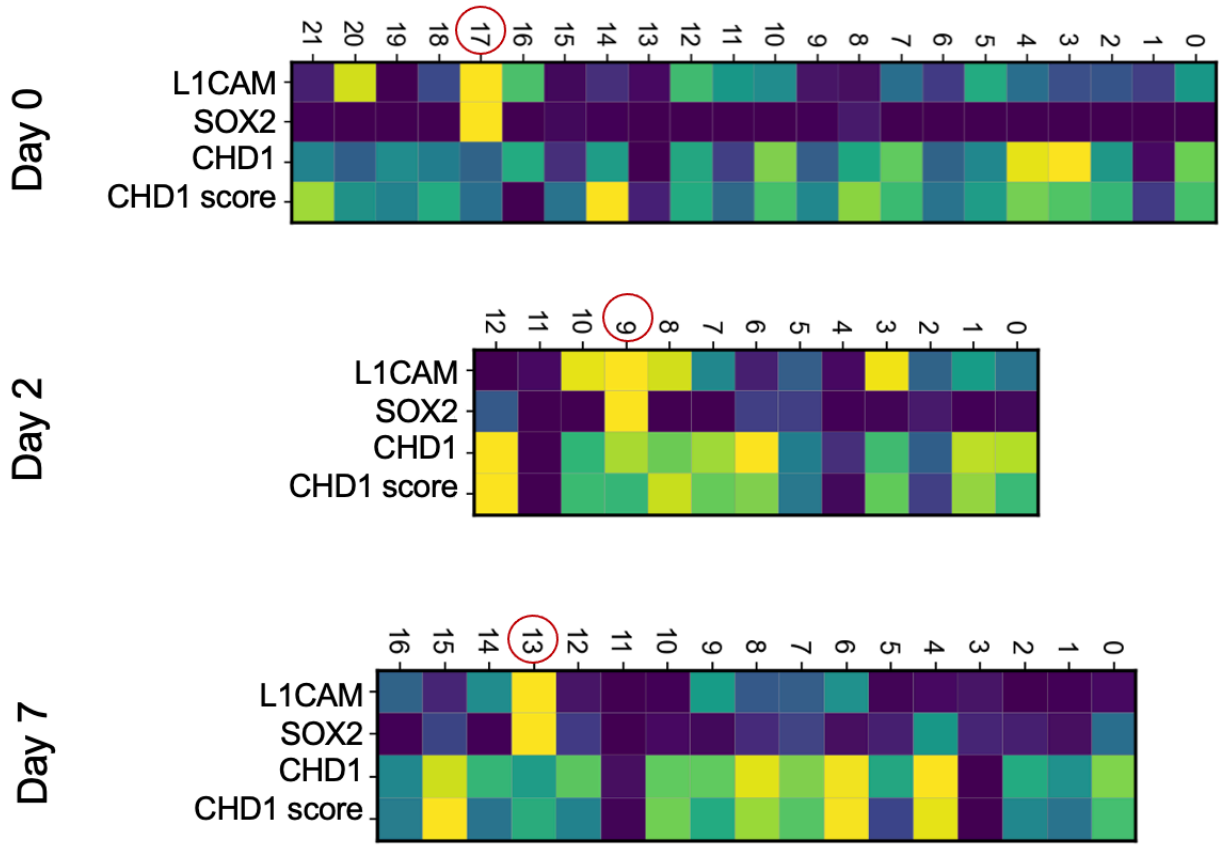

Figure 3-31: Heatmaps show mean L1CAM, SOX2, and CHD1 expression and mean expression of CHD1 target genes (CHD1 score) in the clusters of all three time points. Data by Jin Suk Park.

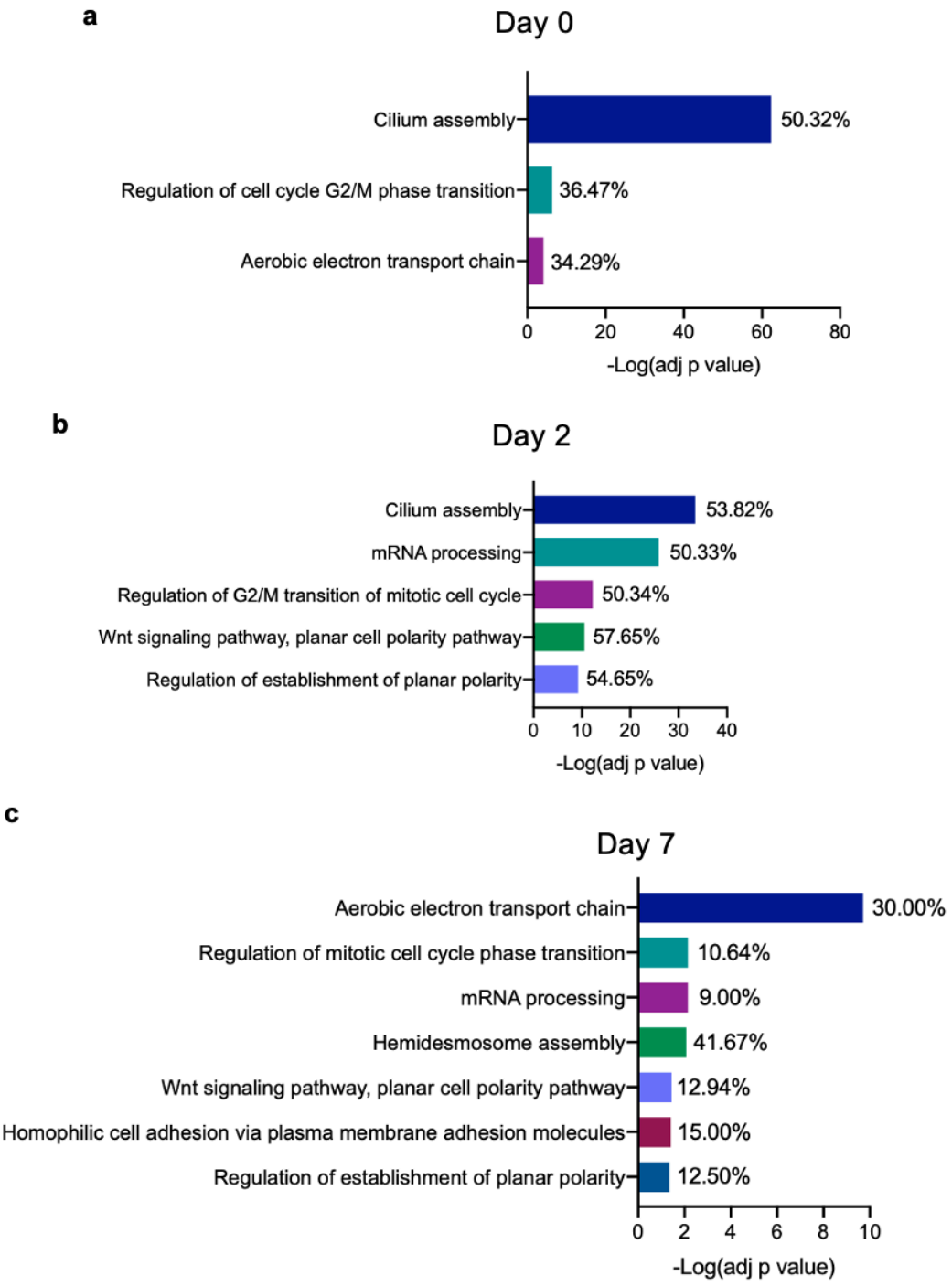

Figure 3-32: PANTHER Gene Ontology analyses of L1CAM+ SOX2+ clusters from the indicated time points of KP LUAD scRNA-seq dataset compared to the other clusters. Highest-scoring biological processes are shown in an unbiased manner (adjusted $p<0.05$). The percentages of the list total are given next to the corresponding GO annotation terms.

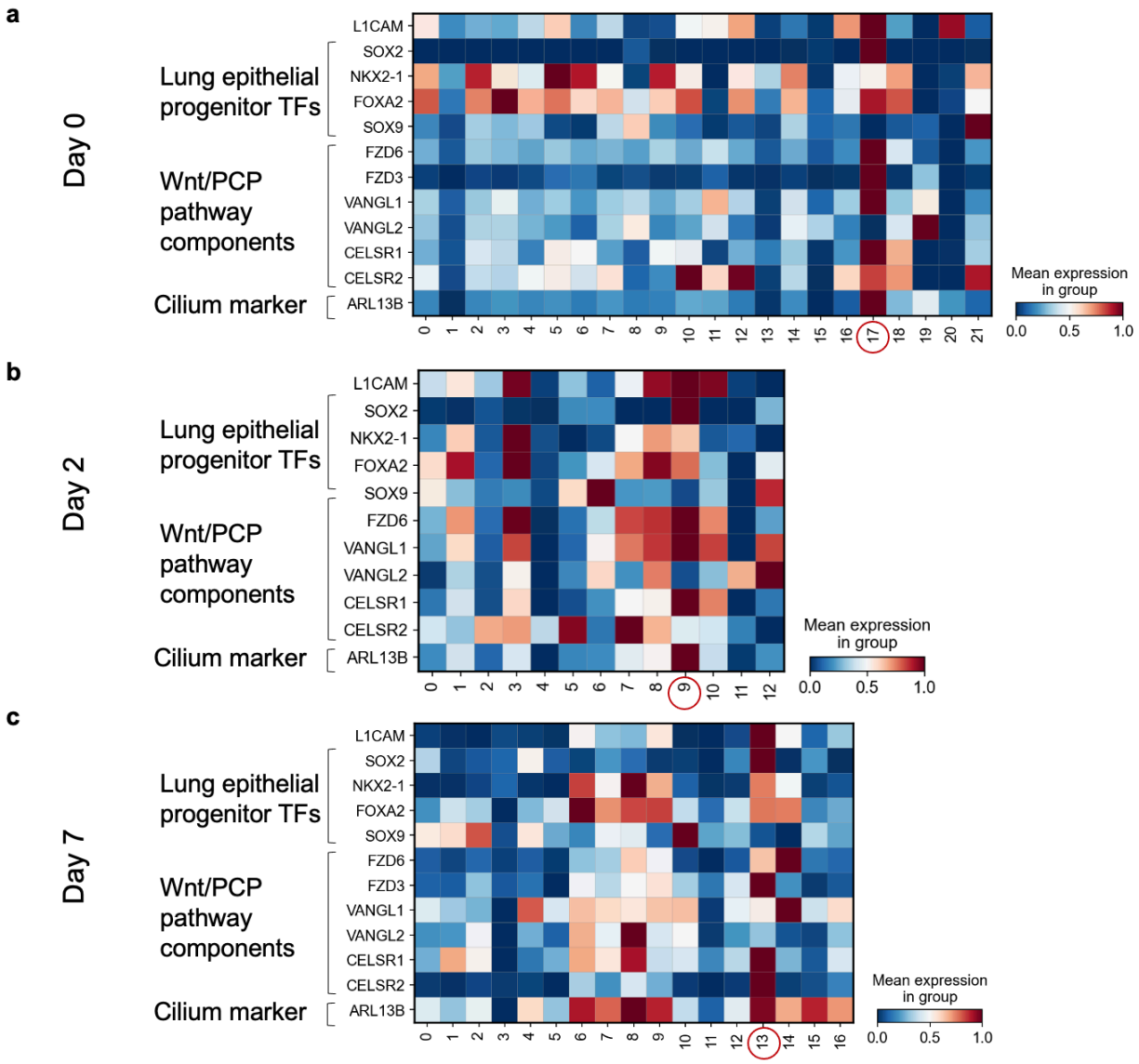

Figure 3-33: The expression of L1CAM, the lung epithelial progenitor transcription factors (TFs), the Wnt/PCP pathway components, and the cilium marker of all KP and KPL1 cells from the three time points in heatmaps colored by mean expression. Red circles mark the L1CAM+/SOX2+ clusters at all time points. Data by Yasemin Kaygusuz and Jin Suk Park.

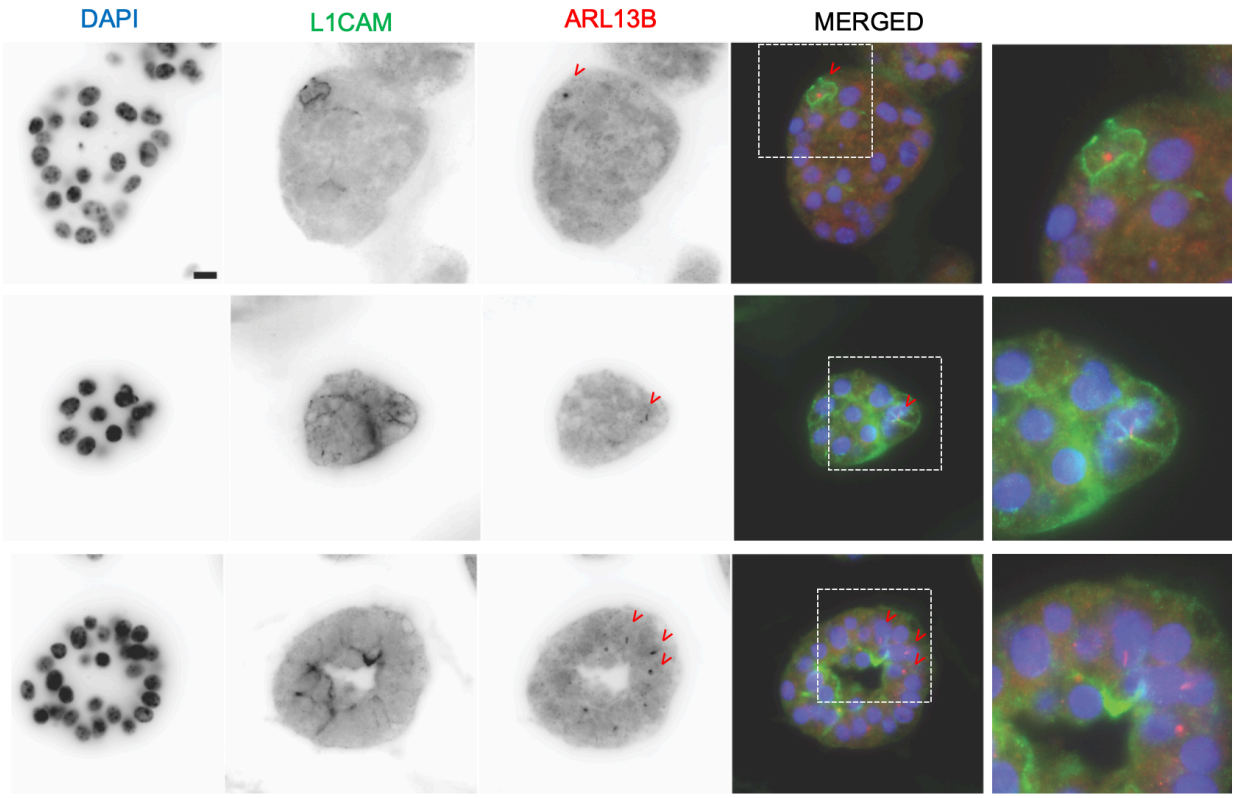

Figure 3-34: Representative images of L1CAM and the cilia marker Arl13b immunofluorescence staining of KP tumoroid (Green: L1CAM, Red: Arl13b, Blue: nuclei, Red arrowheads: cilia). Insets show higher magnification of boxed areas. Scale bar: 10 μm. Data by Jin Suk Park.

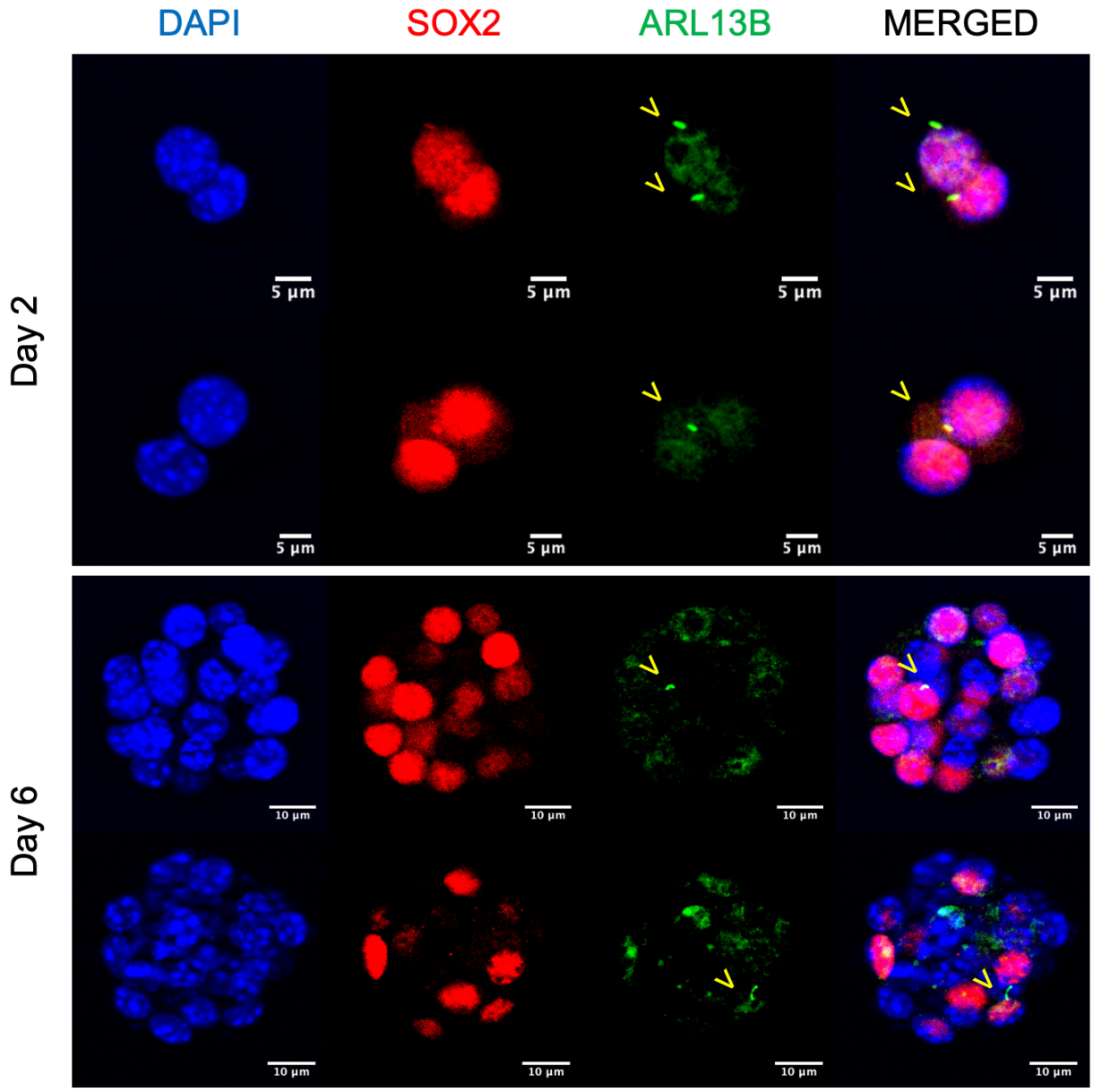

Figure 3-35: Representative images of L1CAM, SOX2, and the cilia marker ARL13B immunofluorescence staining of KP tumoroids cultured *in vitro* for indicated time points (Green: L1CAM, Red: ARL13B, Blue: nuclei, Yellow arrowheads: cilia).

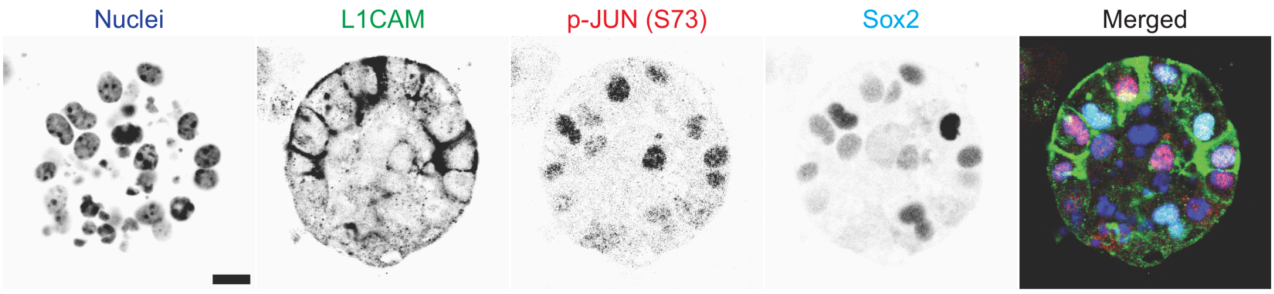

Figure 3-36: (a) Representative images of L1CAM, p-JUN, and Sox2 expression in KP tumoroids by immunofluorescence staining. (green: L1CAM, red: p-JUN (S73), cyan: Sox2, blue: DAPI, nuclei). Scale bar: 10 μm. Data by Jin Suk Park.

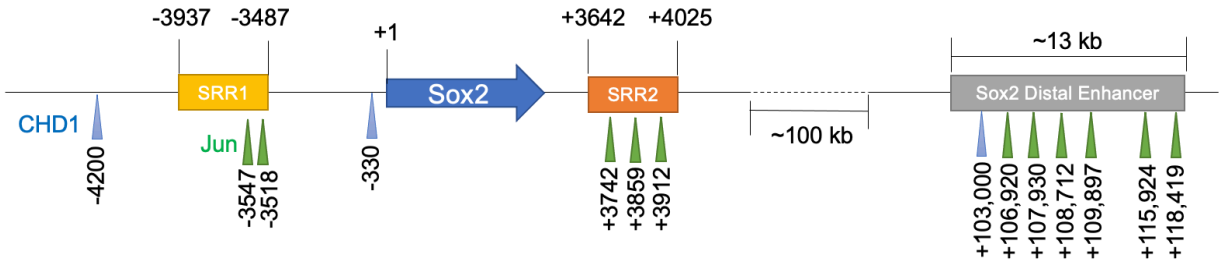

Figure 3-37: Mouse Sox2 locus and the Sox2 distal enhancer shown with the putative CHD1 and Jun binding sites (shown with blue and green arrowheads, respectively) identified by PROMO (SRR: Sox Regulatory Regions).

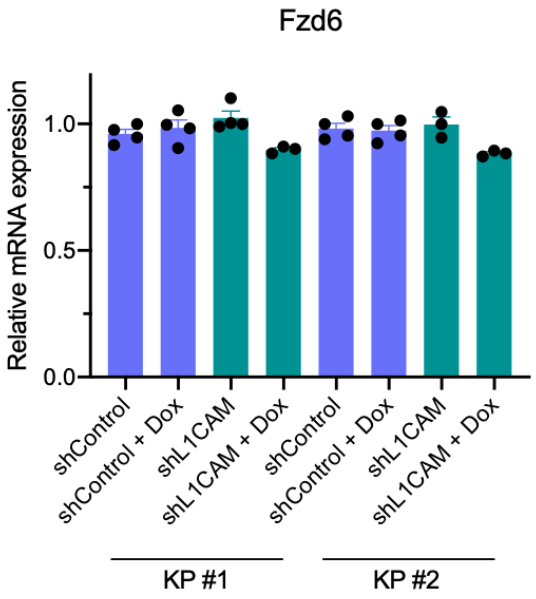

Figure 3-38: Fzd6 mRNA expression quantified by qRT-PCR in two KP tumoroids stably expressing the shRNAs in the presence or absence of doxycycline (Dox) for 2 days before RNA isolation. Data were normalized to Gapdh mRNA levels and to the corresponding shControl samples. Two-tailed unpaired *t* test. N=3 and 4 for each group (mean ± s.e.m.).

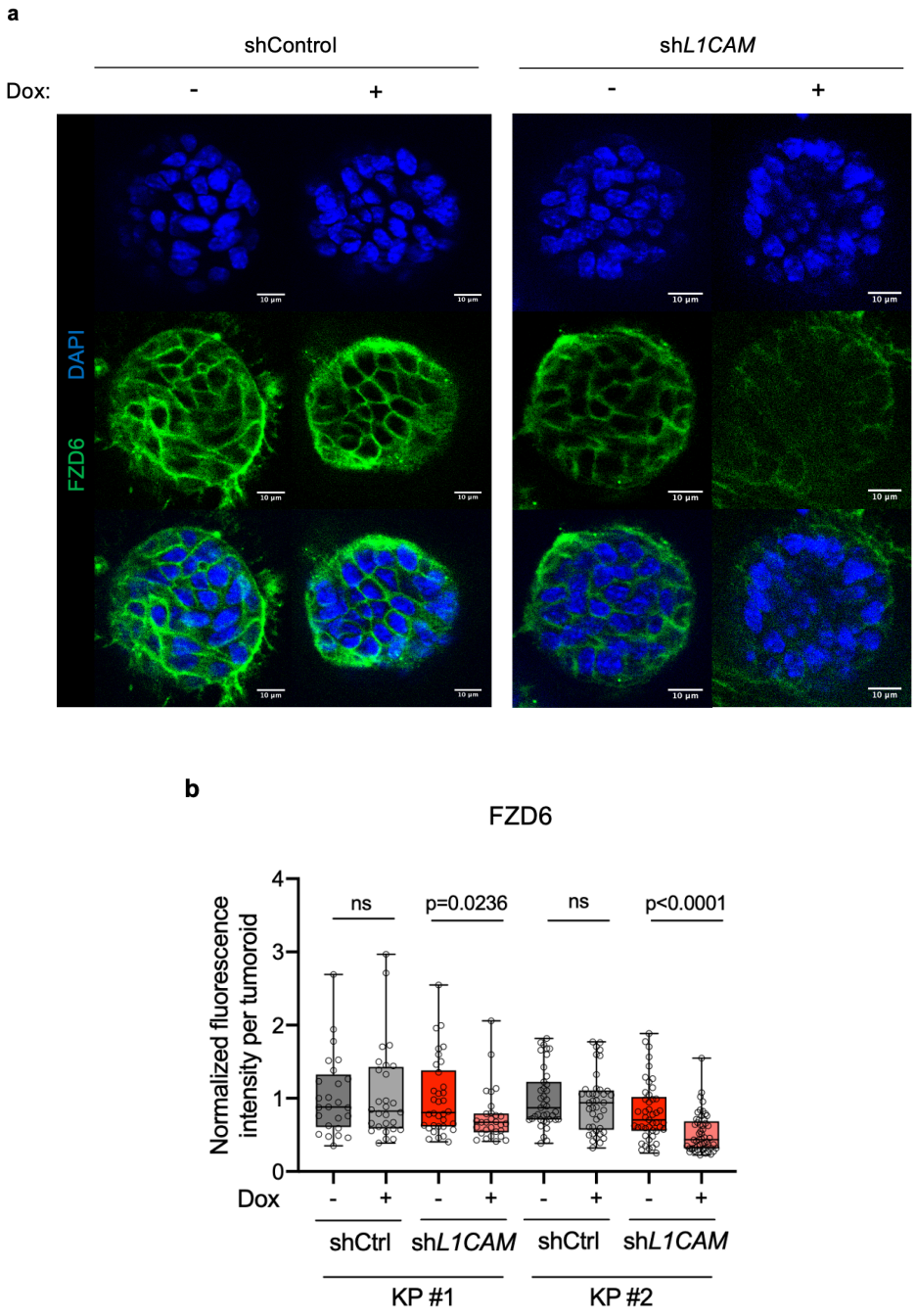

Figure 3-39: (a) Representative images of FZD6 expression in KP tumoroids expressing doxycycline (Dox)-inducible shRNA targeting L1CAM in the presence and absence of Dox for 2 days before staining (green: FZD6, blue: DAPI, nuclei). Data represent 2 biological replicates. (b) Quantification of FZD6 immunofluorescence staining by integrated fluorescence intensity per tumoroid in KP tumoroids expressing shRNAs with or without Dox treatment. Box plots show minimum and maximum with all data points (N= 39, 41, 45, 53, 25, 28, 35, and 29 tumoroids from left to right). Two-tailed Mann-Whitney *U* test.

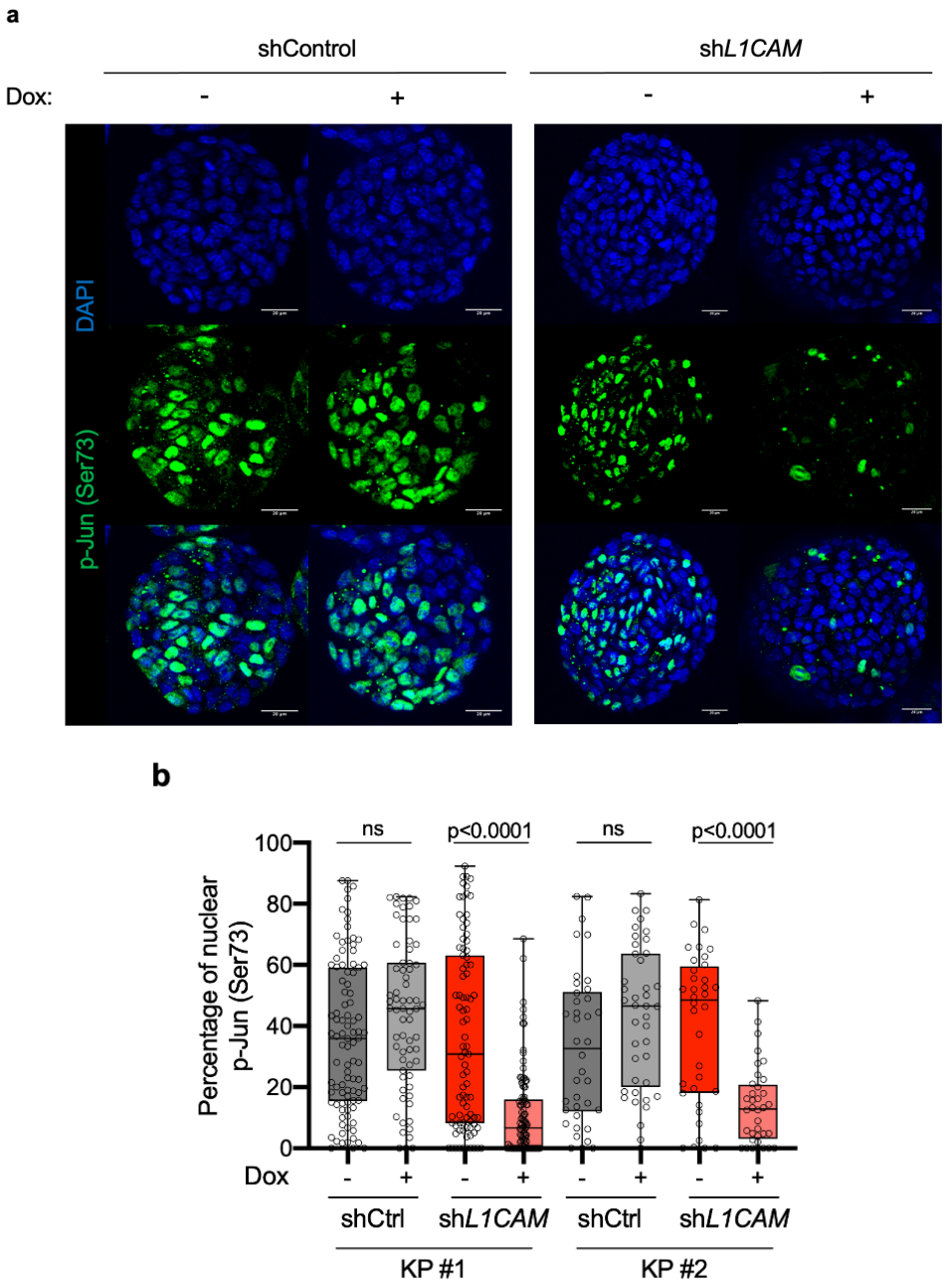

Figure 3-40: (a) Representative images of nuclear phospho-Jun (Ser73) in KP tumoroids expressing doxycycline (Dox)-inducible shRNA targeting L1CAM in the presence and absence of Dox for 2 days before staining (green: phospho-Jun blue: DAPI, nuclei). Data represent 2 biological replicates. (b) Quantification of nuclear phospho-Jun immunofluorescence staining per tumoroid in KP tumoroids expressing shRNAs with or without Dox treatment. Box plots show minimum and maximum with all data points (N= 87, 101, 94, 67, 38, 42, 36, and 36 tumoroids from left to right). Two-tailed Mann-Whitney *U* test.

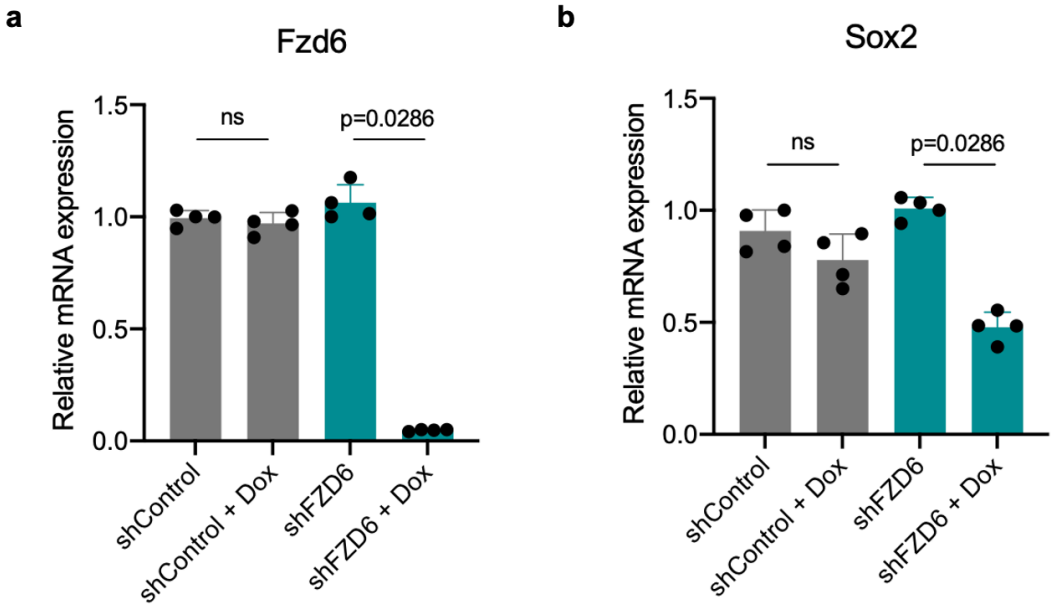

Figure 3-41: (a) Fzd6 and (b) Sox2 mRNA expression quantified by qRT-PCR in KP tumoroids expressing doxycycline-inducible shRNA targeting FZD6 in the presence and absence of doxycycline (Dox) for 2 days. Data were normalized to Gapdh mRNA levels and to the corresponding shControl samples. Two-tailed Mann-Whitney *U* test. N=4 for each group (mean ± s.e.m.).

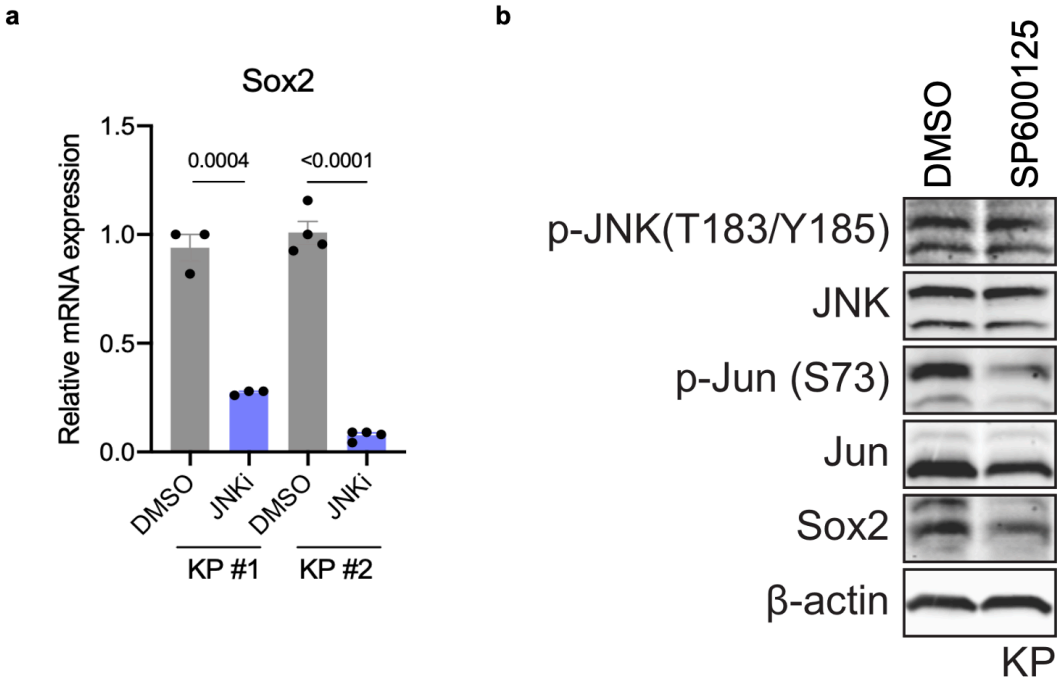

Figure 3-42: (a) Sox2 mRNA expression quantified by qRT-PCR in KP tumoroids treated with the JNK inhibitor SP600125 (JNKi, 20 μM) or vehicle (DMSO) for 24 hours. Data were normalized to Gapdh mRNA levels and to the corresponding DMSO samples. Two-tailed unpaired *t* test. N=3 or 4 for each group (mean ± s.e.m.). Data by Yasemin Kaygusuz. (b) Phospho-JNK, JNK, phospho-Jun, Jun, and Sox2 immunoblots in KP tumoroids treated with the JNK inhibitor SP600125 (20 μM) or vehicle (DMSO). β-actin, loading control. Data by and Jin Suk Park.

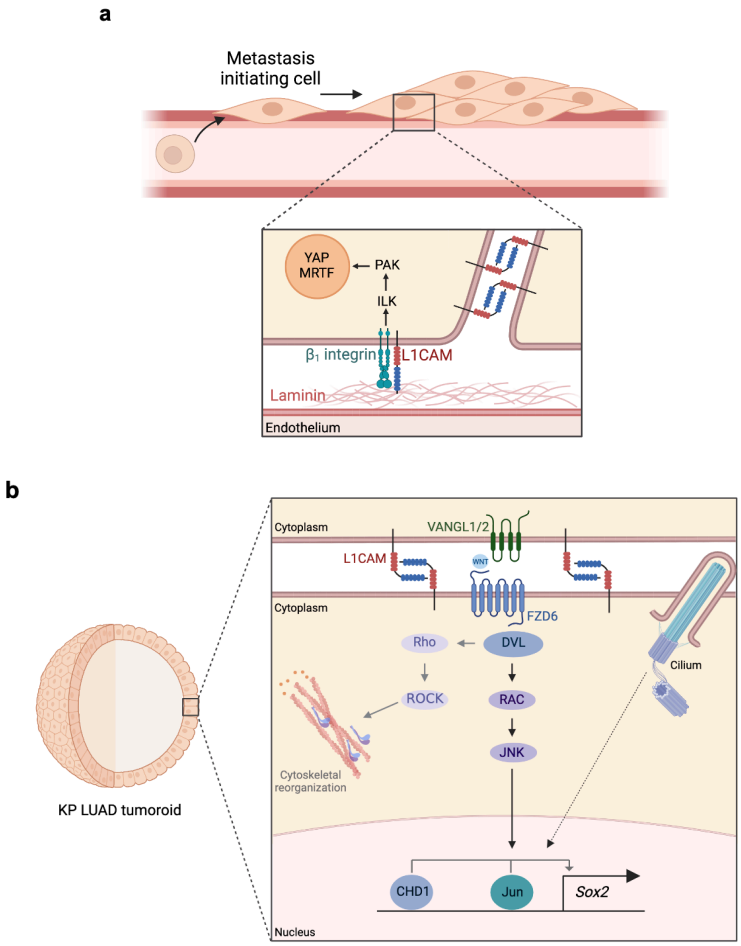

Figure 3-43: (a) A model summarizing the expression and role of L1CAM both at the cell-vascular basal lamina interface and the cell-cell interface in metastasis-initiating cells co-opting blood vessels during metastatic colonization. L1CAM and β1 integrins mediate adhesion to the laminins in vascular basal lamina and activate ILK and PAK, which leads to the activation of YAP and MRTF mechanotransduction transcription factors and metastatic outgrowth. L1CAM expression detected at the cell-cell junctions in metastatic cell clusters possibly indicates L1CAM homophilic interactions. (b) A model demonstrating the role of L1CAM in establishing the SOX2+ progenitor-like state in KP LUAD tumoroids. As KP LUAD cells are dissociated from primary tumors, L1CAM+ cells show superior growth reinitiation capacity in both tumoroid culture and metastatic colonization at distant organ sites. During regrowth as tumoroids and metastases, KP LUAD cells exhibit the SOX2+ progenitor-like state. L1CAM expression at cell-cell junctions promotes the establishment of the WNT/PCP pathway. The activation of the WNT/PCP pathway drives the nuclear translocation of the transcription factor Jun. Jun and the chromatin remodeler CHD1 induce SOX2 expression and promote the SOX2+ progenitor-like state in KP LUAD. Primary cilia are uniquely associated with L1CAM+ SOX2+ cells in KP LUAD tumors and tumoroids; however, whether primary cilia are involved in regulating the SOX2 expression is not clear.

References

1 Massague, J. & Obenauf, A. C. Metastatic colonization by circulating tumour cells. *Nature* **529**, 298-306, doi:10.1038/nature17038 (2016).

2 Klein, C. A. *et al.* Genetic heterogeneity of single disseminated tumour cells in minimal residual cancer. *Lancet* **360**, 683-689, doi:10.1016/S0140-6736(02)09838-0 (2002).

3 Hosseini, H. *et al.* Early dissemination seeds metastasis in breast cancer. *Nature* **540**, 552-558, doi:10.1038/nature20785 (2016).

4 Massague, J. & Ganesh, K. Metastasis-Initiating Cells and Ecosystems. *Cancer Discov* **11**, 971-994, doi:10.1158/2159-8290.CD-21-0010 (2021).

5 Husemann, Y. *et al.* Systemic spread is an early step in breast cancer. *Cancer Cell* **13**, 58-68, doi:10.1016/j.ccr.2007.12.003 (2008).

6 Sanger, N. *et al.* Disseminated tumor cells in the bone marrow of patients with ductal carcinoma in situ. *Int J Cancer* **129**, 2522-2526, doi:10.1002/ijc.25895 (2011).

7 Stott, S. L. *et al.* Isolation and characterization of circulating tumor cells from patients with localized and metastatic prostate cancer. *Sci Transl Med* **2**, 25ra23, doi:10.1126/scitranslmed.3000403 (2010).

8 Fares, J., Fares, M. Y., Khachfe, H. H., Salhab, H. A. & Fares, Y. Molecular principles of metastasis: a hallmark of cancer revisited. *Signal Transduct Target Ther* **5**, 28, doi:10.1038/s41392-020-0134-x (2020).

9 Dongre, A. & Weinberg, R. A. New insights into the mechanisms of epithelial-mesenchymal transition and implications for cancer. *Nat Rev Mol Cell Biol* **20**, 69-84, doi:10.1038/s41580-018-0080-4 (2019).

10 Lambert, A. W., Pattabiraman, D. R. & Weinberg, R. A. Emerging Biological Principles of Metastasis. *Cell* **168**, 670-691, doi:10.1016/j.cell.2016.11.037 (2017).

11 Duda, D. G. *et al.* Malignant cells facilitate lung metastasis by bringing their own soil. *Proc Natl Acad Sci U S A* **107**, 21677-21682, doi:10.1073/pnas.1016234107 (2010).

12 Aceto, N. *et al.* Circulating tumor cell clusters are oligoclonal precursors of breast cancer metastasis. *Cell* **158**, 1110-1122, doi:10.1016/j.cell.2014.07.013 (2014).

13 Gkountela, S. *et al.* Circulating Tumor Cell Clustering Shapes DNA Methylation to Enable Metastasis Seeding. *Cell* **176**, 98-112 e114, doi:10.1016/j.cell.2018.11.046 (2019).

14 Wrenn, E. D. *et al.* Regulation of Collective Metastasis by Nanolumenal Signaling. *Cell* **183**, 395-410 e319, doi:10.1016/j.cell.2020.08.045 (2020).

15 Gay, L. J. & Felding-Habermann, B. Contribution of platelets to tumour metastasis. *Nat Rev Cancer* **11**, 123-134, doi:10.1038/nrc3004 (2011).

16 Placke, T. *et al.* Platelet-derived MHC class I confers a pseudonormal phenotype to cancer cells that subverts the antitumor reactivity of natural killer immune cells. *Cancer Res* **72**, 440-448, doi:10.1158/0008-5472.CAN-11-1872 (2012).

17 Leach, J., Morton, J. P. & Sansom, O. J. Neutrophils: Homing in on the myeloid mechanisms of metastasis. *Mol Immunol* **110**, 69-76, doi:10.1016/j.molimm.2017.12.013 (2019).
18 Valiente, M. *et al.* Serpins promote cancer cell survival and vascular co-option in brain metastasis. *Cell* **156**, 1002-1016, doi:10.1016/j.cell.2014.01.040 (2014).
19 Kienast, Y. *et al.* Real-time imaging reveals the single steps of brain metastasis formation. *Nat Med* **16**, 116-122, doi:10.1038/nm.2072 (2010).
20 Ghajar, C. M. *et al.* The perivascular niche regulates breast tumour dormancy. *Nat Cell Biol* **15**, 807-817, doi:10.1038/ncb2767 (2013).
21 Malladi, S. *et al.* Metastatic Latency and Immune Evasion through Autocrine Inhibition of WNT. *Cell* **165**, 45-60, doi:10.1016/j.cell.2016.02.025 (2016).
22 Pommier, A. *et al.* Unresolved endoplasmic reticulum stress engenders immune-resistant, latent pancreatic cancer metastases. *Science* **360**, doi:10.1126/science.aao4908 (2018).
23 Pantel, K. *et al.* Frequent down-regulation of major histocompatibility class I antigen expression on individual micrometastatic carcinoma cells. *Cancer Res* **51**, 4712-4715 (1991).
24 Koebel, C. M. *et al.* Adaptive immunity maintains occult cancer in an equilibrium state. *Nature* **450**, 903-907, doi:10.1038/nature06309 (2007).
25 Eyob, H. *et al.* Inhibition of ron kinase blocks conversion of micrometastases to overt metastases by boosting antitumor immunity. *Cancer Discov* **3**, 751-760, doi:10.1158/2159-8290.CD-12-0480 (2013).
26 Pan, H. *et al.* 20-Year Risks of Breast-Cancer Recurrence after Stopping Endocrine Therapy at 5 Years. *N Engl J Med* **377**, 1836-1846, doi:10.1056/NEJMoa1701830 (2017).
27 Gao, H. *et al.* The BMP inhibitor Coco reactivates breast cancer cells at lung metastatic sites. *Cell* **150**, 764-779, doi:10.1016/j.cell.2012.06.035 (2012).
28 Park, J. *et al.* Cancer cells induce metastasis-supporting neutrophil extracellular DNA traps. *Sci Transl Med* **8**, 361ra138, doi:10.1126/scitranslmed.aag1711 (2016).
29 De Cock, J. M. *et al.* Inflammation Triggers Zeb1-Dependent Escape from Tumor Latency. *Cancer Res* **76**, 6778-6784, doi:10.1158/0008-5472.CAN-16-0608 (2016).
30 Albrengues, J. *et al.* Neutrophil extracellular traps produced during inflammation awaken dormant cancer cells in mice. *Science* **361**, doi:10.1126/science.aao4227 (2018).
31 Er, E. E. *et al.* Pericyte-like spreading by disseminated cancer cells activates YAP and MRTF for metastatic colonization. *Nat Cell Biol* **20**, 966-978, doi:10.1038/s41556-018-0138-8 (2018).
32 Shibue, T., Brooks, M. W. & Weinberg, R. A. An integrin-linked machinery of cytoskeletal regulation that enables experimental tumor initiation and metastatic colonization. *Cancer Cell* **24**, 481-498, doi:10.1016/j.ccr.2013.08.012 (2013).

33 Cooper, J. & Giancotti, F. G. Integrin Signaling in Cancer: Mechanotransduction, Stemness, Epithelial Plasticity, and Therapeutic Resistance. *Cancer Cell* **35**, 347-367, doi:10.1016/j.ccell.2019.01.007 (2019).
34 Shiozawa, Y. *et al.* Human prostate cancer metastases target the hematopoietic stem cell niche to establish footholds in mouse bone marrow. *J Clin Invest* **121**, 1298-1312, doi:10.1172/JCI43414 (2011).
35 Wang, H. *et al.* The Osteogenic Niche Is a Calcium Reservoir of Bone Micrometastases and Confers Unexpected Therapeutic Vulnerability. *Cancer Cell* **34**, 823-839 e827, doi:10.1016/j.ccell.2018.10.002 (2018).
36 Oskarsson, T. *et al.* Breast cancer cells produce tenascin C as a metastatic niche component to colonize the lungs. *Nat Med* **17**, 867-874, doi:10.1038/nm.2379 (2011).
37 Chen, Q. *et al.* Carcinoma-astrocyte gap junctions promote brain metastasis by cGAMP transfer. *Nature* **533**, 493-498, doi:10.1038/nature18268 (2016).
38 Priego, N. *et al.* STAT3 labels a subpopulation of reactive astrocytes required for brain metastasis. *Nat Med* **24**, 1024-1035, doi:10.1038/s41591-018-0044-4 (2018).
39 Zeng, Q. *et al.* Synaptic proximity enables NMDAR signalling to promote brain metastasis. *Nature* **573**, 526-531, doi:10.1038/s41586-019-1576-6 (2019).
40 Esposito, M., Guise, T. & Kang, Y. The Biology of Bone Metastasis. *Cold Spring Harb Perspect Med* **8**, doi:10.1101/cshperspect.a031252 (2018).
41 Guldner, I. H. *et al.* CNS-Native Myeloid Cells Drive Immune Suppression in the Brain Metastatic Niche through Cxcl10. *Cell* **183**, 1234-1248 e1225, doi:10.1016/j.cell.2020.09.064 (2020).
42 Malanchi, I. *et al.* Interactions between cancer stem cells and their niche govern metastatic colonization. *Nature* **481**, 85-89, doi:10.1038/nature10694 (2011).
43 Chen, Q., Zhang, X. H. & Massague, J. Macrophage binding to receptor VCAM-1 transmits survival signals in breast cancer cells that invade the lungs. *Cancer Cell* **20**, 538-549, doi:10.1016/j.ccr.2011.08.025 (2011).
44 Raulet, D. H., Marcus, A. & Coscoy, L. Dysregulated cellular functions and cell stress pathways provide critical cues for activating and targeting natural killer cells to transformed and infected cells. *Immunol Rev* **280**, 93-101, doi:10.1111/imr.12600 (2017).
45 Kwon, J. & Bakhoum, S. F. The Cytosolic DNA-Sensing cGAS-STING Pathway in Cancer. *Cancer Discov* **10**, 26-39, doi:10.1158/2159-8290.CD-19-0761 (2020).
46 Romero, I. *et al.* T lymphocytes restrain spontaneous metastases in permanent dormancy. *Cancer Res* **74**, 1958-1968, doi:10.1158/0008-5472.CAN-13-2084 (2014).
47 Romero, I., Garrido, F. & Garcia-Lora, A. M. Metastases in immune-mediated dormancy: a new opportunity for targeting cancer. *Cancer Res* **74**, 6750-6757, doi:10.1158/0008-5472.CAN-14-2406 (2014).

48 Basnet, H. *et al.* Flura-seq identifies organ-specific metabolic adaptations during early metastatic colonization. *Elife* **8**, doi:10.7554/eLife.43627 (2019).
49 Piskounova, E. *et al.* Oxidative stress inhibits distant metastasis by human melanoma cells. *Nature* **527**, 186-191, doi:10.1038/nature15726 (2015).
50 Chen, J. *et al.* Gain of glucose-independent growth upon metastasis of breast cancer cells to the brain. *Cancer Res* **75**, 554-565, doi:10.1158/0008-5472.CAN-14-2268 (2015).
51 Knott, S. R. V. *et al.* Asparagine bioavailability governs metastasis in a model of breast cancer. *Nature* **554**, 378-381, doi:10.1038/nature25465 (2018).
52 Yamaguchi, N. *et al.* PCK1 and DHODH drive colorectal cancer liver metastatic colonization and hypoxic growth by promoting nucleotide synthesis. *Elife* **8**, doi:10.7554/eLife.52135 (2019).
53 Nguyen, A. *et al.* PKLR promotes colorectal cancer liver colonization through induction of glutathione synthesis. *J Clin Invest* **126**, 681-694, doi:10.1172/JCI83587 (2016).
54 Dupuy, F. *et al.* PDK1-Dependent Metabolic Reprogramming Dictates Metastatic Potential in Breast Cancer. *Cell Metab* **22**, 577-589, doi:10.1016/j.cmet.2015.08.007 (2015).
55 Pascual, G. *et al.* Targeting metastasis-initiating cells through the fatty acid receptor CD36. *Nature* **541**, 41-45, doi:10.1038/nature20791 (2017).
56 Jin, X. *et al.* A metastasis map of human cancer cell lines. *Nature* **588**, 331-336, doi:10.1038/s41586-020-2969-2 (2020).
57 Gupta, P. B., Pastushenko, I., Skibinski, A., Blanpain, C. & Kuperwasser, C. Phenotypic Plasticity: Driver of Cancer Initiation, Progression, and Therapy Resistance. *Cell Stem Cell* **24**, 65-78, doi:10.1016/j.stem.2018.11.011 (2019).
58 Yuan, S., Norgard, R. J. & Stanger, B. Z. Cellular Plasticity in Cancer. *Cancer Discov* **9**, 837-851, doi:10.1158/2159-8290.CD-19-0015 (2019).
59 Varga, J. & Greten, F. R. Cell plasticity in epithelial homeostasis and tumorigenesis. *Nat Cell Biol* **19**, 1133-1141, doi:10.1038/ncb3611 (2017).
60 Biswas, D. *et al.* A clonal expression biomarker associates with lung cancer mortality. *Nat Med* **25**, 1540-1548, doi:10.1038/s41591-019-0595-z (2019).
61 Hu, Z., Li, Z., Ma, Z. & Curtis, C. Multi-cancer analysis of clonality and the timing of systemic spread in paired primary tumors and metastases. *Nat Genet* **52**, 701-708, doi:10.1038/s41588-020-0628-z (2020).
62 Reiter, J. G. *et al.* Minimal functional driver gene heterogeneity among untreated metastases. *Science* **361**, 1033-1037, doi:10.1126/science.aat7171 (2018).
63 Turajlic, S. & Swanton, C. Metastasis as an evolutionary process. *Science* **352**, 169-175, doi:10.1126/science.aaf2784 (2016).
64 Zhao, Z. M. *et al.* Early and multiple origins of metastatic lineages within primary tumors. *Proc Natl Acad Sci U S A* **113**, 2140-2145, doi:10.1073/pnas.1525677113 (2016).

65 Robinson, D. R. *et al.* Integrative clinical genomics of metastatic cancer. *Nature* **548**, 297-303, doi:10.1038/nature23306 (2017).
66 Jamal-Hanjani, M. *et al.* Tracking the Evolution of Non-Small-Cell Lung Cancer. *N Engl J Med* **376**, 2109-2121, doi:10.1056/NEJMoa1616288 (2017).
67 Denny, S. K. *et al.* Nfib Promotes Metastasis through a Widespread Increase in Chromatin Accessibility. *Cell* **166**, 328-342, doi:10.1016/j.cell.2016.05.052 (2016).
68 Ganesh, K. *et al.* L1CAM defines the regenerative origin of metastasis-initiating cells in colorectal cancer. *Nat Cancer* **1**, 28-45, doi:10.1038/s43018-019-0006-x (2020).
69 LaFave, L. M. *et al.* Epigenomic State Transitions Characterize Tumor Progression in Mouse Lung Adenocarcinoma. *Cancer Cell* **38**, 212-228 e213, doi:10.1016/j.ccell.2020.06.006 (2020).
70 Latil, M. *et al.* Cell-Type-Specific Chromatin States Differentially Prime Squamous Cell Carcinoma Tumor-Initiating Cells for Epithelial to Mesenchymal Transition. *Cell Stem Cell* **20**, 191-204 e195, doi:10.1016/j.stem.2016.10.018 (2017).
71 Roe, J. S. *et al.* Enhancer Reprogramming Promotes Pancreatic Cancer Metastasis. *Cell* **170**, 875-888 e820, doi:10.1016/j.cell.2017.07.007 (2017).
72 Vanharanta, S. *et al.* Epigenetic expansion of VHL-HIF signal output drives multiorgan metastasis in renal cancer. *Nat Med* **19**, 50-56, doi:10.1038/nm.3029 (2013).
73 Gomes, A. P. *et al.* Dynamic Incorporation of Histone H3 Variants into Chromatin Is Essential for Acquisition of Aggressive Traits and Metastatic Colonization. *Cancer Cell* **36**, 402-417 e413, doi:10.1016/j.ccell.2019.08.006 (2019).
74 Yuan, S. *et al.* Global Regulation of the Histone Mark H3K36me2 Underlies Epithelial Plasticity and Metastatic Progression. *Cancer Discov* **10**, 854-871, doi:10.1158/2159-8290.CD-19-1299 (2020).
75 de Sousa, E. M. F. & de Sauvage, F. J. Cellular Plasticity in Intestinal Homeostasis and Disease. *Cell Stem Cell* **24**, 54-64, doi:10.1016/j.stem.2018.11.019 (2019).
76 Dekoninck, S. & Blanpain, C. Stem cell dynamics, migration and plasticity during wound healing. *Nat Cell Biol* **21**, 18-24, doi:10.1038/s41556-018-0237-6 (2019).
77 Barker, N. *et al.* Identification of stem cells in small intestine and colon by marker gene Lgr5. *Nature* **449**, 1003-1007, doi:10.1038/nature06196 (2007).
78 Ayyaz, A. *et al.* Single-cell transcriptomes of the regenerating intestine reveal a revival stem cell. *Nature* **569**, 121-125, doi:10.1038/s41586-019-1154-y (2019).
79 Tian, H. *et al.* A reserve stem cell population in small intestine renders Lgr5-positive cells dispensable. *Nature* **478**, 255-259, doi:10.1038/nature10408 (2011).

80 Serra, D. *et al.* Self-organization and symmetry breaking in intestinal organoid development. *Nature* **569**, 66-72, doi:10.1038/s41586-019-1146-y (2019).
81 Fumagalli, A. *et al.* Plasticity of Lgr5-Negative Cancer Cells Drives Metastasis in Colorectal Cancer. *Cell Stem Cell* **26**, 569-578 e567, doi:10.1016/j.stem.2020.02.008 (2020).
82 Han, T. *et al.* Lineage Reversion Drives WNT Independence in Intestinal Cancer. *Cancer Discov* **10**, 1590-1609, doi:10.1158/2159-8290.CD-19-1536 (2020).
83 Morral, C. *et al.* Zonation of Ribosomal DNA Transcription Defines a Stem Cell Hierarchy in Colorectal Cancer. *Cell Stem Cell* **26**, 845-861 e812, doi:10.1016/j.stem.2020.04.012 (2020).
84 Altevogt, P., Doberstein, K. & Fogel, M. L1CAM in human cancer. *Int J Cancer* **138**, 1565-1576, doi:10.1002/ijc.29658 (2016).
85 Siegel, R. L., Miller, K. D., Fuchs, H. E. & Jemal, A. Cancer statistics, 2022. *CA Cancer J Clin* **72**, 7-33, doi:10.3322/caac.21708 (2022).
86 Thai, A. A., Solomon, B. J., Sequist, L. V., Gainor, J. F. & Heist, R. S. Lung cancer. *Lancet* **398**, 535-554, doi:10.1016/S0140-6736(21)00312-3 (2021).
87 Howlader, N. *et al.* The Effect of Advances in Lung-Cancer Treatment on Population Mortality. *N Engl J Med* **383**, 640-649, doi:10.1056/NEJMoa1916623 (2020).
88 Herbst, R. S., Morgensztern, D. & Boshoff, C. The biology and management of non-small cell lung cancer. *Nature* **553**, 446-454, doi:10.1038/nature25183 (2018).
89 Zappa, C. & Mousa, S. A. Non-small cell lung cancer: current treatment and future advances. *Transl Lung Cancer Res* **5**, 288-300, doi:10.21037/tlcr.2016.06.07 (2016).
90 Islami, F. *et al.* Proportion and number of cancer cases and deaths attributable to potentially modifiable risk factors in the United States. *CA Cancer J Clin* **68**, 31-54, doi:10.3322/caac.21440 (2018).
91 Asselin-Labat, M. L. & Filby, C. E. Adult lung stem cells and their contribution to lung tumourigenesis. *Open Biol* **2**, 120094, doi:10.1098/rsob.120094 (2012).
92 Sainz de Aja, J., Dost, A. F. M. & Kim, C. F. Alveolar progenitor cells and the origin of lung cancer. *J Intern Med* **289**, 629-635, doi:10.1111/joim.13201 (2021).
93 Ding, L. *et al.* Somatic mutations affect key pathways in lung adenocarcinoma. *Nature* **455**, 1069-1075, doi:10.1038/nature07423 (2008).
94 Dogan, S. *et al.* Molecular epidemiology of EGFR and KRAS mutations in 3,026 lung adenocarcinomas: higher susceptibility of women to smoking-related KRAS-mutant cancers. *Clin Cancer Res* **18**, 6169-6177, doi:10.1158/1078-0432.CCR-11-3265 (2012).
95 Karatrasoglou, E. A. *et al.* Association between PD-L1 expression and driver gene mutations in non-small cell lung cancer patients: correlation

with clinical data. *Virchows Arch* **477**, 207-217, doi:10.1007/s00428-020-02756-1 (2020).
96 Nakajima, E. C. *et al.* FDA Approval Summary: Sotorasib for KRAS G12C-Mutated Metastatic NSCLC. *Clin Cancer Res* **28**, 1482-1486, doi:10.1158/1078-0432.CCR-21-3074 (2022).
97 Spagnuolo, A., Maione, P. & Gridelli, C. The treatment of advanced non-small cell lung cancer harboring KRAS mutation: a new class of drugs for an old target-a narrative review. *Transl Lung Cancer Res* **11**, 1199-1216, doi:10.21037/tlcr-21-948 (2022).
98 Skoulidis, F. *et al.* Sotorasib for Lung Cancers with KRAS p.G12C Mutation. *N Engl J Med* **384**, 2371-2381, doi:10.1056/NEJMoa2103695 (2021).
99 Parsons, S., Maldonado, E. B. & Prasad, V. Comparison of Drugs Used for Adjuvant and Metastatic Therapy of Colon, Breast, and Non-Small Cell Lung Cancers. *JAMA Netw Open* **3**, e202488, doi:10.1001/jamanetworkopen.2020.2488 (2020).
100 Karacz, C. M., Yan, J., Zhu, H. & Gerber, D. E. Timing, Sites, and Correlates of Lung Cancer Recurrence. *Clin Lung Cancer* **21**, 127-135 e123, doi:10.1016/j.cllc.2019.12.001 (2020).
101 Uramoto, H. & Tanaka, F. Recurrence after surgery in patients with NSCLC. *Transl Lung Cancer Res* **3**, 242-249, doi:10.3978/j.issn.2218-6751.2013.12.05 (2014).
102 Hutter, C. & Zenklusen, J. C. The Cancer Genome Atlas: Creating Lasting Value beyond Its Data. *Cell* **173**, 283-285, doi:10.1016/j.cell.2018.03.042 (2018).
103 Laughney, A. M. *et al.* Regenerative lineages and immune-mediated pruning in lung cancer metastasis. *Nat Med* **26**, 259-269, doi:10.1038/s41591-019-0750-6 (2020).
104 Marjanovic, N. D. *et al.* Emergence of a High-Plasticity Cell State during Lung Cancer Evolution. *Cancer Cell* **38**, 229-246 e213, doi:10.1016/j.ccell.2020.06.012 (2020).
105 Zhou, S. *et al.* The ABC transporter Bcrp1/ABCG2 is expressed in a wide variety of stem cells and is a molecular determinant of the side-population phenotype. *Nat Med* **7**, 1028-1034, doi:10.1038/nm0901-1028 (2001).
106 Obenauf, A. C. *et al.* Therapy-induced tumour secretomes promote resistance and tumour progression. *Nature* **520**, 368-372, doi:10.1038/nature14336 (2015).
107 Faget, D. V., Ren, Q. & Stewart, S. A. Unmasking senescence: context-dependent effects of SASP in cancer. *Nat Rev Cancer* **19**, 439-453, doi:10.1038/s41568-019-0156-2 (2019).
108 Gajewski, T. F. *et al.* Immune resistance orchestrated by the tumor microenvironment. *Immunol Rev* **213**, 131-145, doi:10.1111/j.1600-065X.2006.00442.x (2006).
109 Gajewski, T. F. *et al.* Cancer immunotherapy strategies based on overcoming barriers within the tumor microenvironment. *Curr Opin Immunol* **25**, 268-276, doi:10.1016/j.coi.2013.02.009 (2013).

110 Jenkins, R. W., Barbie, D. A. & Flaherty, K. T. Mechanisms of resistance to immune checkpoint inhibitors. *Br J Cancer* **118**, 9-16, doi:10.1038/bjc.2017.434 (2018).
111 Bailey, J. M. *et al.* Sonic hedgehog promotes desmoplasia in pancreatic cancer. *Clin Cancer Res* **14**, 5995-6004, doi:10.1158/1078-0432.CCR-08-0291 (2008).
112 Olive, K. P. *et al.* Inhibition of Hedgehog signaling enhances delivery of chemotherapy in a mouse model of pancreatic cancer. *Science* **324**, 1457-1461, doi:10.1126/science.1171362 (2009).
113 Quail, D. F. *et al.* The tumor microenvironment underlies acquired resistance to CSF-1R inhibition in gliomas. *Science* **352**, aad3018, doi:10.1126/science.aad3018 (2016).
114 Rathjen, F. G. & Schachner, M. Immunocytological and biochemical characterization of a new neuronal cell surface component (L1 antigen) which is involved in cell adhesion. *EMBO J* **3**, 1-10, doi:10.1002/j.1460-2075.1984.tb01753.x (1984).
115 Moos, M. *et al.* Neural adhesion molecule L1 as a member of the immunoglobulin superfamily with binding domains similar to fibronectin. *Nature* **334**, 701-703, doi:10.1038/334701a0 (1988).
116 Maten, M. V., Reijnen, C., Pijnenborg, J. M. A. & Zegers, M. M. L1 Cell Adhesion Molecule in Cancer, a Systematic Review on Domain-Specific Functions. *Int J Mol Sci* **20**, doi:10.3390/ijms20174180 (2019).
117 Maness, P. F. & Schachner, M. Neural recognition molecules of the immunoglobulin superfamily: signaling transducers of axon guidance and neuronal migration. *Nat Neurosci* **10**, 19-26, doi:10.1038/nn1827 (2007).
118 Dahme, M. *et al.* Disruption of the mouse L1 gene leads to malformations of the nervous system. *Nat Genet* **17**, 346-349, doi:10.1038/ng1197-346 (1997).
119 Fransen, E. *et al.* L1 knockout mice show dilated ventricles, vermis hypoplasia and impaired exploration patterns. *Hum Mol Genet* **7**, 999-1009, doi:10.1093/hmg/7.6.999 (1998).
120 Fransen, E., Van Camp, G., Vits, L. & Willems, P. J. L1-associated diseases: clinical geneticists divide, molecular geneticists unite. *Hum Mol Genet* **6**, 1625-1632, doi:10.1093/hmg/6.10.1625 (1997).
121 Gorka, B. *et al.* NrCAM, a neuronal system cell-adhesion molecule, is induced in papillary thyroid carcinomas. *Br J Cancer* **97**, 531-538, doi:10.1038/sj.bjc.6603915 (2007).
122 He, L. H. *et al.* CHL1 is involved in human breast tumorigenesis and progression. *Biochem Biophys Res Commun* **438**, 433-438, doi:10.1016/j.bbrc.2013.07.093 (2013).
123 Brummendorf, T., Kenwrick, S. & Rathjen, F. G. Neural cell recognition molecule L1: from cell biology to human hereditary brain malformations. *Curr Opin Neurobiol* **8**, 87-97, doi:10.1016/s0959-4388(98)80012-3 (1998).
124 Kulahin, N. *et al.* Fibronectin type III (FN3) modules of the neuronal cell adhesion molecule L1 interact directly with the fibroblast growth factor

(FGF) receptor. *Mol Cell Neurosci* **37**, 528-536, doi:10.1016/j.mcn.2007.12.001 (2008).
125 Nagaraj, K. *et al.* Pathogenic human L1-CAM mutations reduce the adhesion-dependent activation of EGFR. *Hum Mol Genet* **18**, 3822-3831, doi:10.1093/hmg/ddp325 (2009).
126 Loers, G. & Schachner, M. Recognition molecules and neural repair. *J Neurochem* **101**, 865-882, doi:10.1111/j.1471-4159.2006.04409.x (2007).
127 Herron, L. R., Hill, M., Davey, F. & Gunn-Moore, F. J. The intracellular interactions of the L1 family of cell adhesion molecules. *Biochem J* **419**, 519-531, doi:10.1042/BJ20082284 (2009).
128 Mechtersheimer, S. *et al.* Ectodomain shedding of L1 adhesion molecule promotes cell migration by autocrine binding to integrins. *J Cell Biol* **155**, 661-673, doi:10.1083/jcb.200101099 (2001).
129 Pancook, J. D. *et al.* Expression and regulation of the neural cell adhesion molecule L1 on human cells of myelomonocytic and lymphoid origin. *J Immunol* **158**, 4413-4421 (1997).
130 Doberstein, K. *et al.* L1-CAM expression in ccRCC correlates with shorter patients survival times and confers chemoresistance in renal cell carcinoma cells. *Carcinogenesis* **32**, 262-270, doi:10.1093/carcin/bgq249 (2011).
131 Gavert, N. *et al.* L1, a novel target of beta-catenin signaling, transforms cells and is expressed at the invasive front of colon cancers. *J Cell Biol* **168**, 633-642, doi:10.1083/jcb.200408051 (2005).
132 Geismann, C. *et al.* Up-regulation of L1CAM in pancreatic duct cells is transforming growth factor beta1- and slug-dependent: role in malignant transformation of pancreatic cancer. *Cancer Res* **69**, 4517-4526, doi:10.1158/0008-5472.CAN-08-3493 (2009).
133 Huszar, M. *et al.* Up-regulation of L1CAM is linked to loss of hormone receptors and E-cadherin in aggressive subtypes of endometrial carcinomas. *J Pathol* **220**, 551-561, doi:10.1002/path.2673 (2010).
134 Pfeifer, M. *et al.* L1CAM expression in endometrial carcinomas is regulated by usage of two different promoter regions. *BMC Mol Biol* **11**, 64, doi:10.1186/1471-2199-11-64 (2010).
135 Kallunki, P., Edelman, G. M. & Jones, F. S. Tissue-specific expression of the L1 cell adhesion molecule is modulated by the neural restrictive silencer element. *J Cell Biol* **138**, 1343-1354, doi:10.1083/jcb.138.6.1343 (1997).
136 Ballas, N. & Mandel, G. The many faces of REST oversee epigenetic programming of neuronal genes. *Curr Opin Neurobiol* **15**, 500-506, doi:10.1016/j.conb.2005.08.015 (2005).
137 Majumder, S. REST in good times and bad: roles in tumor suppressor and oncogenic activities. *Cell Cycle* **5**, 1929-1935, doi:10.4161/cc.5.17.2982 (2006).
138 Wagoner, M. P. *et al.* The transcription factor REST is lost in aggressive breast cancer. *PLoS Genet* **6**, e1000979, doi:10.1371/journal.pgen.1000979 (2010).

139 Kreisler, A. *et al.* Regulation of the NRSF/REST gene by methylation and CREB affects the cellular phenotype of small-cell lung cancer. *Oncogene* **29**, 5828-5838, doi:10.1038/onc.2010.321 (2010).
140 Chong, Y. *et al.* MicroRNA-503 acts as a tumor suppressor in osteosarcoma by targeting L1CAM. *PLoS One* **9**, e114585, doi:10.1371/journal.pone.0114585 (2014).
141 Doberstein, K. *et al.* miR-21-3p is a positive regulator of L1CAM in several human carcinomas. *Cancer Lett* **354**, 455-466, doi:10.1016/j.canlet.2014.08.020 (2014).
142 Schirmer, U. *et al.* Role of miR-34a as a suppressor of L1CAM in endometrial carcinoma. *Oncotarget* **5**, 462-472, doi:10.18632/oncotarget.1552 (2014).
143 Kato, K. *et al.* DNA hypomethylation at the CpG island is involved in aberrant expression of the L1 cell adhesion molecule gene in colorectal cancer. *Int J Oncol* **35**, 467-476, doi:10.3892/ijo_00000358 (2009).
144 Schirmer, U. *et al.* Epigenetic regulation of L1CAM in endometrial carcinoma: comparison to cancer-testis (CT-X) antigens. *BMC Cancer* **13**, 156, doi:10.1186/1471-2407-13-156 (2013).
145 Gavert, N., Vivanti, A., Hazin, J., Brabletz, T. & Ben-Ze'ev, A. L1-mediated colon cancer cell metastasis does not require changes in EMT and cancer stem cell markers. *Mol Cancer Res* **9**, 14-24, doi:10.1158/1541-7786.MCR-10-0406 (2011).
146 Shapiro, B., Tocci, P., Haase, G., Gavert, N. & Ben-Ze'ev, A. Clusterin, a gene enriched in intestinal stem cells, is required for L1-mediated colon cancer metastasis. *Oncotarget* **6**, 34389-34401, doi:10.18632/oncotarget.5360 (2015).
147 Basu, S., Gavert, N., Brabletz, T. & Ben-Ze'ev, A. The intestinal stem cell regulating gene ASCL2 is required for L1-mediated colon cancer progression. *Cancer Lett* **424**, 9-18, doi:10.1016/j.canlet.2018.03.022 (2018).
148 Fang, Q. X., Zheng, X. C. & Zhao, H. J. L1CAM is involved in lymph node metastasis via ERK1/2 signaling in colorectal cancer. *Am J Transl Res* **12**, 837-846 (2020).
149 Novak-Hofer, I. The L1 cell adhesion molecule as a target for radioimmunotherapy. *Cancer Biother Radiopharm* **22**, 175-184, doi:10.1089/cbr.2007.342 (2007).
150 Weidle, U. H., Eggle, D. & Klostermann, S. L1-CAM as a target for treatment of cancer with monoclonal antibodies. *Anticancer Res* **29**, 4919-4931 (2009).
151 Wolterink, S. *et al.* Therapeutic antibodies to human L1CAM: functional characterization and application in a mouse model for ovarian carcinoma. *Cancer Res* **70**, 2504-2515, doi:10.1158/0008-5472.CAN-09-3730 (2010).
152 Giordano, M. & Cavallaro, U. Different Shades of L1CAM in the Pathophysiology of Cancer Stem Cells. *J Clin Med* **9**, doi:10.3390/jcm9051502 (2020).

153 Song, I. H. *et al.* Development of a Theranostic Convergence Bioradiopharmaceutical for Immuno-PET Based Radioimmunotherapy of L1CAM in Cholangiocarcinoma Model. *Clin Cancer Res* **25**, 6148-6159, doi:10.1158/1078-0432.CCR-19-1157 (2019).
154 Hoefnagel, C. A. *et al.* A comparison of targeting of neuroblastoma with mIBG and anti L1-CAM antibody mAb chCE7: therapeutic efficacy in a neuroblastoma xenograft model and imaging of neuroblastoma patients. *Eur J Nucl Med* **28**, 359-368 (2001).
155 Andersch, L. *et al.* CD171- and GD2-specific CAR-T cells potently target retinoblastoma cells in preclinical in vitro testing. *BMC Cancer* **19**, 895, doi:10.1186/s12885-019-6131-1 (2019).
156 Hong, H. *et al.* L1 Cell Adhesion Molecule-Specific Chimeric Antigen Receptor-Redirected Human T Cells Exhibit Specific and Efficient Antitumor Activity against Human Ovarian Cancer in Mice. *PLoS One* **11**, e0146885, doi:10.1371/journal.pone.0146885 (2016).
157 Park, J. R. *et al.* Adoptive transfer of chimeric antigen receptor re-directed cytolytic T lymphocyte clones in patients with neuroblastoma. *Mol Ther* **15**, 825-833, doi:10.1038/sj.mt.6300104 (2007).
158 Butler, M. T. & Wallingford, J. B. Planar cell polarity in development and disease. *Nat Rev Mol Cell Biol* **18**, 375-388, doi:10.1038/nrm.2017.11 (2017).
159 Davey, C. F. & Moens, C. B. Planar cell polarity in moving cells: think globally, act locally. *Development* **144**, 187-200, doi:10.1242/dev.122804 (2017).
160 Adler, P. N. The frizzled/stan pathway and planar cell polarity in the Drosophila wing. *Curr Top Dev Biol* **101**, 1-31, doi:10.1016/B978-0-12-394592-1.00001-6 (2012).
161 Goodrich, L. V. & Strutt, D. Principles of planar polarity in animal development. *Development* **138**, 1877-1892, doi:10.1242/dev.054080 (2011).
162 Lawrence, P. A. & Casal, J. The mechanisms of planar cell polarity, growth and the Hippo pathway: some known unknowns. *Dev Biol* **377**, 1-8, doi:10.1016/j.ydbio.2013.01.030 (2013).
163 Peng, Y. & Axelrod, J. D. Asymmetric protein localization in planar cell polarity: mechanisms, puzzles, and challenges. *Curr Top Dev Biol* **101**, 33-53, doi:10.1016/B978-0-12-394592-1.00002-8 (2012).
164 Yang, Y. & Mlodzik, M. Wnt-Frizzled/planar cell polarity signaling: cellular orientation by facing the wind (Wnt). *Annu Rev Cell Dev Biol* **31**, 623-646, doi:10.1146/annurev-cellbio-100814-125315 (2015).
165 Chen, W. S. *et al.* Asymmetric homotypic interactions of the atypical cadherin flamingo mediate intercellular polarity signaling. *Cell* **133**, 1093-1105, doi:10.1016/j.cell.2008.04.048 (2008).
166 Lawrence, P. A., Casal, J. & Struhl, G. Cell interactions and planar polarity in the abdominal epidermis of Drosophila. *Development* **131**, 4651-4664, doi:10.1242/dev.01351 (2004).

167 Strutt, H. & Strutt, D. Differential stability of flamingo protein complexes underlies the establishment of planar polarity. *Curr Biol* **18**, 1555-1564, doi:10.1016/j.cub.2008.08.063 (2008).
168 Usui, T. *et al.* Flamingo, a seven-pass transmembrane cadherin, regulates planar cell polarity under the control of Frizzled. *Cell* **98**, 585-595, doi:10.1016/s0092-8674(00)80046-x (1999).
169 Struhl, G., Casal, J. & Lawrence, P. A. Dissecting the molecular bridges that mediate the function of Frizzled in planar cell polarity. *Development* **139**, 3665-3674, doi:10.1242/dev.083550 (2012).
170 Jenny, A., Darken, R. S., Wilson, P. A. & Mlodzik, M. Prickle and Strabismus form a functional complex to generate a correct axis during planar cell polarity signaling. *EMBO J* **22**, 4409-4420, doi:10.1093/emboj/cdg424 (2003).
171 Jenny, A., Reynolds-Kenneally, J., Das, G., Burnett, M. & Mlodzik, M. Diego and Prickle regulate Frizzled planar cell polarity signalling by competing for Dishevelled binding. *Nat Cell Biol* **7**, 691-697, doi:10.1038/ncb1271 (2005).
172 Boutros, M., Paricio, N., Strutt, D. I. & Mlodzik, M. Dishevelled activates JNK and discriminates between JNK pathways in planar polarity and wingless signaling. *Cell* **94**, 109-118, doi:10.1016/s0092-8674(00)81226-x (1998).
173 Eaton, S., Wepf, R. & Simons, K. Roles for Rac1 and Cdc42 in planar polarization and hair outgrowth in the wing of Drosophila. *J Cell Biol* **135**, 1277-1289, doi:10.1083/jcb.135.5.1277 (1996).
174 Paricio, N., Feiguin, F., Boutros, M., Eaton, S. & Mlodzik, M. The Drosophila STE20-like kinase misshapen is required downstream of the Frizzled receptor in planar polarity signaling. *EMBO J* **18**, 4669-4678, doi:10.1093/emboj/18.17.4669 (1999).
175 Winter, C. G. *et al.* Drosophila Rho-associated kinase (Drok) links Frizzled-mediated planar cell polarity signaling to the actin cytoskeleton. *Cell* **105**, 81-91, doi:10.1016/s0092-8674(01)00298-7 (2001).
176 Wu, J., Roman, A. C., Carvajal-Gonzalez, J. M. & Mlodzik, M. Wg and Wnt4 provide long-range directional input to planar cell polarity orientation in Drosophila. *Nat Cell Biol* **15**, 1045-1055, doi:10.1038/ncb2806 (2013).
177 Chu, C. W. & Sokol, S. Y. Wnt proteins can direct planar cell polarity in vertebrate ectoderm. *Elife* **5**, doi:10.7554/eLife.16463 (2016).
178 Heisenberg, C. P. *et al.* Silberblick/Wnt11 mediates convergent extension movements during zebrafish gastrulation. *Nature* **405**, 76-81, doi:10.1038/35011068 (2000).
179 Qian, D. *et al.* Wnt5a functions in planar cell polarity regulation in mice. *Dev Biol* **306**, 121-133, doi:10.1016/j.ydbio.2007.03.011 (2007).
180 Carvajal-Gonzalez, J. M., Roman, A. C. & Mlodzik, M. Positioning of centrioles is a conserved readout of Frizzled planar cell polarity signalling. *Nat Commun* **7**, 11135, doi:10.1038/ncomms11135 (2016).

181 Wallingford, J. B. Planar cell polarity and the developmental control of cell behavior in vertebrate embryos. *Annu Rev Cell Dev Biol* **28**, 627-653, doi:10.1146/annurev-cellbio-092910-154208 (2012).
182 Tada, M. & Smith, J. C. Xwnt11 is a target of Xenopus Brachyury: regulation of gastrulation movements via Dishevelled, but not through the canonical Wnt pathway. *Development* **127**, 2227-2238, doi:10.1242/dev.127.10.2227 (2000).
183 Wallingford, J. B. *et al.* Dishevelled controls cell polarity during Xenopus gastrulation. *Nature* **405**, 81-85, doi:10.1038/35011077 (2000).
184 Carmona-Fontaine, C. *et al.* Contact inhibition of locomotion in vivo controls neural crest directional migration. *Nature* **456**, 957-961, doi:10.1038/nature07441 (2008).
185 Theveneau, E. *et al.* Collective chemotaxis requires contact-dependent cell polarity. *Dev Cell* **19**, 39-53, doi:10.1016/j.devcel.2010.06.012 (2010).
186 Chai, G., Goffinet, A. M. & Tissir, F. Celsr3 and Fzd3 in axon guidance. *Int J Biochem Cell Biol* **64**, 11-14, doi:10.1016/j.biocel.2015.03.013 (2015).
187 Qu, Y. *et al.* Genetic evidence that Celsr3 and Celsr2, together with Fzd3, regulate forebrain wiring in a Vangl-independent manner. *Proc Natl Acad Sci U S A* **111**, E2996-3004, doi:10.1073/pnas.1402105111 (2014).
188 Glasco, D. M. *et al.* The mouse Wnt/PCP protein Vangl2 is necessary for migration of facial branchiomotor neurons, and functions independently of Dishevelled. *Dev Biol* **369**, 211-222, doi:10.1016/j.ydbio.2012.06.021 (2012).
189 Qu, Y. *et al.* Atypical cadherins Celsr1-3 differentially regulate migration of facial branchiomotor neurons in mice. *J Neurosci* **30**, 9392-9401, doi:10.1523/JNEUROSCI.0124-10.2010 (2010).
190 Yang, T., Bassuk, A. G., Stricker, S. & Fritzsch, B. Prickle1 is necessary for the caudal migration of murine facial branchiomotor neurons. *Cell Tissue Res* **357**, 549-561, doi:10.1007/s00441-014-1925-6 (2014).
191 Gerdes, J. M. *et al.* Disruption of the basal body compromises proteasomal function and perturbs intracellular Wnt response. *Nat Genet* **39**, 1350-1360, doi:10.1038/ng.2007.12 (2007).
192 Ross, A. J. *et al.* Disruption of Bardet-Biedl syndrome ciliary proteins perturbs planar cell polarity in vertebrates. *Nat Genet* **37**, 1135-1140, doi:10.1038/ng1644 (2005).
193 Simons, M. *et al.* Inversin, the gene product mutated in nephronophthisis type II, functions as a molecular switch between Wnt signaling pathways. *Nat Genet* **37**, 537-543, doi:10.1038/ng1552 (2005).
194 Anastas, J. N. *et al.* A protein complex of SCRIB, NOS1AP and VANGL1 regulates cell polarity and migration, and is associated with breast cancer progression. *Oncogene* **31**, 3696-3708, doi:10.1038/onc.2011.528 (2012).
195 Gujral, T. S. *et al.* A noncanonical Frizzled2 pathway regulates epithelial-mesenchymal transition and metastasis. *Cell* **159**, 844-856, doi:10.1016/j.cell.2014.10.032 (2014).

196 Luga, V. *et al.* Exosomes mediate stromal mobilization of autocrine Wnt-PCP signaling in breast cancer cell migration. *Cell* **151**, 1542-1556, doi:10.1016/j.cell.2012.11.024 (2012).
197 MacMillan, C. D. *et al.* Stage of breast cancer progression influences cellular response to activation of the WNT/planar cell polarity pathway. *Sci Rep* **4**, 6315, doi:10.1038/srep06315 (2014).
198 Yamamoto, H. *et al.* Wnt5a signaling is involved in the aggressiveness of prostate cancer and expression of metalloproteinase. *Oncogene* **29**, 2036-2046, doi:10.1038/onc.2009.496 (2010).
199 Zhang, L. *et al.* A lateral signalling pathway coordinates shape volatility during cell migration. *Nat Commun* **7**, 11714, doi:10.1038/ncomms11714 (2016).
200 Rodriguez-Hernandez, I. *et al.* WNT11-FZD7-DAAM1 signalling supports tumour initiating abilities and melanoma amoeboid invasion. *Nat Commun* **11**, 5315, doi:10.1038/s41467-020-18951-2 (2020).
201 Marshall, W. F. & Rosenbaum, J. L. Intraflagellar transport balances continuous turnover of outer doublet microtubules: implications for flagellar length control. *J Cell Biol* **155**, 405-414, doi:10.1083/jcb.200106141 (2001).
202 Long, H. & Huang, K. Transport of Ciliary Membrane Proteins. *Front Cell Dev Biol* **7**, 381, doi:10.3389/fcell.2019.00381 (2019).
203 Ishikawa, H. & Marshall, W. F. Ciliogenesis: building the cell's antenna. *Nat Rev Mol Cell Biol* **12**, 222-234, doi:10.1038/nrm3085 (2011).
204 Bangs, F. & Anderson, K. V. Primary Cilia and Mammalian Hedgehog Signaling. *Cold Spring Harb Perspect Biol* **9**, doi:10.1101/cshperspect.a028175 (2017).
205 Wheway, G., Nazlamova, L. & Hancock, J. T. Signaling through the Primary Cilium. *Front Cell Dev Biol* **6**, 8, doi:10.3389/fcell.2018.00008 (2018).
206 Ezratty, E. J., Pasolli, H. A. & Fuchs, E. A Presenilin-2-ARF4 trafficking axis modulates Notch signaling during epidermal differentiation. *J Cell Biol* **214**, 89-101, doi:10.1083/jcb.201508082 (2016).
207 Ezratty, E. J. *et al.* A role for the primary cilium in Notch signaling and epidermal differentiation during skin development. *Cell* **145**, 1129-1141, doi:10.1016/j.cell.2011.05.030 (2011).
208 Huang, P. & Schier, A. F. Dampened Hedgehog signaling but normal Wnt signaling in zebrafish without cilia. *Development* **136**, 3089-3098, doi:10.1242/dev.041343 (2009).
209 Ocbina, P. J., Tuson, M. & Anderson, K. V. Primary cilia are not required for normal canonical Wnt signaling in the mouse embryo. *PLoS One* **4**, e6839, doi:10.1371/journal.pone.0006839 (2009).
210 Abdelhamed, Z. A. *et al.* Variable expressivity of ciliopathy neurological phenotypes that encompass Meckel-Gruber syndrome and Joubert syndrome is caused by complex de-regulated ciliogenesis, Shh and Wnt signalling defects. *Hum Mol Genet* **22**, 1358-1372, doi:10.1093/hmg/dds546 (2013).

211 Cano, D. A., Murcia, N. S., Pazour, G. J. & Hebrok, M. Orpk mouse model of polycystic kidney disease reveals essential role of primary cilia in pancreatic tissue organization. *Development* **131**, 3457-3467, doi:10.1242/dev.01189 (2004).
212 Lin, F. *et al.* Kidney-specific inactivation of the KIF3A subunit of kinesin-II inhibits renal ciliogenesis and produces polycystic kidney disease. *Proc Natl Acad Sci U S A* **100**, 5286-5291, doi:10.1073/pnas.0836980100 (2003).
213 Wheway, G. *et al.* Aberrant Wnt signalling and cellular over-proliferation in a novel mouse model of Meckel-Gruber syndrome. *Dev Biol* **377**, 55-66, doi:10.1016/j.ydbio.2013.02.015 (2013).
214 Korkaya, H. & Wicha, M. S. HER-2, notch, and breast cancer stem cells: targeting an axis of evil. *Clin Cancer Res* **15**, 1845-1847, doi:10.1158/1078-0432.CCR-08-3087 (2009).
215 de Sousa, E. M. F. & Vermeulen, L. Wnt Signaling in Cancer Stem Cell Biology. *Cancers (Basel)* **8**, doi:10.3390/cancers8070060 (2016).
216 Merchant, A. A. & Matsui, W. Targeting Hedgehog--a cancer stem cell pathway. *Clin Cancer Res* **16**, 3130-3140, doi:10.1158/1078-0432.CCR-09-2846 (2010).
217 Menzl, I. *et al.* Loss of primary cilia occurs early in breast cancer development. *Cilia* **3**, 7, doi:10.1186/2046-2530-3-7 (2014).
218 Yuan, K. *et al.* Primary cilia are decreased in breast cancer: analysis of a collection of human breast cancer cell lines and tissues. *J Histochem Cytochem* **58**, 857-870, doi:10.1369/jhc.2010.955856 (2010).
219 Hassounah, N. B. *et al.* Inhibition of Ciliogenesis Promotes Hedgehog Signaling, Tumorigenesis, and Metastasis in Breast Cancer. *Mol Cancer Res* **15**, 1421-1430, doi:10.1158/1541-7786.MCR-17-0034 (2017).
220 Hassounah, N. B. *et al.* Primary cilia are lost in preinvasive and invasive prostate cancer. *PLoS One* **8**, e68521, doi:10.1371/journal.pone.0068521 (2013).
221 Han, Y. G. *et al.* Dual and opposing roles of primary cilia in medulloblastoma development. *Nat Med* **15**, 1062-1065, doi:10.1038/nm.2020 (2009).
222 Wong, S. Y. *et al.* Primary cilia can both mediate and suppress Hedgehog pathway-dependent tumorigenesis. *Nat Med* **15**, 1055-1061, doi:10.1038/nm.2011 (2009).
223 Risson, E., Nobre, A. R., Maguer-Satta, V. & Aguirre-Ghiso, J. A. The current paradigm and challenges ahead for the dormancy of disseminated tumor cells. *Nat Cancer* **1**, 672-680, doi:10.1038/s43018-020-0088-5 (2020).
224 Vera-Ramirez, L., Vodnala, S. K., Nini, R., Hunter, K. W. & Green, J. E. Autophagy promotes the survival of dormant breast cancer cells and metastatic tumour recurrence. *Nat Commun* **9**, 1944, doi:10.1038/s41467-018-04070-6 (2018).

225 Samatov, T. R., Wicklein, D. & Tonevitsky, A. G. L1CAM: Cell adhesion and more. *Prog Histochem Cytochem* **51**, 25-32, doi:10.1016/j.proghi.2016.05.001 (2016).
226 Jung, P. *et al.* Isolation and in vitro expansion of human colonic stem cells. *Nat Med* **17**, 1225-1227, doi:10.1038/nm.2470 (2011).
227 Sato, T. *et al.* Long-term expansion of epithelial organoids from human colon, adenoma, adenocarcinoma, and Barrett's epithelium. *Gastroenterology* **141**, 1762-1772, doi:10.1053/j.gastro.2011.07.050 (2011).
228 Okayasu, I. *et al.* A novel method in the induction of reliable experimental acute and chronic ulcerative colitis in mice. *Gastroenterology* **98**, 694-702, doi:10.1016/0016-5085(90)90290-h (1990).
229 Miyoshi, H., Ajima, R., Luo, C. T., Yamaguchi, T. P. & Stappenbeck, T. S. Wnt5a potentiates TGF-beta signaling to promote colonic crypt regeneration after tissue injury. *Science* **338**, 108-113, doi:10.1126/science.1223821 (2012).
230 Madison, B. B. *et al.* Cis elements of the villin gene control expression in restricted domains of the vertical (crypt) and horizontal (duodenum, cecum) axes of the intestine. *J Biol Chem* **277**, 33275-33283, doi:10.1074/jbc.M204935200 (2002).
231 Hallmann, R. *et al.* Expression and function of laminins in the embryonic and mature vasculature. *Physiol Rev* **85**, 979-1000, doi:10.1152/physrev.00014.2004 (2005).
232 Simon-Assmann, P. *et al.* The laminins: role in intestinal morphogenesis and differentiation. *Ann N Y Acad Sci* **859**, 46-64, doi:10.1111/j.1749-6632.1998.tb11110.x (1998).
233 Kleinman, H. K. *et al.* Basement membrane complexes with biological activity. *Biochemistry* **25**, 312-318, doi:10.1021/bi00350a005 (1986).
234 Lemmon, V., Farr, K. L. & Lagenaur, C. L1-mediated axon outgrowth occurs via a homophilic binding mechanism. *Neuron* **2**, 1597-1603, doi:10.1016/0896-6273(89)90048-2 (1989).
235 Hall, H., Carbonetto, S. & Schachner, M. L1/HNK-1 carbohydrate- and beta 1 integrin-dependent neural cell adhesion to laminin-1. *J Neurochem* **68**, 544-553, doi:10.1046/j.1471-4159.1997.68020544.x (1997).
236 Barker, N. *et al.* Crypt stem cells as the cells-of-origin of intestinal cancer. *Nature* **457**, 608-611, doi:10.1038/nature07602 (2009).
237 Schwitalla, S. *et al.* Intestinal tumorigenesis initiated by dedifferentiation and acquisition of stem-cell-like properties. *Cell* **152**, 25-38, doi:10.1016/j.cell.2012.12.012 (2013).
238 Shimokawa, M. *et al.* Visualization and targeting of LGR5(+) human colon cancer stem cells. *Nature* **545**, 187-192, doi:10.1038/nature22081 (2017).
239 de Sousa e Melo, F. *et al.* A distinct role for Lgr5(+) stem cells in primary and metastatic colon cancer. *Nature* **543**, 676-680, doi:10.1038/nature21713 (2017).

240 Rompolas, P. *et al.* Spatiotemporal coordination of stem cell commitment during epidermal homeostasis. *Science* **352**, 1471-1474, doi:10.1126/science.aaf7012 (2016).
241 Tata, P. R. *et al.* Dedifferentiation of committed epithelial cells into stem cells in vivo. *Nature* **503**, 218-223, doi:10.1038/nature12777 (2013).
242 Stange, D. E. *et al.* Differentiated Troy+ chief cells act as reserve stem cells to generate all lineages of the stomach epithelium. *Cell* **155**, 357-368, doi:10.1016/j.cell.2013.09.008 (2013).
243 Yui, S. *et al.* YAP/TAZ-Dependent Reprogramming of Colonic Epithelium Links ECM Remodeling to Tissue Regeneration. *Cell Stem Cell* **22**, 35-49 e37, doi:10.1016/j.stem.2017.11.001 (2018).
244 Kiefel, H. *et al.* L1CAM: a major driver for tumor cell invasion and motility. *Cell Adh Migr* **6**, 374-384, doi:10.4161/cam.20832 (2012).
245 Rud, A. K. *et al.* Detection of disseminated tumor cells in lymph nodes from patients with early stage non-small cell lung cancer. *Diagn Pathol* **11**, 50, doi:10.1186/s13000-016-0504-4 (2016).
246 Gontan, C. *et al.* Sox2 is important for two crucial processes in lung development: branching morphogenesis and epithelial cell differentiation. *Dev Biol* **317**, 296-309, doi:10.1016/j.ydbio.2008.02.035 (2008).
247 Ochieng, J. K. *et al.* Sox2 regulates the emergence of lung basal cells by directly activating the transcription of Trp63. *Am J Respir Cell Mol Biol* **51**, 311-322, doi:10.1165/rcmb.2013-0419OC (2014).
248 Tompkins, D. H. *et al.* Sox2 activates cell proliferation and differentiation in the respiratory epithelium. *Am J Respir Cell Mol Biol* **45**, 101-110, doi:10.1165/rcmb.2010-0149OC (2011).
249 Zhang, S., Xiong, X. & Sun, Y. Functional characterization of SOX2 as an anticancer target. *Signal Transduct Target Ther* **5**, 135, doi:10.1038/s41392-020-00242-3 (2020).
250 Jackson, E. L. *et al.* Analysis of lung tumor initiation and progression using conditional expression of oncogenic K-ras. *Genes Dev* **15**, 3243-3248, doi:10.1101/gad.943001 (2001).
251 Jackson, E. L. *et al.* The differential effects of mutant p53 alleles on advanced murine lung cancer. *Cancer Res* **65**, 10280-10288, doi:10.1158/0008-5472.CAN-05-2193 (2005).
252 Winslow, M. M. *et al.* Suppression of lung adenocarcinoma progression by Nkx2-1. *Nature* **473**, 101-104, doi:10.1038/nature09881 (2011).
253 Tischler, V. *et al.* L1CAM protein expression is associated with poor prognosis in non-small cell lung cancer. *Mol Cancer* **10**, 127, doi:10.1186/1476-4598-10-127 (2011).
254 Jia, M., Yu, S., Gao, H. & Sun, P. L. Spread Through Air Spaces (STAS) in Lung Cancer: A Multiple-Perspective and Update Review. *Cancer Manag Res* **12**, 2743-2752, doi:10.2147/CMAR.S249790 (2020).
255 Sullivan, J. P. *et al.* Aldehyde dehydrogenase activity selects for lung adenocarcinoma stem cells dependent on notch signaling. *Cancer Res* **70**, 9937-9948, doi:10.1158/0008-5472.CAN-10-0881 (2010).

256 Zuo, W. *et al.* p63(+)Krt5(+) distal airway stem cells are essential for lung regeneration. *Nature* **517**, 616-620, doi:10.1038/nature13903 (2015).
257 Vaughan, A. E. *et al.* Lineage-negative progenitors mobilize to regenerate lung epithelium after major injury. *Nature* **517**, 621-625, doi:10.1038/nature14112 (2015).
258 Kim, C. F. *et al.* Identification of bronchioalveolar stem cells in normal lung and lung cancer. *Cell* **121**, 823-835, doi:10.1016/j.cell.2005.03.032 (2005).
259 Eenjes, E. *et al.* SOX21 modulates SOX2-initiated differentiation of epithelial cells in the extrapulmonary airways. *Elife* **10**, doi:10.7554/eLife.57325 (2021).
260 Lachmann, A. *et al.* ChEA: transcription factor regulation inferred from integrating genome-wide ChIP-X experiments. *Bioinformatics* **26**, 2438-2444, doi:10.1093/bioinformatics/btq466 (2010).
261 Consortium, E. P. An integrated encyclopedia of DNA elements in the human genome. *Nature* **489**, 57-74, doi:10.1038/nature11247 (2012).
262 Dhanasekaran, R. *et al.* The MYC oncogene - the grand orchestrator of cancer growth and immune evasion. *Nat Rev Clin Oncol* **19**, 23-36, doi:10.1038/s41571-021-00549-2 (2022).
263 Das, B. *et al.* MYC Regulates the HIF2alpha Stemness Pathway via Nanog and Sox2 to Maintain Self-Renewal in Cancer Stem Cells versus Non-Stem Cancer Cells. *Cancer Res* **79**, 4015-4025, doi:10.1158/0008-5472.CAN-18-2847 (2019).
264 Kwan, K. Y., Shen, J. & Corey, D. P. C-MYC transcriptionally amplifies SOX2 target genes to regulate self-renewal in multipotent otic progenitor cells. *Stem Cell Reports* **4**, 47-60, doi:10.1016/j.stemcr.2014.11.001 (2015).
265 Lusser, A., Urwin, D. L. & Kadonaga, J. T. Distinct activities of CHD1 and ACF in ATP-dependent chromatin assembly. *Nat Struct Mol Biol* **12**, 160-166, doi:10.1038/nsmb884 (2005).
266 Konev, A. Y. *et al.* CHD1 motor protein is required for deposition of histone variant H3.3 into chromatin in vivo. *Science* **317**, 1087-1090, doi:10.1126/science.1145339 (2007).
267 Gaspar-Maia, A. *et al.* Chd1 regulates open chromatin and pluripotency of embryonic stem cells. *Nature* **460**, 863-868, doi:10.1038/nature08212 (2009).
268 Lee, H. R., Yang, S. J., Choi, H. K., Kim, J. A. & Oh, I. H. The Chromatin Remodeling Complex CHD1 Regulates the Primitive State of Mesenchymal Stromal Cells to Control Their Stem Cell Supporting Activity. *Stem Cells Dev* **30**, 363-373, doi:10.1089/scd.2020.0166 (2021).
269 Griffon, A. *et al.* Integrative analysis of public ChIP-seq experiments reveals a complex multi-cell regulatory landscape. *Nucleic Acids Res* **43**, e27, doi:10.1093/nar/gku1280 (2015).
270 Hammal, F., de Langen, P., Bergon, A., Lopez, F. & Ballester, B. ReMap 2022: a database of Human, Mouse, Drosophila and Arabidopsis regulatory regions from an integrative analysis of DNA-binding sequencing

experiments. *Nucleic Acids Res* **50**, D316-D325, doi:10.1093/nar/gkab996 (2022).
271 Tomioka, M. *et al.* Identification of Sox-2 regulatory region which is under the control of Oct-3/4-Sox-2 complex. *Nucleic Acids Res* **30**, 3202-3213, doi:10.1093/nar/gkf435 (2002).
272 Zhou, H. Y. *et al.* A Sox2 distal enhancer cluster regulates embryonic stem cell differentiation potential. *Genes Dev* **28**, 2699-2711, doi:10.1101/gad.248526.114 (2014).
273 Mi, H., Muruganujan, A., Ebert, D., Huang, X. & Thomas, P. D. PANTHER version 14: more genomes, a new PANTHER GO-slim and improvements in enrichment analysis tools. *Nucleic Acids Res* **47**, D419-D426, doi:10.1093/nar/gky1038 (2019).
274 Corda, G. & Sala, A. Non-canonical WNT/PCP signalling in cancer: Fzd6 takes centre stage. *Oncogenesis* **6**, e364, doi:10.1038/oncsis.2017.69 (2017).
275 Lu, Z. *et al.* DKK1 maintained cancer stem-like properties of esophageal carcinoma cells via ALDH1A1/SOX2 axis. *Int J Clin Exp Pathol* **10**, 9489-9495 (2017).
276 Seino, M. *et al.* Requirement of JNK signaling for self-renewal and tumor-initiating capacity of ovarian cancer stem cells. *Anticancer Res* **34**, 4723-4731 (2014).
277 Okada, M. *et al.* Targeting the K-Ras--JNK axis eliminates cancer stem-like cells and prevents pancreatic tumor formation. *Oncotarget* **5**, 5100-5112, doi:10.18632/oncotarget.2087 (2014).
278 Yoon, C. *et al.* Chemotherapy Resistance in Diffuse-Type Gastric Adenocarcinoma Is Mediated by RhoA Activation in Cancer Stem-Like Cells. *Clin Cancer Res* **22**, 971-983, doi:10.1158/1078-0432.CCR-15-1356 (2016).
279 Liu, Y., Zhang, X., Wang, J., Yang, J. & Tan, W. F. JNK is required for maintaining the tumor-initiating cell-like properties of acquired chemoresistant human cancer cells. *Acta Pharmacol Sin* **36**, 1099-1106, doi:10.1038/aps.2015.58 (2015).
280 Zheng, H., Wu, L., Fan, J. & Yuan, H. Zinc finger protein 501 maintains glioblastoma cell growth through enhancing Frizzled-6 expression. *Neurosci Res* **182**, 15-24, doi:10.1016/j.neures.2022.06.003 (2022).
281 Katoh, M. Canonical and non-canonical WNT signaling in cancer stem cells and their niches: Cellular heterogeneity, omics reprogramming, targeted therapy and tumor plasticity (Review). *Int J Oncol* **51**, 1357-1369, doi:10.3892/ijo.2017.4129 (2017).
282 Chen, Y., Chen, Z., Tang, Y. & Xiao, Q. The involvement of noncanonical Wnt signaling in cancers. *Biomed Pharmacother* **133**, 110946, doi:10.1016/j.biopha.2020.110946 (2021).
283 Ebnet, K. *et al.* Regulation of cell polarity by cell adhesion receptors. *Semin Cell Dev Biol* **81**, 2-12, doi:10.1016/j.semcdb.2017.07.032 (2018).
284 Paridaen, J. T., Wilsch-Brauninger, M. & Huttner, W. B. Asymmetric inheritance of centrosome-associated primary cilium membrane directs

ciliogenesis after cell division. *Cell* **155**, 333-344, doi:10.1016/j.cell.2013.08.060 (2013).
285 Jaafar Marican, N. H., Cruz-Migoni, S. B. & Borycki, A. G. Asymmetric Distribution of Primary Cilia Allocates Satellite Cells for Self-Renewal. *Stem Cell Reports* **6**, 798-805, doi:10.1016/j.stemcr.2016.04.004 (2016).
286 Messeguer, X. *et al.* PROMO: detection of known transcription regulatory elements using species-tailored searches. *Bioinformatics* **18**, 333-334, doi:10.1093/bioinformatics/18.2.333 (2002).
287 Farre, D. *et al.* Identification of patterns in biological sequences at the ALGGEN server: PROMO and MALGEN. *Nucleic Acids Res* **31**, 3651-3653, doi:10.1093/nar/gkg605 (2003).
288 Batlle, E. & Clevers, H. Cancer stem cells revisited. *Nat Med* **23**, 1124-1134, doi:10.1038/nm.4409 (2017).
289 Celia-Terrassa, T. & Kang, Y. Metastatic niche functions and therapeutic opportunities. *Nat Cell Biol* **20**, 868-877, doi:10.1038/s41556-018-0145-9 (2018).
290 Oskarsson, T., Batlle, E. & Massague, J. Metastatic stem cells: sources, niches, and vital pathways. *Cell Stem Cell* **14**, 306-321, doi:10.1016/j.stem.2014.02.002 (2014).
291 Bastock, R., Strutt, H. & Strutt, D. Strabismus is asymmetrically localised and binds to Prickle and Dishevelled during Drosophila planar polarity patterning. *Development* **130**, 3007-3014, doi:10.1242/dev.00526 (2003).
292 Devenport, D. & Fuchs, E. Planar polarization in embryonic epidermis orchestrates global asymmetric morphogenesis of hair follicles. *Nat Cell Biol* **10**, 1257-1268, doi:10.1038/ncb1784 (2008).
293 Stahley, S. N., Basta, L. P., Sharan, R. & Devenport, D. Celsr1 adhesive interactions mediate the asymmetric organization of planar polarity complexes. *Elife* **10**, doi:10.7554/eLife.62097 (2021).
294 Platt, R. J. *et al.* CRISPR-Cas9 knockin mice for genome editing and cancer modeling. *Cell* **159**, 440-455, doi:10.1016/j.cell.2014.09.014 (2014).